Vladimir Boskovic, Dipl.-Ing.

Local heat treatment of advanced high strength steels to reduce springback

DISSERTATION

zur Erlangung des akademischen Grades

Doktor der technischen Wissenschaften

eingereicht an der

Technischen Universität Graz

Betreuer

Univ.-Prof. Dipl.-Ing. Dr.techn. Christof Sommitsch
Institut für Werkstoffkunde, Fügetechnik und Umformtechnik

Graz, im März 2024

EIDESSTATTLICHE ERKLÄRUNG

Ich erkläre an Eides statt, dass ich die vorliegende Arbeit selbstständig verfasst, andere als die angegebenen Quellen/Hilfsmittel nicht benutzt, und die den benutzten Quellen wörtlich und inhaltlich entnommen Stellen als solche kenntlich gemacht habe. Das in TUGRAZonline hochgeladene Textdokument ist mit der vorliegenden Dissertation identisch.

Datum	Unterschrift

To my wife and children
For their love, support, and patience

Gutachter:

Univ.-Prof. Dipl.-Ing. Dr.techn. Christof Sommitsch

Institut für Werkstoffkunde, Fügetechnik und Umformtechnik

Univ.-Prof. Dipl.-Ing. Dr.techn. Bernhard Sonderegger

Institut für Metallische Konstruktionswerkstoffe

Johannes Kepler Universität Linz

Abstract

High-strength steel (HSS) and advanced high-strength steel (AHSS) have recently seen a steady increase in their use for deep drawing of automobile components. The considerable potential of these steels to improve crash resistance of lightweight structures has driven this trend. However, challenges remain in counteracting the associated springback of these types of steel that leads to the reduced dimensional accuracy of deep drawn components. Springback primarily manifests as elastic deformation occurring when the formed component is released from the forming tool. Therefore, mitigation measures must be found to minimize elastic stresses directly within forming operations. There have been several proposed methods in the literature to address this springback issue when forming HSS of AHSS, such as: varying the blank holder force, utilizing counterpunch in sheet bending and the application of inductive heating to the flange region in deep drawing. In this thesis, an introduction to a hybrid forming-heating process is given, and a specialized tool is designed and constructed to test the suitability of local heat treatment – when applied directly after deep-drawing but before the formed part is released. Furthermore, the feasibility for a semi-industrial scale application of this hybrid technique to solve the material inherent springback issue is considered. Steel grades tested with the tool range from 780 MPa to 1180 MPa and heating treatment peak temperatures of 500°C and 900°C were employed. The results of hybrid forming-heating experiments are thoroughly discussed and analyzed in detail with the assistance of finite element (FE) simulations.

Kurzfassung

In den letzten Jahren hat die Verwendung von hochfestem Stahl (HSS) und weiterentwickeltem hochfestem Stahl (AHSS) für das Tiefziehen von Automobilkomponenten stetig zugenommen, da diese Stahltypen großes Potenzial für die Herstellung leichter Strukturen mit verbesserter Crashsicherheit zeigen. Allerdings wird die elastische Rückfederug als ernsthaftes Problem betrachtet, da sie die Kontrolle der dimensionalen Spezifikationen von Komponenten sehr herausfordernd macht. Springback kann hauptsächlich als elastische Verformung betrachtet werden, die auftritt, wenn das geformte Bauteil aus dem Formwerkzeug gelöst wird. Daher ist es äußerst effektiv, Maßnahmen zur Minimierung elastischer Spannungen direkt in den Umformoperationen in den Fokus zu rücken. In der Literatur werden verschiedene technologische Konzepte vorgeschlagen, um die Rückfederung beim Umformen von HSS oder AHSS-Blechen zu reduzieren: Variation der Unterzugkraft oder induktive Erwärmung des Flanschbereichs beim Tiefziehen sowie Verwendung eines Gegenstempels beim Biegen von Blechen. In dieser Arbeit wird das Konzept eines hybriden Umform-Wärmebehandlungsprozesses vorgestellt. Ein Werkzeug wird entworfen und hergestellt, um eine lokale Wärmebehandlung von tiefgezogenen Bauteilen unmittelbar nach Abschluss des Umformhubes, d.h. kurz vor dem Herausnehmen des geformten Bauteils aus dem Werkzeug, zu ermöglichen. Die vorliegende Arbeit untersucht die Machbarkeit, im halbindustriellen Maßstab, dieses Prototyp-Werkzeugs zur Lösung des Rückfederung-Problems einzusetzen. Die ausgewählten Stahlsorten, die auf dem Werkzeug getestet werden sollen, haben eine Zugfestigkeit von 780 MPa bis 1180 MPa. Die Wärmebehandlung des Materials wird mit Spitzen-Temperaturen von 500°C und 900°C durchgeführt. Die Ergebnisse der hybriden Umform-Wärmebehandlungsversuche werden im Detail diskutiert und mithilfe von Finite-Elemente-Simulationen analysiert.

Table of content

Symbol directory and list of abbreviations

Symbol	Unit	Description
F	N	Punch force
k_f	MPa	Yield stress
n	-	Hardening exponent
R_p	MPa	Yield strength
r	-	Lankford parameter
$r_{0,45,90}$	-	Lankford parameter determined at 0°, 45° and 90 ° to the rolling direction
r_f	°	Draw ring radius, after forming
r_i	°	Draw ring radius, initial
s or T	mm	Sheet thickness
ε_p	-	Plastic strain
$\dot{\varepsilon}$	1/s	Strain rate
λ	W/mK	Thermal conductivity
φ' and φ''	-	Convex function of deviatoric stress tensor
φ_1	-	Strain in direction x
φ_2	-	Strain in direction y
φ_3	-	Strain in direction z
σ_{ij}	MPa	Yield stress three dimensional
E	N/m^2	Modulus of elasticity
G	N/m^2	Shear modulus
L_0	mm	Initial length
L	mm	Current length
A_{c1}	°C	Boundary temperature
Θ	°	Bending angle
ν		Poisson's ratio
τ	MPa	Shear stress
β		Drawing ratio

AHSS	Advanced high strength steel
BCC	Body-centred cubic materials
BFH	Blank holder force
BIW	Body in White
CP	Complex phase steel
DP	Dual phase steel
FCC	Faced-centred cubic materials
FEM	Finite element method
HSLA	High-strength low-alloy steel
HSS	High strength steel
IMAT	Institute of Materials Science, Joining and Forming
MS	Martensitic steel
TWIP	Twinning-induced plasticity
UTS	Ultimate tensile strength
YS	Yield strength

1 Introduction

The automotive industry spent the last two decades trying to come up with ways of producing low-mass, low-emission vehicles, which are light and fuel-efficient to meet the demands of both the consumers and regulations imposed by authorities worldwide. [1]

This pushed industry to develop and produce innovative engines to meet the above challenges. However, another possible solution was to be found in producing lighter vehicles by using thinner sheets when producing car body parts. [2]

During this period, safety organizations had the safety requirements strengthened, as casualties in vehicle-related accidents rose to unacceptable numbers. Thus, having been faced with a contradiction that proved impossible to solve with the materials at hand, the time came for the steel being used to be reinvented to match these new requirements. [2] [3]

Figure 1 shows a Comparative Life Cycle GHG Emissions for two contender body structure and closure materials. AHSS-intensive vehicles and Aluminum-intensive vehicles were comprehensibly tested and compared to a baseline using Life Cycle Assessment (LCA) methods. Aluminum-intensive vehicles show a higher total lifetime GHG emissions when compared to AHSS-intensive vehicles, for every vehicle class tested. [4]

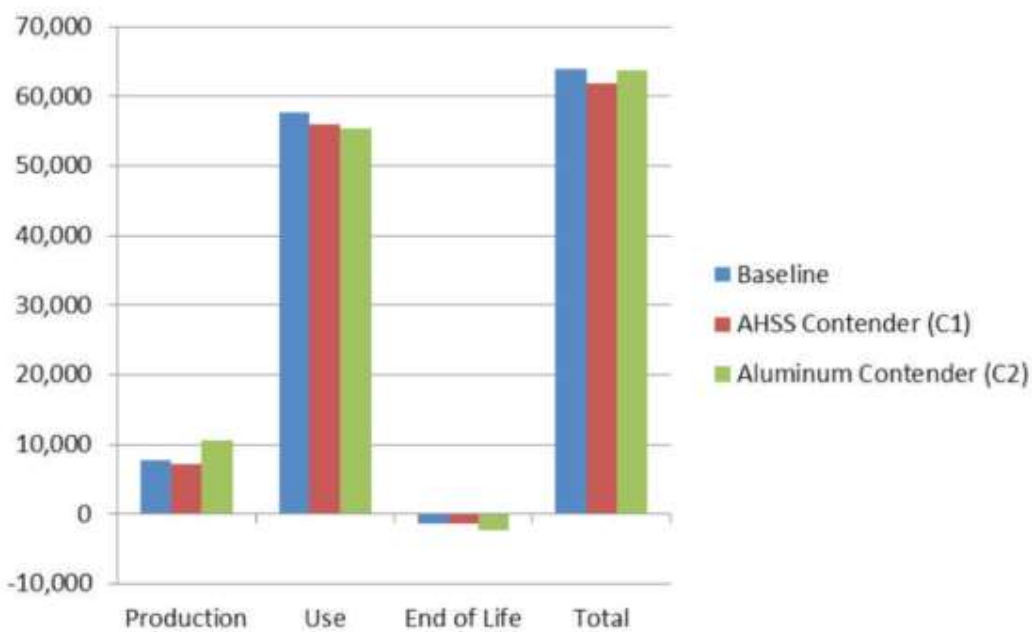

Figure 1 Common body structure, and closure material, GHG material production emissions accounting for part mass-reduction estimates [4]

For more than ten years, the characteristics and the use of Advanced High Strength Steels (or AHSS) has given the industry the desired results in terms of both safety whilst maintaining its lightweight. Its higher

strength allows the production of crash-relevant parts, without losing any safety performance and when compared to steel grades previously used, the sheet thickness is lower. [2]

AHSS parts, which are currently used in the industry, can be divided into two groups in accordance with their production needs. Based on differing mechanical requirements, automotive parts are produced either via “cold forming” of via “hot forming” with both these processes having both advantages and disadvantages. [5]

While it is more economically sound as a production technique, cold forming does have a significant drawback. Vehicle producers have a major problem with the appearance of undesired residual stresses involved when using cold forming in production, namely: The so-called springback, which is an elastically driven change in shape and form of a part upon unloading. After a part is formed this is the most significant problematic issue resulting from cold forming. [6]

Figure 2 shows how material property differences between dual phase (DP) and high-strength low-alloy (HSLA) steels leads to different stress distributions, resulting in different dimensional accuracy.

Figure 2 Two channels made sequentially in the same die, with different mechanical properties leading to different springback [7]

Warm sheet metal forming can be implemented to overcome this springback forming issue. This thesis presents and discusses a new hybrid process developed, which includes local heat treatment to reduce springback in deep drawing of AHSS. The goal is to create a technical solution, that may be later developed further for industrial use application.

Chapter 1. Introduction of springback concept and motivation for this thesis.

Chapter 2. An overview of the forming technology and a comprehensive look into the basics of deep drawing, classification and application of AHSS, to further explain the springback issue. At its conclusion, it discusses the compensation of elastic springback and a short overview of the possibilities of induction heating will be given.

Chapter 3. Aims and objectives of this thesis. The work and analysis is based on the deductive methodology.

Chapter 4. Experimental results of the thesis. It explains the materials and the methods used for the qualitative and quantitative characterization of springback phenomena. It also elaborates how and in which way the tool is used in these tests, including the results of the mechanical testing of different materials with different parameters. Furthermore, simulation models will be introduced, which are employed to explain the stress relieving theory.

Finally, Chapter 5. is a conclusion of the thesis and a brief summary of further developments needed for future industrial application.

2 Literature review

The following chapter gives an overview of the methods and the technologies, which are the basis for resolving formability issues. It is comprised of a multitude of literature reviews which deal with the main topics of interest. Firstly, the technologies used in the automotive industry while producing vehicle parts will be taken into consideration. This overview will include research into the Advanced High Strength Steels as well. Furthermore, a systematic look into the issue of springback, focusing on explaining the concept of springback and what causes it, while taking into consideration the microstructure of the material itself and the geometry of the sheet blank, is presented. Finally, induction heating will be briefly explained as it is an important factor in this thesis.

2.1 Deep drawing fundamentals

When producing a hollow body, deep drawing of sheet metal, which is used in numerous industry branches, is considered to be one of the most important non-cutting processes for the production in several industrial sectors. For instance, white goods, packaging industry and vehicle industry all utilize the production of components via sheet metal forming. This is when a flat sheet of metal is formed into complex, three-dimensional geometries through the process of compression form pulling. The main advantage of this process is that through tensile compression, sheet metal can be formed without resulting in the modification of steel thickness. [8] The process typically employs a punch, a die (drawing ring) and a binder, see Figure 3.

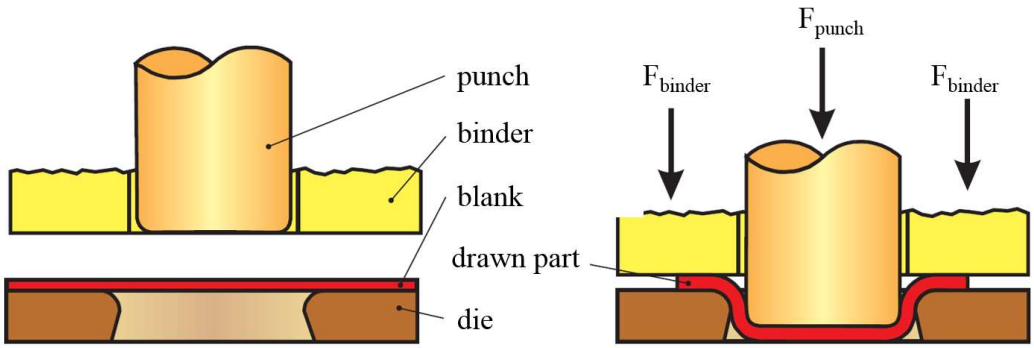

Figure 3 Schematic representation of deep drawing with a rigid tool [9]

Flat metal sheet, known as blank, is initially clamped between the blank holder and die through a defined blank holder force. The prestressed sheet of metal is then pushed in the direction indicated in the diagram via the punch to manipulate it beyond the drawing ring radius. During this first process the base is shaped, thus resulting in the creation of a bi-axial strain condition. Stretch-forming stress occurs in this area, due

to tensile stress in the radial and tangential directions. The drawing gap of the tool is defined by the distance between the outside of the punch and the inside of the die. If this gap is too small, or otherwise too large, there is a risk of component failure. During this process, it is essential that no sheet metal flows from the outside to the inside, so that the bottom of the component will be formed only through the thickness of the sheet metal. Depending on what radius ratios were employed during this process, there is the possibility that cracks may form in the vicinity of the drawing ring and the punch radius. Through further increase in the drawing depth, the drawing force from the floor to the frame (component wall) is then transferred into the flange zone. It is at this point that the deep-drawing process actually begins by drawing the blank from the outside in, under a pre-determined pressure between the binder and the die. In the outer area of the flange, a thickening of the material occurs, due to tensile and compressive stresses. In the flange area, normal stresses occur due to the binder force. The so-called plane strain occurs in the component frame and in the outlet of the stamp edge rounding, due to radial and tangential tensile stresses. [8] [10] [11]

Figure 4 shows the prevailing strain conditions on a deep-drawn part section.

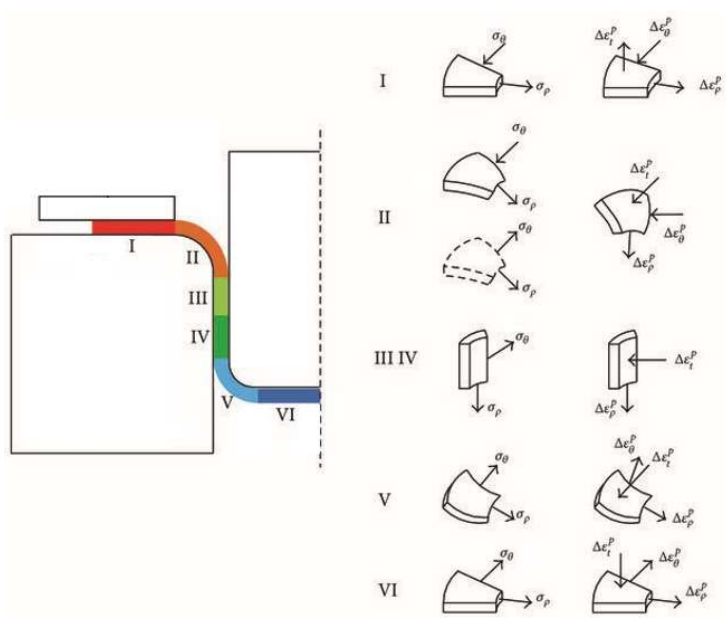

Figure 4 Strain representation of the forming zone, force transmission zone and load path [12]

Deep drawing operations, more specifically their process design, can be recognized by both a wrinkling and the characteristic appearance of splits in the wall or bottom area of the part, which indicate the process boundary. Avoiding wrinkling is achievable by increasing the binder force. This however, will simultaneously increase the likelihood of material failure by causing more cracks (splits). A schematic representation of the interaction between binder force and the wrinkling and appearance of splits given in Figure 5 demonstrates this phenomenon.

To summarize, low binder force leads to the appearance of wrinkles. Using the optimal binder force ensures the maximum drawing depth, without the occurrence of material failure. When producing parts with more complex geometries, such as the flange, wall or bottom, it is possible to implement the same principle shown in Figure 5 [13]

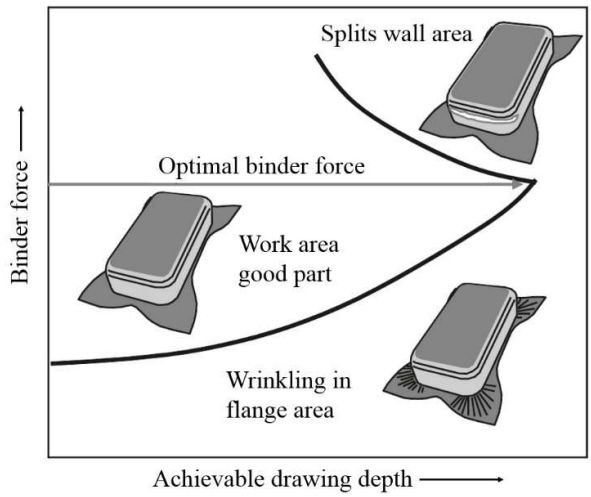

Figure 5 Operational diagram for the adjustment of binder force for a rectangular shaped cup [14]

When designing a simple cup, a relevant parameter while drawing parts is the limit drawing ratio β. More precisely, the limit drawing ratio β establishes the maximum allowable blank diameter, relative to a given punch diameter, that can be drawn without generating cracks in the wall section of the part. [13] [8]

The following process parameters are influencing the drawing ratio for deep drawing processes:

- Material properties
- Blank thickness
- Blank size
- Blank position
- Tribological properties (sheet and/or tool surface, lubrication, etc.)
- Punch,die and draw radius
- Gap between punch and die
- Binder force
- Draw beads

Slip and twinning are the two processes that cause plastic deformation of metal, with slip being the more frequent cause. Slip is a consequence of the movement of dislocations, and therefore the mobility of the dislocation is at the center of the ease of deformation. Applied stress is necessary to overcome lattice friction while the dislocation is moving through the lattice. These friction stresses, commonly known as Peierls-Nabarro stresses are often overcome by the dislocations by utilizing thermal energy. Peierls-

Nabarro stress are the main obstacle when employing bcc metals, such as steel, thus in these cases, temperature becomes a major factor. [15] [16]

When considering forming at elevated temperature, it is important to differentiate warm forming from hot forming. The micro-structure remains stable in warm forming, while in hot forming, re-crystallization, grain growth and other changes to the microstructure do arise. In warm forming, the temperature range is characterized by utilizing a factor 0.3 to 0.5 of the melting temperature. The term hot forming is used for temperatures exceeding a factor 0.5 of melting temperature mark. [15] [16]

As this review will demonstrate, warm sheet metal forming is possible with a partially heated blank. This concept results in the possible advantage of decreased springback through various factors and will be further discussed in a subsequent chapter.

2.2 Classification and application of AHSS

When considering the steel portfolio, one is faced with the fact that Advanced High Strength Steels (AHSS) are the group that has shown the most innovations implemented. Constant developments and the introduction of completely new grades, after having been used with great success within the automotive industry for more than 10 years, has ensured an increasing range of use. Their ability to meet a variety of needs in the body of a vehicle is a result of the multi-phase micro-structures achieved by the consolidated production methods used.

Currently, the following five main groups of classification are used for AHSS in the automotive industry:

- Mild Steels (abbreviated as MS, not to be confused with Martensitic Steels)
- (Conventional) High-Strength Steels (abbreviated as HSS)
- First-generation Advanced High-Strength Steels (abbreviated as AHSS)
- Second-generation Advanced High-Strength Steels
- Third-generation Advanced High-Strength Steels

Billur et al. [17] described the First generation of AHSS usually as having a martensitic microstructure, allowing for additional strength, however also less formable. Improving formability required additional phases. Dual-phase (DP) steels for example, contain ferrite in addition to their martensitic microstructure. In Complex-phase (CP) steels, which exhibit more coexistent microstructures bainite is found in addition to ferrite and marstensite.

The Second generation, as stated by Billur et al. [18], is characterized by an austenitic microstructure allowing for a higher level of formability with the drawback of being metastable in most cases at room temperature. The final price of these steels can be significantly increased by an ad hoc use of high-alloy elements. Twinning-Induced Plasticity steels (TWIP) and Austenitic Stainless steels (Aust. SS) are examples of this practice.

In order to solve the issues presented by above mentioned steel grades, a third generation of AHSS is being tested. Lower cost and higher levels of formability are the focus points of the next generation of AHSS as stated by Billur et al. [19]. The production processes such as Quenching and Partitioning (Q&P) or creating TRIP-aided Bainitic Ferrite (TBF) are the reason for their exceptional mechanical properties. In addition to this, third generation steels with a variety of properties are being tested, and extensively so, by NanoSteel Co. ©

The latter classification can be seen in Figure 6. This diagram displays the strength and elongation ranges of different generations of AHSS in comparison to previous steel grades in a Strength-Elongation curve.

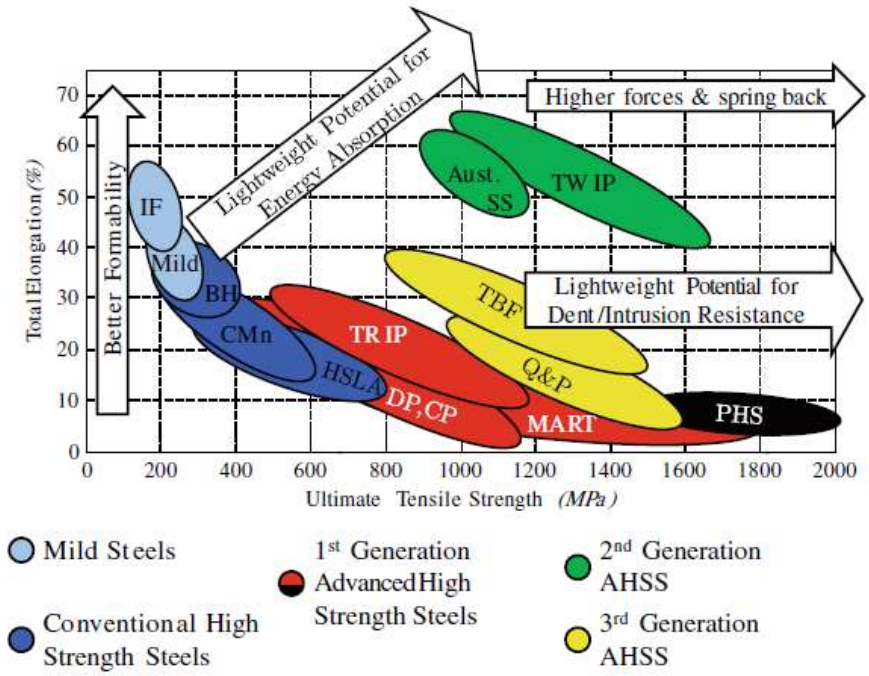

Figure 6 "Banana Curve" – Material classification tensile strength vs. total elongation [17]

According to Zuidema et al. [3], the use of a new generation of materials in recent years, which are more advanced, is the key to the reduction of weight. Their study showcases 29% savings in Body-in-White vehicle weight. [3] The Body-in-White is an industry term that refers to the production stage before any moving parts (doors, hoods, etc.) were added and painting have been applied. At this stage only the sheet metal components have been welded together. [20]

Zuidema et al. [3] further state that weight reduction is dependent on their content of AHSS and the generation they belong to. The possibility of implementing car parts with thinner walls, which is possible when using AHSS is the main reason behind this. Due to the increment of the tensile strength in emerging steel generations and the improvement in their formability and mechanical properties, they will very likely continue to be applied in BiW in the future so that the trend in weight reduction continues.

The mentioned progression, which is displayed in Figure 7, demonstrates the effect that different generations of steels have on weight reduction. The best results are expected to be coincide with the emergence of third-generation AHSS.

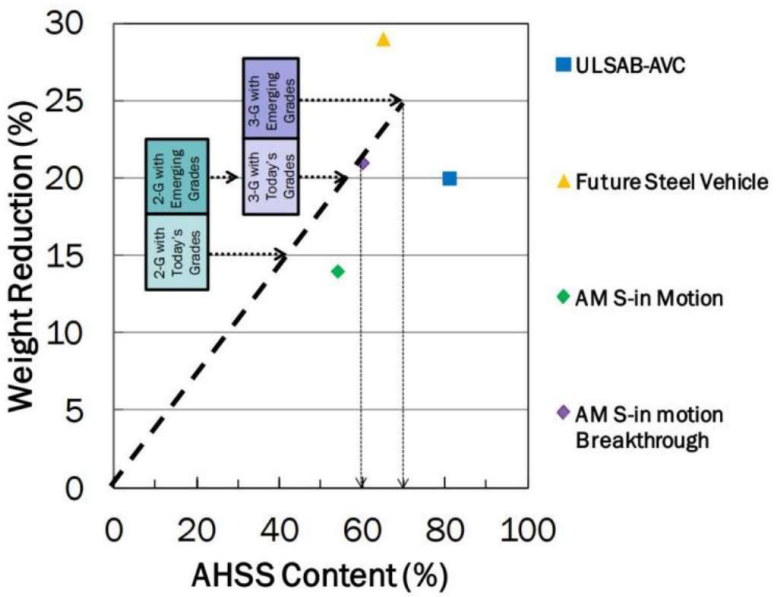

Figure 7 Progress in weight reduction of increasing AHSS content and generation [3]

Through their study on material applications for weight reduction in the future, Zuidema et al. [3] predicted the primary BiW potentials for lightweight in 2025. The study focused on the usage of both current and emerging generations of steel and their ability to reduce weight in the BiW, in relation to a 2009 baseline. As shown in Table 1, it is expected to reach an average of 25 % reduction in the year 2025. This will be achieved through developments made as a result of the expertise of the preceding generations.

Table 1 AHSS Grades as potential for weight reduction [3]

AHSS Grade	Potential for weight reduction
Conventional steels	0% (no reduction)
Current 2nd Generation AHSS	15 %
Emerging 2nd Generation AHSS	20 %
Current 3rd Gen. AHSS	20 %
Emerging 3rd Generation AHSS	25 %

EuroCarBody conferences, [21] yearly benchmark meetings, are organized by Automotive Circle International as an opportunity to study the trends and the use of material mix in BiW. At these events, around 10 cars of different segments are analyzed, with the resulting technical findings, including a detailed report of the BiW material mixture being presented. As an example of a model presented in EuroCarBody, Figure 8 shows the material mix of the 2015 Alfa Romeo Gulietta which belongs to the C-vehicle-sector. The dramatic increase in the inclusion of AHS steels for Body in White components is shown in Table 2.

Materials: corresponding metallurgical classes		RGB colour code
Steels	**Low Strength Steels:** Mild steels	R 153, G 204, B 255
	High Strength Steels (HSS): High Strength Interstitial-free Steels (HSIF), Bake Hardening Steels (BH), High Strength Low Alloy Steels (HSLA)	R 051, G 102, B 255
	Advanced High Strength Steels (AHSS): Dual Phase Steels (DP), Transformation Induced Plasticity Steels (TRIP)	R 255, G 153, B 204
	Stainless steels: Austenitic stainless steels	R 051, G 051, B 153
	Ultra High Strength Steels (UHSS): Complex Phase Steels (CP), Martensitic Steels (MS)	R 204, G 153, B 255
	Press Hardened Steels (PHS)	R 128, G 000, B 128
Aluminium	**Aluminium sheets:** 7xxx series	R 051, G 204, B 153
	Aluminium sheets: 6xxx series	R 000, G 255, B 000
	Aluminium sheets: 5xxx series	R 204, G 255, B 204
	Aluminium extrusion profiles	R 153, G 204, B 000
	Cast aluminium	R 051, G 153, B 102
	Magnesium	R 255, G 255, B 000
Plastics	**Fibre reinforced plastics**	R 255, G 000, B 000
	Duroplastics, including Sheet Molding Compound (SMC)	R 255, G 153, B 000
	Thermoplastics	R 153, G 051, B 000
Other materials, namely:_____		R 192, G 192, B 192

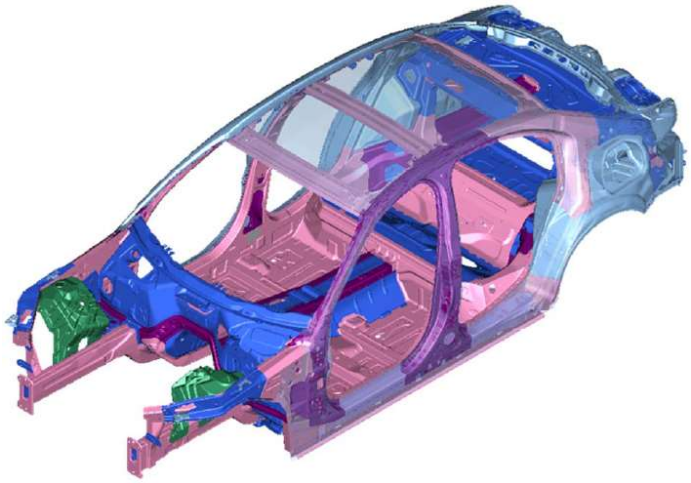

Figure 8 Body in white - Alfa Romeo Gulietta 2015 including RGB color code according to the metallurgical class of the used materials [21]

Table 2 Dramatical increase of AHS steels for Body in White components [21]

Vehicle	Year - Segment	AHSS (DP, TRIP)	UHSS (CP,Mart)	LSS (Mild Steels)	HSS (IF,BH, HSLA)	Press hardened steels (PHS)
Nissan Ariya	`22-C	17,8%	1,8%	26,5%	13,4%	9,4%
Toyota bZ4X	`22-C	25,0%	11,6%	39,3%	8,9%	13,4%
Volkswagen ID.Buzz	`22-M	26,0%	14,0%	14,0%	10,0%	31,0%
Opel Mokka	`21-B	20,9%		44,9%	22,6%	11,6%
Peugeot 308	`21-C	19,9%	8,0%	24,6%	36,2%	12,6%
Rivian R1T	`21-M	21,0%	12,0%	26,0%	10,0%	
Honda e	`20-B	29,8%	0,3%	45,4%	17,3%	6,2%
Skoda Octavia	`20-C	10,0%	2,9%	26,3%	39,7%	20,6%
Subaru Outback	`20-D	31,0%		47,9%	11,7%	7,7%
Volvo XC40	`20-J	23,9%		28,7%	28,4%	10,4%
Volkswagen ID.4	`20-C	11,9%	1,0%	29,8%	26,4%	24,6%
Mustang Mach-E	`20-C	11,6%	7,7%	22,2%	26,3%	24,9%
Reno Clio	`19-B	15,0%	3,5%	37,7%	33,5%	8,4%
Audi e-tron	`19-J	21,7%	0,8%	12,9%	27,3%	23,6%
Scania NTG	`18	17,0%		6,0%	73,0%	4,0%
GMC Sierra / Chervolet Silv	`18	11,9%	7,2%	21,6%	39,4%	5,5%
BMW 8 Series Coupe	`18 -S	9,0%	1,0%	9,0%	29,0%	21,0%
Volvo V60	`18 - C	18,4%		28,8%	20,8%	24,6%
Infiniti QX50	`18 - D	33,0%		45,0%	17,0%	
Audi A6 / A7 sportback	`18 - E	19,4%	1,0%	23,2%	19,9%	19,7%
PSA DS3 crossback	`18 - B	15,6%	3,9%	34,3%	30,9%	11,6%
Mercedes - Benz A Class	`18 - C	35,5%	0,7%	24,6%	26,4%	9,5%
Ford Fokus	`18 - C	9,3%	2,4%	33,7%	21,7%	31,6%
Audi A8	`17 - F	11,1%		0,3%	990,0%	13,4%
Renault Koleos	`17 - D	19,1%	3,4%	50,5%	21,5%	3,2%
Chervolet Bolt	`17 - B	23,3%	9,2%	14,6%	23,8%	11,8%
Subaru Impreza	`17 - C	27,5%		51,5%	11,7%	7,5%
VW Polo	`17 - A	9,2%	1,3%	30,3%	38,2%	21,0%
Volvo XC60	`17 - J	16,7%		28,5%	18,0%	26,3%
Honda Accord	`17 - D	18,7%		41,5%	21,9%	11,6%
BMW 6 Series GT	`17 - E	8,0%	1,0%	13,0%	33,0%	17,0%
Alfa Romeo Giulietta	`16 - C	31,0%	3,0%	15,0%	23,0%	12,0%
Volvo X90	`16 - D	15,5%		27,8%	17,4%	28,9%
Audi A5	`16 -D	24,1%		31,0%	28,7%	14,3%
Audi Q7	`15 - D	14,9%		10,3%	15,7%	9,2%
Cadilac CT6	`15 - E	7,6%	0,2%	6,9%	12,7%	10,5%
Renault Espace	`15 - D	7,0%	2,0%	28,0%	34,0%	12,0%
Fiat 500X	`14 - C	21,9%	0,5%	23,5%	40,6%	10,0%
Mazda 2	`14 - B	24,5%	13,7%	37,1%	23,0%	1,7%
Peugeot 308	`14 - C	20,9%		29,2%	33,3%	10,3%
Subaru WRX	`14 - D	35,0%	3,0%	51,0%	7,0%	2,0%
Mercedes C-Class	`14 - D	8,9%	5,4%	12,0%	36,2%	11,9%

In accordance with the material used for its production and its function, each automotive component demands a specific production process. Hot forming and cold forming are the two most commonly used processes. They encompass the different steps used while reshaping metals plastically either at room temperature (cold forming) or above the re-crystallization temperature of the material (hot forming). However, different steel grades are suitable for different processes and this work focuses on press stamping or pressing and its use in cold and hot forming. This refers to the use of sheet blank in part production. The crash-relevant components described previously comply with these requirements, which indicate that the thickness of a part is almost the same as its initial sheet blank. [5]

Severe springback after the forming process makes the use of these steels in the automotive industry quite difficult and somewhat limited. Controlling this issue requires an additional investment in tool design and allowing for the component tolerances to be fulfilled. However, this means longer development times and higher costs. With draw beads the right level force and regulation of the clamping force, it is possible to achieve a reduction in springback. When considering possible solutions to the reduction of sprinngback, a smaller tool radius, lower tool clearence and higher clamping forces must be considered. The use of modified tools (also called “false” tools) or overbending are possible solutions when compensating for springback.

2.3 Description of materials

The types of deformation implemented on sheets of metal as part of the forming process in the automotive industry while constructing the car body are as follows: the elastic strain, the plastic strain and finally failure. In the case of steel, there is a linear relationship between the stress and the elastic deformation. [22] Relationship described by Hooke's law:

$$\sigma_{ij} = \sum C_{ij}\ \varepsilon_p \tag{1}$$

σ_{ij} and ε_p are the components of the three-dimensional stress and strain tensor and c_{ij} the elastic constants of the material. Assuming a uni-axial stress state and an isotropic one material behavior, the equations for the normal stress σ and the shear stress τ, are the following: [23]

$$\sigma = E\ \varepsilon \tag{2}$$

$$\tau = G\ \gamma \tag{3}$$

The elongation ε is defined by the change in length in relation to the initial length, while the shear τ from the arc-tangent of the ratio of displacement in the thrust direction to the initial length. In equations above the material constants of the modulus of elasticity E and the shear modulus G are introduced. Assuming constant volume, the shear modulus can be calculated during of the deformation via the Poisson's ratio ν converted to the modulus of elasticity. [24]

$$\nu = \frac{E}{2G} - 1 \tag{4}$$

In order for plastic flow to occur in the workpiece during forming, the stress that actually occurs must reach a material characteristic level. In forming technology, it is therefore customary to refer the acting force F to the actual cross-section or its area S. The yield stress k_f is defined as.

$$k_f = \frac{F}{S} \tag{5}$$

In calculating the strength of materials, it is customary to define the strain ε for the uni-axial tensile test as a change in length $L_1 - L_0$ in relation to the initial length L_0:

$$\varepsilon = \int_{L_0}^{L_1} \frac{dL}{L0} = \frac{L1 - Lo}{L0} \tag{6}$$

Since there are usually large plastic changes in shape when implementing forming technology, the engineer's strain defined is not suitable for describing the distortion. Instead, the degree of deformation φ, in which the change in length is related to the current length L, is often used:

$$\varphi = \int_{L_0}^{L_1} \frac{dL}{L} = ln \frac{L1}{L0} \tag{7}$$

The flow curve is defined as:

$$k_f(\varphi) \tag{8}$$

represents the range of the generally non-linear relationship between the strain ϕ and the stress, which is necessary for a uni-axial stress state in order for yield to occur. In the case of multi-axial stress states, the onset of yielding depends not only on one stress component, but also on the entire stress tensor. The transition from uni-axial to multi-axial stress states is determined by yield conditions, e.g. von Tresca and von Mises, for which an equivalent stress σ_v is calculated and compared with the yield stress k_f via its equivalent strain φ_v [8]. φ_v' defines the comparative strain rate.

Von Mises:

$$\varphi_v' = \sqrt{\frac{2}{3}(\varphi_1' + \varphi_2' + \varphi_3')} \tag{9}$$

$$\varphi_v = \int_{t_0}^{t_1} \varphi_v' \, \mathrm{dt}$$

Treca: $$\varphi_v' = \max(\varphi_1', \varphi_2', \varphi_3') \quad (10)$$

$$\varphi_v = \max(\varphi_1, \varphi_2, \varphi_3)$$

The deformability of a material is understood to mean the equivalent degree of deformation that can be achieved at break. Determining the deformability is generally difficult, since the degree of deformation achieved at fracture depends on various factors. Even in the case of uni-axial stress, the resultant degree of deformation depends on the type of stress, the rate of deformation and the temperature.

At higher temperatures, recovery and re-crystallization processes take place in the material as a result of thermal activation [8]. Whether it is correct to employ re-crystallization or crystal recovery to achieve the desired result, must be decided on a case-by-case basis. Both processes take place with a finite, temperature-dependent speed. The course of the flow curve is influenced by hardening as a result of the increase in dislocation density during forming and by the decrease in dislocation density as a result of crystal recovery or re-crystallization. The flow curves are therefore strongly dependent on the strain rate φ' in addition to the temperature T and the degree of strain φ. In the case of an infinitely high strain rate, an adiabatic flow curve is obtained (i.e., the strain heat cannot be derived). In principle, the ability to change shape increases with increasing temperature and decreases with increasing strain rate (see Figure 9). In general, according to [25], cold and warm flow curves can be formulated as below:

$$k_f\ (\varphi_v, \varphi_v^{`}) = C\varphi_v^n, \varphi_v^{`m} \quad (11)$$

The hardening exponent n is a measure of strain hardening and depends on the micro-structure of the material. Increasing values of the strength properties correspond to a smaller n-value and reduce the formability of a material. A larger n value reduces the material's tendency to manifest localized constriction during stretch forming, which results in higher uniform elongation.

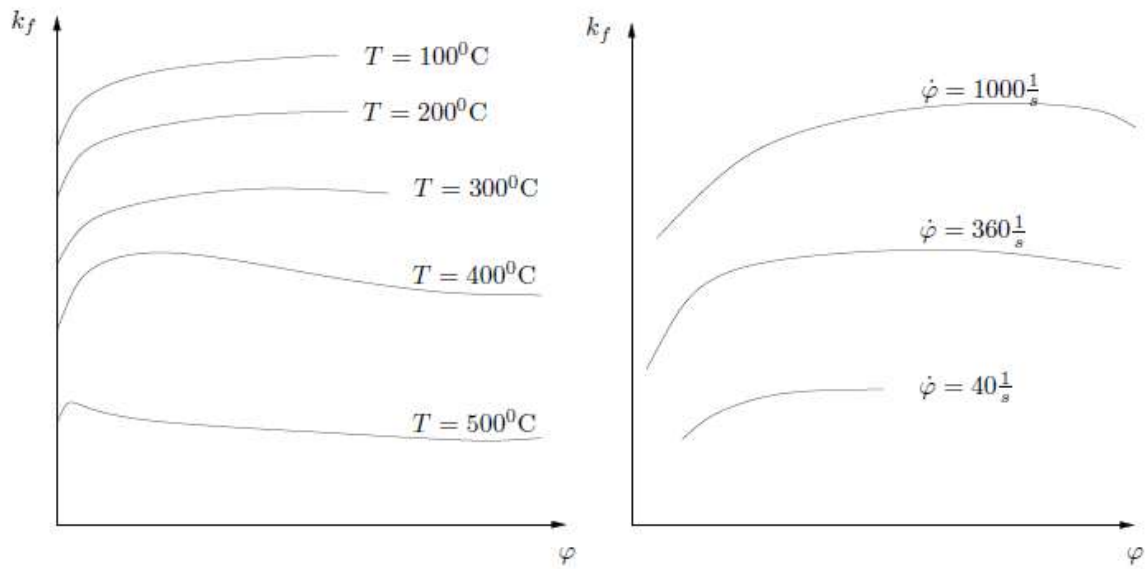

Figure 9 Schematic representation of flow stress curves obtained at different temperature and strain rate [8]

The exponent m depends on temperature and material. Values for C, m and n are tabulated in [8].

The relationship for cold flow curves results from the following equation

$$k_f\ (\varphi\ \ ) = C\varphi_v^n \tag{12}$$

Elasticity is related to interatomic forces; hence Young's modulus is generally direction dependent. If the material is anisotropic, knowledge of the yield location is also required. Yield locus curves are the locus for all combinations of stress components where plastic flow occurs. The plastic anisotropy of the rolled sheet is described by so-called r-values, which characterize the yield stress ratios in the longitudinal (r0) and width (r90) directions. [26]

2.4 Springback – fundaments and evaluation

When trying to develop a tool design or to define the accurate process parameters in sheet metal stamping operations it is vital to predict springback correctly. Establishing mechanisms for springback compensation and applying them, if possible, in a serial process is the main focus.

2.4.1 Definition and concepts

Springback by definition is the attempt of a formed flat-rolled metal to go back to its original position upon the release of the forming force. When considering cold forming, it is the most significant issue to take into account as it can cause stamping instability and can affect the required tolerances. Consequently, this issue disregards the successful completion of the final desired shape, and it is greatly undesired in every production process. [6] [27] Furthermore, it is expected to appear more frequently in the automotive industry due to the cold forming of AHSS. Figure 10 shows a representation of springback in the bending of a sheet metal.

The uneven distribution of atoms along the cross section creates the elastic recovery of the material, which is the principal factor behind the occurrence of springback. During the forming process, compression is found in newly created bends along the inner region, while stretching can be found along the outer region. Therefore, the atoms exhibit greater density on the inside of each bend in comparison to the outside of the bend. Forces that initiate material backsliding are created by this dissimilarity in densities.

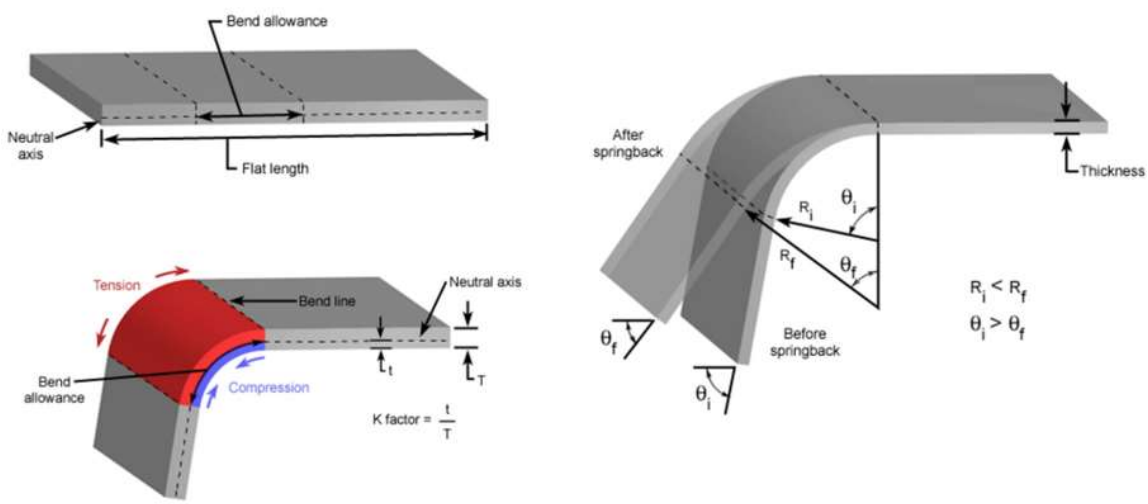

Figure 10 Springback in the bending of a sheet metal [28]

According to Sumikawa et al. [29], the magnitude of the mentioned phenomenon is mainly dependent on three factors: the Bauschinger effect, the average Young´s Modulus and the elasto-plastic anisotropy.

- The Bauschinger effect is a material behavior where appear softening, or reduction of the yield stress, upon reloading posterior to the unloading. It appears after reversing the direction of the stress, after compression followed by tension, or shear followed by contrary-direction shear. This effect aggravates for different steel grades. In their study, Sumikawa et al. [29] compared the

Bauschinger effect of a conventional HSS (HSLA590, with 622 MPa UTS) and an AHSS (DP980, with 986 MPa UTS), and they concluded that the Bauschinger effect was greater in the AHSS. [29] Figure 11 shows the schematic strain-stress curve for the Bauschinger effect. This effect can result in anisotropic behavior, meaning the material's response to mechanical forces depends on the loading direction.

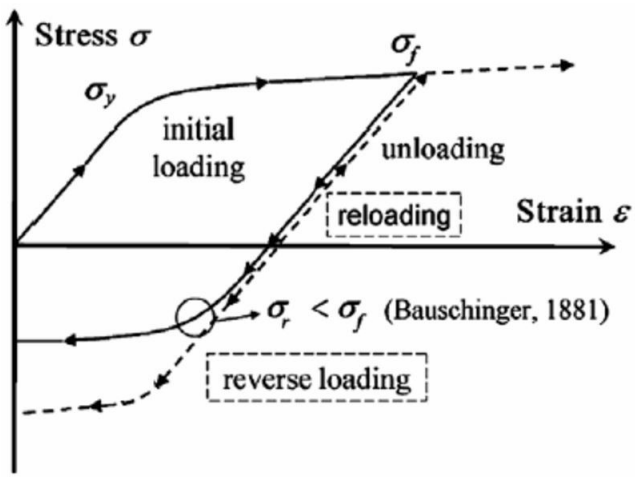

Figure 11 Schematic stress-strain curve that exhibits the Bauschinger effect [30]

- The **Young´s Modulus** or modulus of elasticity (*E*) defines the relationship between the material´s stress and strain. According to Sumikawa et al. [29], it is characterized as a stress-strain gradient during each unloading for the Bauschinger effect and it decreases gradually with plastic deformation. Therefore, it can be represented as the slope of the elasticity of a material in the stress-strain curve. [31] Figure 12 shows the representation of the modulus of elasticity for aluminum and steel. Sumikawa et al. [29] concluded that an increase of the average modulus of elasticity reduced the springback measured.

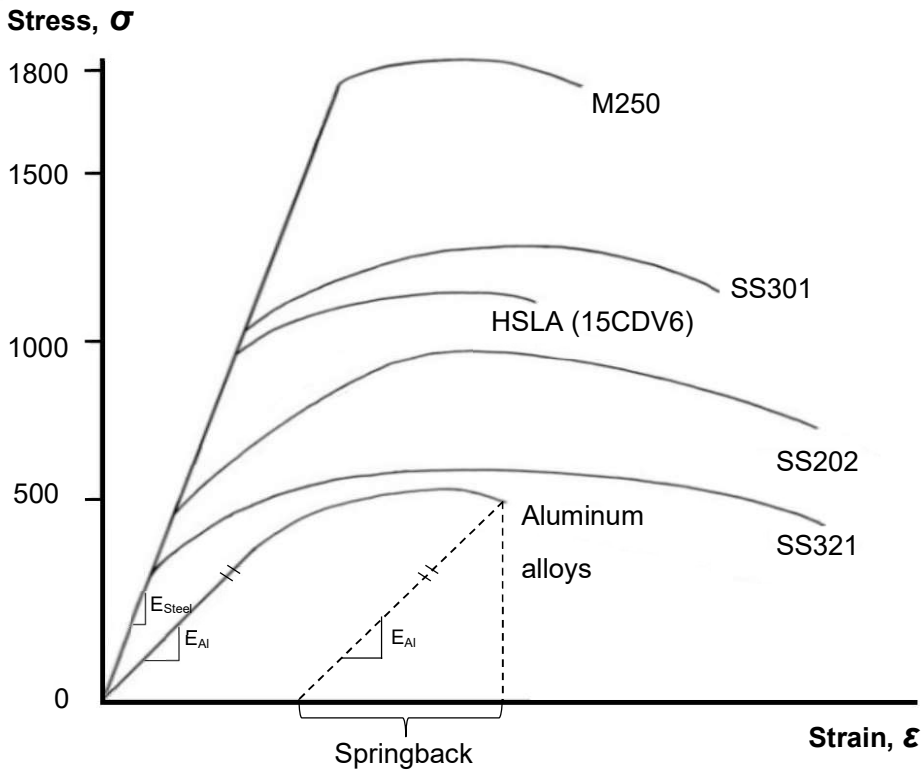

Figure 12 Representative stress-strain curve of various aerospace alloys [32]

Figure 12 shows that those materials belonging to the same group of steels exhibit the same strain-stress relationship properties. Their formability characteristics specify their yield point and their ultimate strength.

- **Elasto-plastic anisotropies** are characterized by steel parts having different properties in different directions as a consequence of the rolling direction during sheet production. This phenomenon is a result of the oriented microstructures, producing residual stresses after forming [29] that lead to various amounts of springback.

2.4.2 Representation of springback

As stated previously, springback will arise after any cold forming process and no forming type can prevent its appearance. Two methods will be presented that epitomise springback. Firstly, an evaluation of springback in an elastic and perfectly plastic material is presented, since it demonstrates the basics of this phenomenon. Secondly, a study of springback in real sheet metal forming is presented.

Elastic-plastic bending

The springback in an elastic, perfectly plastic material can be represented as a function of the difference between bending and resulting bend angles, $\Delta\theta$, according to Marciniak et al. [33] Their study shows how

loading and unloading affect springback in the absence of any tensions. When a moment, M, is applied into a sheet with a certain thickness, t, the latter is bent into a particular angle, θ, causing a curvature 1/ρ. Taking the neutral surface of the blank, whose length is l, as a reference, equation: [33]

$$\theta = l \ \frac{1}{\rho} \tag{13}$$

By differentiating equation, where l is constant

$$\frac{\Delta\theta}{\theta} = \frac{\Delta(1/\rho)}{1/\rho} \tag{14}$$

The stress-strain curve for an elastic, perfectly plastic material is given in figure 13. In a reverse loading situation, the condition Δσ1 = -2S can occur without the material entering into plastic state due to the characteristics of the material. S is the flow stress of the material, which is defined as the value of the stress required to immediately deform the material plastically.

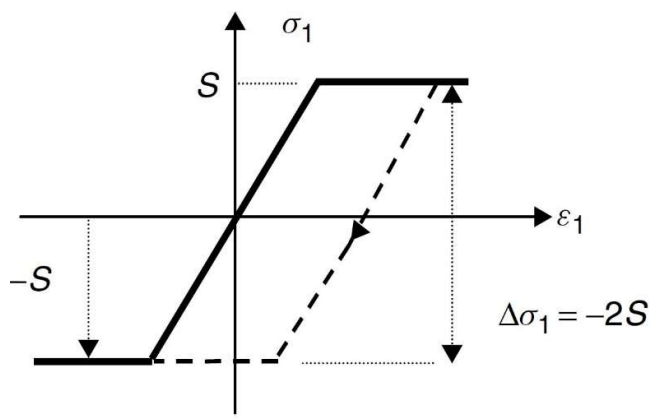

Figure 13 Elastic, perfectly plastic material model with reverse loading [33]

At this point, the assumption of the studies by Marciniak et al. [33] and Sluzalec et al. [34] should be cited, where they define the relationship between the bending moment, M, and the curvature of the neutral surface as in equation:

$$\frac{1}{\rho} = \frac{M}{EJ} \tag{15}$$

Assuming that the unloading of the mentioned moment, M, will be an elastic process, then the equation can be written in a different form and thus giving equation:

$$\frac{\Delta M}{J} = \frac{\Delta\sigma_1}{y} = \frac{\Delta\sigma_{1max}}{t/2} = E\,\Delta\left(\frac{1}{\rho}\right) \tag{16}$$

If plasticity has been fully achieved during the loading, then the model resembles that shown in Figure 14, whose unloading curve fulfils the condition of triangle proportionality. [33] Therefore, for a change in moment –Mp

$$\frac{\Delta(1/\rho)}{(1/\rho)_e} = \frac{\Delta M}{M_e} = \frac{-M_p}{M_e} \tag{17}$$

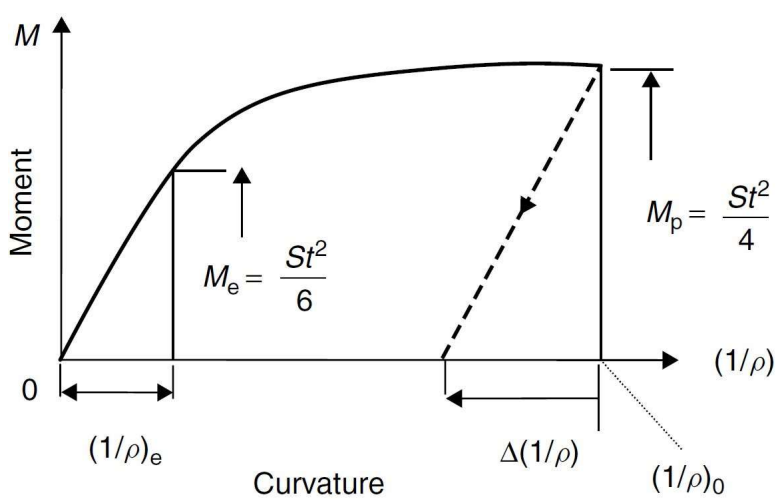

Figure 14 Moment, curvature diagram for an elastic, perfectly plastic sheet showing unloading from a fully plastic moment [33]

Where $(1/\rho)_e$ is the curvature at the moment of limit elastic bending, that is, the curvature before entering plasticity. Marciniak et al. [33] demonstrated that the mentioned curvature is as shown in equation:

$$\left(\frac{1}{\rho}\right)_{e} = \frac{2S}{Et} \tag{18}$$

Their study also demonstrated that the ratio of the fully plastic moment, Mp, and the limiting elastic moment, M_e, ration is 3/2

$$\Delta\left(\frac{1}{\rho}\right) = -\frac{3}{2}\left(\frac{1}{\rho}\right)_{e} = -3\frac{S}{Et} \tag{19}$$

After unloading the sheet from a curvature (1/ρ)0, the change in curvature will be proportional and thus given by equation:

$$\frac{\Delta(1/\rho)}{(1/\rho)0} = -3\frac{S}{E}\frac{\rho 0}{t} \tag{20}$$

Finally, considering the result of previous equation, the previous calculation can be written in the form of the change in bend angle, shown in equation 21

$$\Delta\theta \approx -3\,\frac{S}{E}\frac{\rho 0}{t}\,\theta \tag{21}$$

This equation, according to Marciniak et al. [33], is only an approximation and it has been assumed that the blank is bent to nearly fully plastic state. However, it shows that the springback is proportional to:

- the ratio $\frac{S}{E}$, which is the ratio of flow stress to Young´s Modulus
- the bend ratio $\frac{\rho 0}{t}$
- the bend angle, θ

Therefore, it is deduced that the springback can be represented as a function of the difference between bending and bent angles and it will increase with:

- smaller sheet thicknesses
- higher strength of material

Sheet metal forming

In real sheet metal forming processes, a blank holder is used to entirely clamp the part. Hence, the motion is limited during plastic deformation, unlike in pure bending. Furthermore, the residual stresses act as a deterrent for ideal situations and the tensions are dispersed unequally across the blank thickness. Those residual stresses are a result of the anisotropies after undergoing plastic deformation. These non-uniformities are created by the different phases found in the crystallographic microstructure of steel and the rolling direction used during sheet production. [29] [35]

Schmidt-Jürgensen [35], represented springback as a result of the elastic-plastic behaviour during sheet metal forming. This behaviour is characterized by a distribution of stresses, which stays in balance with the external force provided by the press, as shown in Figure 15a. The areas where the stresses do not exceed the yield point deform only elastically. When the external force of the press is removed, it originates an unloading moment, M_e, which in case of purely elastic deformation, it would be equal to the original bending moment. This is shown in Figure 15b. According to Schmidt-Jürgensen et al., in an elastic-plastic deformation, the stress distribution can be determined by adding the loading state of the first case and the unloading moment of the second, as seen in Figure 15c. If the unloading moments are large enough, the originated tensions can cause a new plastic state which is the resultant springback.

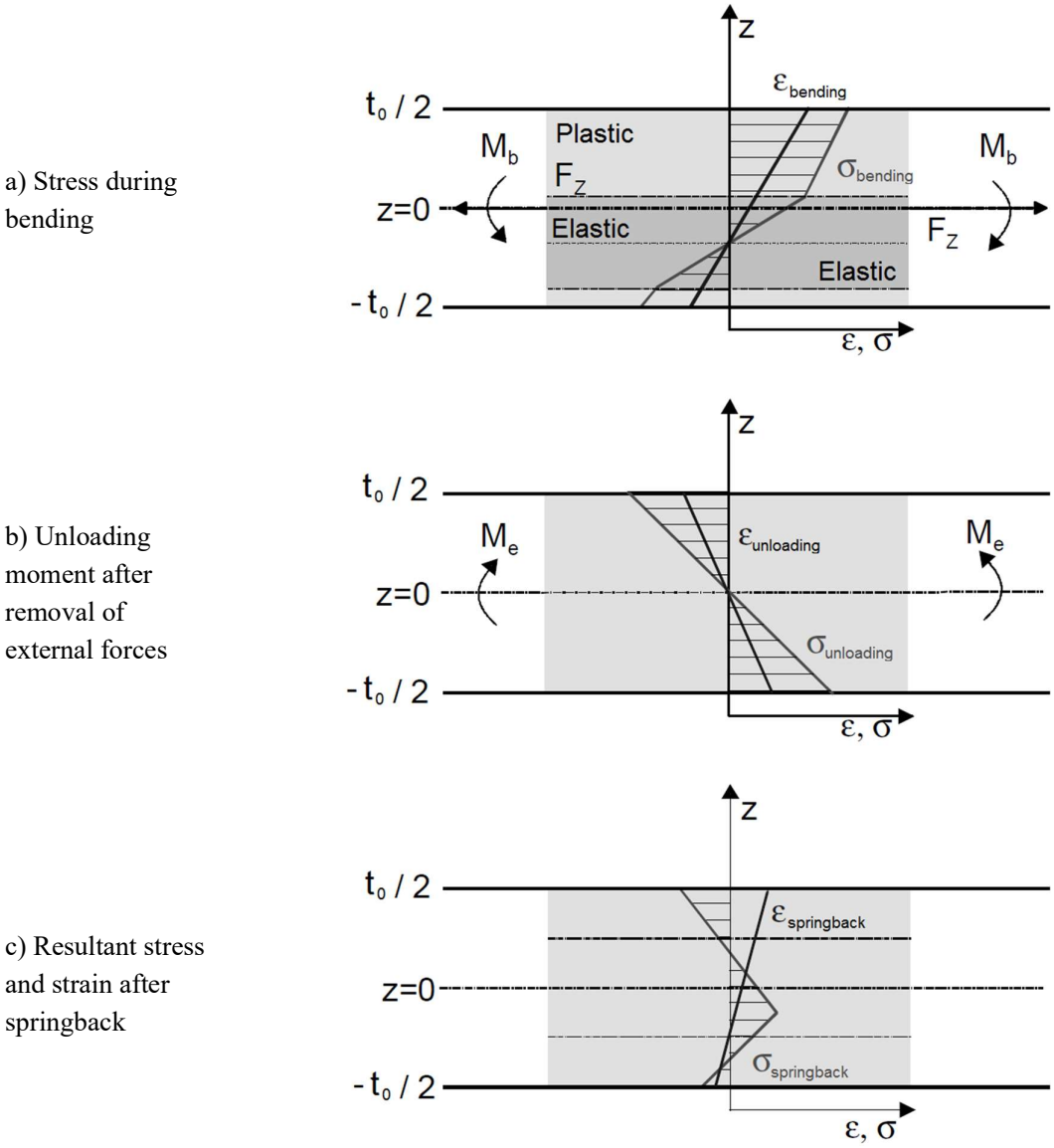

Figure 15 Stress and strain distributions before and after springback in a sheet metal [35]

2.4.3 Major influential input parameters

This chapter is a summary of a research made to identify the factors which influence springback on a greater scale. It has been studied according to the input parameters of the sheet blanks and of the press.

Characteristics of the sheet blank

As stated by Marciniak et al. [33], thickness of the blank and the mechanical strength are the two main characteristics of the blank that affected the springback in ideal situations. In real sheet metal forming

these two factors heavily influence the springback. A study by Albut [36] determined that the decrease of sheet thickness leads to a greater springback effect.

In term of the effect of the mechanical strength, Doege et al. [10] studied three different steel grades, including one AHSS grade (TRIP 700), after hat-shaped bending. The blanks all had identical shape and thickness (1.46 mm ± 0.02 mm) and the same press input parameters were introduced. However, their values of the tensile strength changed. In increasing order of tensile strength values, H340LA was the softest, while TRIP700 was the strongest. The study came to the conclusion that the greater the UTS, the more springback it presented. This was due to the higher concentration of residual strength in the parts with higher UTS. Figure 16 shows the change in springback behaviour of hat-shaped parts with different tensile strengths.

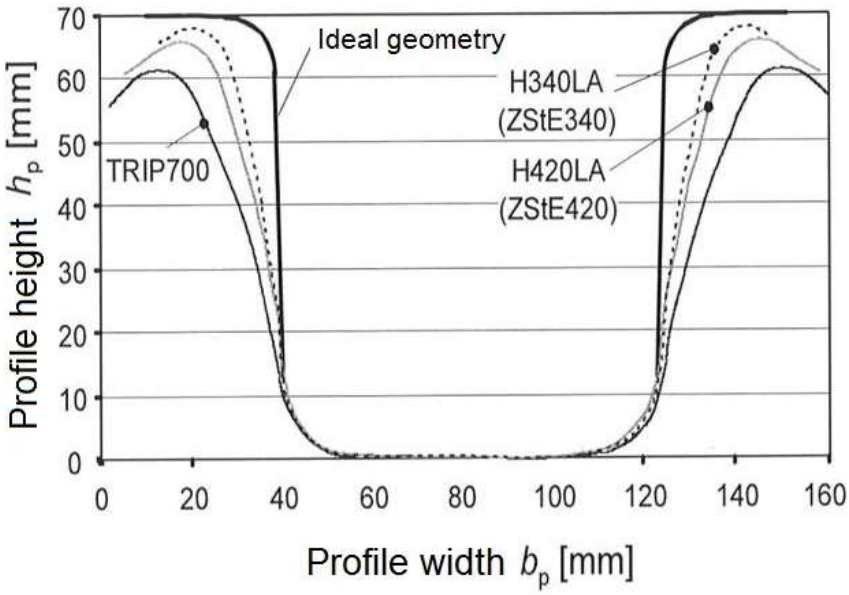

Figure 16 Springback in hat-shaped bending of AHSS [10]

Blank holder force

The final springback result change with every variation to the selected input parameters. A study by Woellner et al. [37] on stamping of AHSS on 1.5 mm thickness shows that the blank holder force has a direct influence on the springback. Having conducted a simulation they concluded that an initial high BHF, as well as a progressively high BHF, improved the issue of springback; especially with those materials with a high tensile strength.

Friction coefficient

The amount of springback is also dependent on the friction coefficient between the blank and the forming die. If more friction is present while forming, there will be less springback, according to Srinivasan et al. [38]. Their study specified that the lubricant viscosity influences the friction, thus it affects directly to the springback. They concluded that, the more viscous the lubricant, the bigger appearance of springback.

Rolling direction

When a sheet blank is produced, the material goes under several rolling mills. As a result of this, distinguishable linear marks all along the blank can be observed and are known as the rolling direction. These lines are important at the time the blank is placed in the forming tools. A study by Albut et al. [39] concluded that, after simulating the behaviour of two mild steels with tensile strengths of 381 MPa and 458 MPa, setting the rolling direction perpendicularly to the deformation of the bends can reduce the springback by about 6.5 %. According to the study, this reduction value increases with bigger tensile strengths, as mentioned previously.

Design of the tool

The tool used to give the final shape to the part determines the final springback due to its geometry. Chikalthankar et al. [40] listed the major variable parameters on the punches used in pure sheet metal bending. For example, they determine that using tools with a smaller punch angle will lead to higher springback deformation of the blank. The punch radius, punch height and opening of the die are other factors listed in this study.

Reducing springback is dependent on having control over these important factors. However higher costs due to longer production times may occur if these actions are implemented without proper guidance. To this end, there are several studies available which will be used as a basis for this work.

2.4.4 Methods for springback prediction and evaluation

Several numerical calculations and guidelines can be used to measure springback with the main purpose being to provide, given different parameters, an estimation of the behaviour of springback. While some of those behavioral approximations are possible via the implementation of modern software solutions, only simple numerical approaches will be addressed in this work. Many of these approaches are a result of independent studies, which will be referred to in the first place. Secondly, those evaluation approaches given by certified organizations of standards will be explained.

Analytical calculation

The springback can be measured analytically according to different approaches. The most common approach is related to the over-bending of the sheet, which causes a bending angle, θ_i, and a final bent angle, θ_f, as seen in figure 10. One calculation for this approach has been given in equation, which allows the obtainment of the difference between angles after springback. For this end, the initial angle, the flow stress to Young´s Modulus ratio, the curvature and the thickness of the blank are needed.

In addition, the springback factor of a material, K_s, can be calculated. According to Sachs et al. [41], this parameter is the result of the ratio between the final and the initial angles, and it is given by equation.

$$K_s = \frac{\theta_f}{\theta_i} = \frac{(2r_i / t) + 1}{(2r_f / t) + 1} \tag{22}$$

This calculation also takes into consideration the curvature radii generated in the over-bending, r_i and r_f, which can also be observed in figure 10.

Moreover, one final approach estimates the ratio between the initial and final radii. For this consideration, Oehler et al. [11] analysed the bending process as a purely elastic, with the assumption that when $r_i > 2t$, the applied bending moments generate a plane deformation, as shown in equation:

$$\frac{r_i}{r_f} = 1 + 4\left[\frac{r_i R_e}{Et}\right]^3 - 3\left[\frac{r_i R_e}{Et}\right] \tag{23}$$

By using this approach, the final radius after springback, r_f, can be released and calculated. The radius of initial over-bending is needed, as well as properties of the blank and the materials, such as the blank thickness, t, the Young´s modulus, E, and the yield strength, R_e.

2.4.5 Methods for reduced springback

Various strategies can aid in reducing springback after forming. Some of these involve geometrical methods, such as incorporating stiffening features into the part shape, as well as modifying addendum and binder surfaces. [3] [42]Another approach involves altering the stress-strain conditions in the part. This can be achieved through methods such as applying additional restraining forces or implementing adjustable and controllable blank holding forces that vary over time in relation to punch travel, thereby facilitating forming with alternating blank drawing. [3] [5] [42]

Kuriyama introduces four possible processes to form a hat profile with reduced springback: e.g. form-draw process [43]. World auto steel shows advances in die process concepts such as programmable blankholder and drawbeads integrated in upper binder or active draw beads [44]. S. Sadagopan et al. [45] explains the influence of tool radii, tool gap and drawbead restraining force on springback. M. Linnepe et al. [46] present a patented smartform process from company Thyssenkrupp. In this publication they focus on the smallest possible size of forming blanks with no flange. Thyssenkrupp explains that technology allows UHSS to be processed by cold forming in a dimensionally stable way with almost no springback [47]. Löbbe et al. [48] introduce the heat-assisted sheet forming for a better control of springback. In the Nippon steel technical report, Yoshida et al. [49] show a basic concept of countermeasures against springback, such as crash forming tension control or emboss/bead. Löbbe et al. [50] [51] explain a new process of controlled springback in bending. Temperature measurements are carried out using thermal cameras to calibrate the process. The tool rapidly cools the heated sheet and brings it into the desired position. Siswanto et al. [52] show potential of using a variable blank holder force, where the springback error can be decreased and the dimensional deviation falls in the predefined tolerance range. Ulibarri et al. [53] explain a reduction of the Young modulus with the increment of the strain and ductility of Inconel 718. They use an intermediate heat treatment process. Cui et al. [54] introduce electromagnetic forming as a high-speed forming (300mm/s) method that can deform a workpiece through magnetic force using the electromagnetic induction theorem and can reduce springback. Pepelnjak et al. [55] [56] explain the deep drawing process with local heating at the flange region of a DP600 steel sheet to increase the drawing limit and as an effect to reduce springback. Lim [57] presents the control of material-flow using an adjustable blank holder force enhancing part quality and consistency in stamping. Lawanwong et al. [58] present a novel technology called double-action bending (DAB) in order to eliminate springback in hat shape forming of AHSS. Woellner et al. [59] conclude that the use of a higher blank holder force on the final half process step could reduce the springback. Maeno et al. [60] demonstrate a temperature control

of hot deep drawing with focus on contact/no-contact in the flange gap. Jia et al. [61] discuss about the post-stretching in forming process by stake bead application. They minimize springback but cause severely unacceptable sidewall curl. Zhou and Kannan [62] present the effect on springback from combining draw and stake beads together, in a controlled hybrid bead, to effectuate a post-stretching process in U shape parts. Springback control and material restricting effect were observed. [63] Konieczny [64] explains how implementing side ribs on material DP800 can reduce springback. Fekete [65] shows a 10% reduction of springback even at DP980 strength level through beads in the wall. Mihail et al. [66] introduce the solution for GM Chevy B-Pillar inner part. They stamp the part several times and finally restrike the die with draft angle in order to reduce springback. Mousavi and Brosius [67] show that springback behavior of sheet metal parts can be reduced by increasing the peak-to-valley height difference during a lubricant free forming process with macrostructured tools. In contrast, Park et al. [68] explain a bottoming approach to reduce springback.

2.5 Induction heating

Numerous industries use induction heating with a wide range of applications. It is commonly used in the casting industry to melt large metal blocks. An induction coil, a flux concentrator, a phase advancing/resonance capacitor, a step-down transformer and switched power electronics are necessary parts for setting up an induction heating system. These will each be individually discussed in detail, following a theoretical background. [16] [69]

2.5.1 Theoretical background

The application of an alternating current creates a magnetic field. Placing an object which can conduct electricity, inside or near the coil causes eddy currents to affect said object (Faraday´s law) and heat will be the byproduct of the Joule effect. This, elementary electromagnetic phenomenon behind induction heating is given in Figure 17. [16]

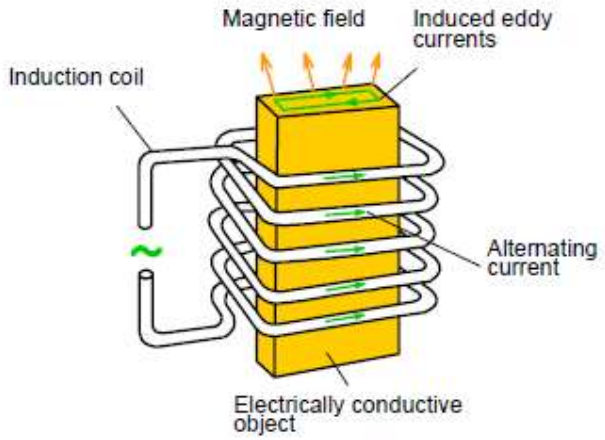

Figure 17 Magnetic fields of currents [16]

The rate of heating is contingent upon several factors, including the introduced current, its frequency and intensity, and material properties such as specific heat, magnetic permeability, and electrical resistivity. Electrical resistivity denotes a material's capacity to impede the conduction of an electric current and is inversely related to electrical conductivity. Additionally, electrical resistivity fluctuates with temperature. In the case of pure metals, resistivity can often be approximated using a linear expression [16]

$$\rho(T) = \rho_0\big(1 + \alpha(T - T_0)\big) \tag{24}$$

where $\rho(T)$ is the resistivity at temperature T, ρ_0 is the resistivity at the temperature T_0 and α is the temperature coefficient.

Comparing the electrical resistance material properties of aluminum to that of steel determines that steel, with its higher electrical resistivity will require less heating time in an induction heater than aluminum. Furthermore, the increasing temperature of a steel part in the induction oven does have the effect of increasing its electrical resistance, which in turn assists in increasing the effectiveness of induction heating. Likewise, the magnetic permeability of a metallic material (usually given relative to air, μr) will determine how easily an induction heater can generate an internal heating current in a metal part. It similarly has a temperature dependence that increases inductive heating efficiency with increasing temperature up to the Curie temperature, at which point ferromagnetic materials such as iron/steel lose their magnetic properties and hence inductive heating efficiency is reduced. The behavior of metals in an induction heater is strongly determined by a metal's ability to conduct magnetic flux. Paramagnetic metals ($\mu r > 1$) have a high magnetic permeability (especially ferromagnetic materials) when compared to diamagnetic materials ($\mu r < 1$), and typically have a magnetic permeability dependence on both temperature and applied magnetic field intensity. Figure 18 illustrates the relative magnetic permeability, μr, as a function of temperature and magnetic field intensity (H) for medium carbon steel. [69] [16]

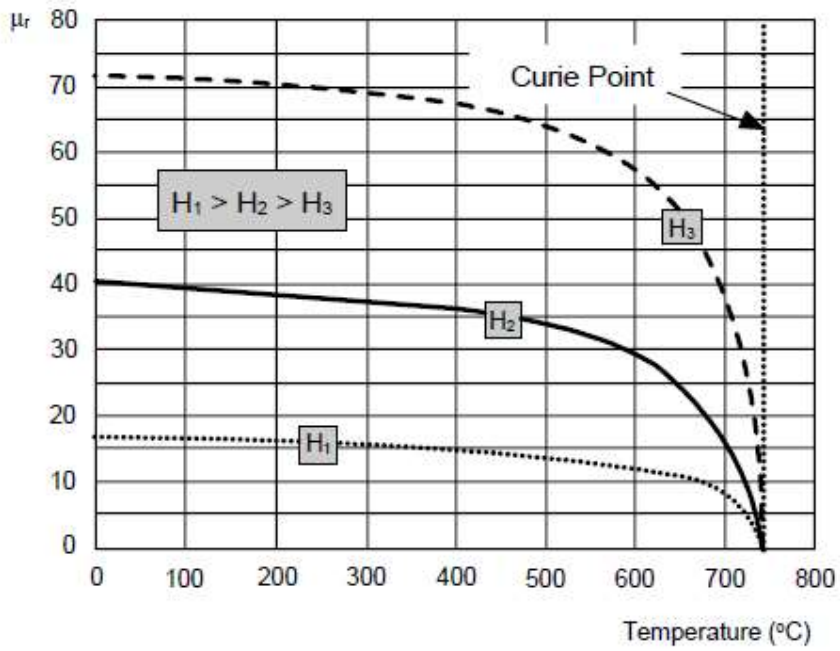

Figure 18 Effects of temperature and field intensity on relative permeability of medium carbon steel [69]

Induction heating efficiency is greatly enhanced in magnetic materials by the hysteresis effect produced by the alternating magnetic field of the induction coil heater. The friction generated by the time-lag of induced magnetic dipoles in the material switching orientation under the influence of the external alternating magnetic field (commonly known as hysteresis), produces heat. This heat is however generated mostly at the surface of a metal part due to the skin-effect confining most of the magnetically induced current to a thin surface layer of the metal. These surface eddy currents are heavily influenced by the magnetic permeability and electrical resistivity of the material, and by the frequency and strength of the externally applied magnetic field. All these factors contribute to the penetration depth at which the heating power is most efficiently transferred to the material. Various other electromagnetic phenomena, such as the proximity effect, can also affect heating power transfer. [69] [16]

2.5.2 Induction coil

Copper tubes, adapted to the specific processes, are typically used to make induction coils. The coil endures high temperatures not only because of the alternating current passing through the coil, but also from the resulting induced voltage due to the alternating magnetic field that tries to penetrate the coil. A cooling liquid is often used to flush the coil cavity. A newer approach to solve this problem is to use litz cables with air cooling, thus rendering liquid cooling unnecessary. [69] [16]

2.5.3 Flux concentrator

To maximize the permeation of magnetic flux to the entire metal workpiece, a flux concentrator, constructed from a high-permeability conductor, can be integrated into the forming tool. Ideally a flux concentrator will have a high magnetic permeability, a high saturation magnetization and a high electrical resistivity (in at least one direction). To achieve this flux concentrators are made from laminated structures, ferrites or soft-magnetic composites (such as isolated iron particles in a polymer matrix). For the warm forming process presented in this chapter, a soft-magnetic composite would satisfy the requirements. Permedyn, is an example material that would be suitable for machining into complex geometries to provide flux concentration, of three-dimensional magnetic fields, into complex geometry metal workpieces in a forming tool. [69] [16]

2.5.4 Induction heated tool for deep drawing

As detailed in the preceding chapter, an induction heating system is comprised of several components, namely: at its core is an induction coil and a magnetic flux conductor, ancillary to these is a phase advancing/resonance capacitor, a step-down transformer and switched power electronics. The induction coil and magnetic flux conductor are combined and fully integrated into the forming tool, whereas the capacitor and transformer are not. Since the blank must be heated in the radii regions the inductive heating unit can be either positioned in the blank holder or within the die itself. Figure 19 shows a tool setup where the induction heating unit is directly integrated into the blank holder. [16]

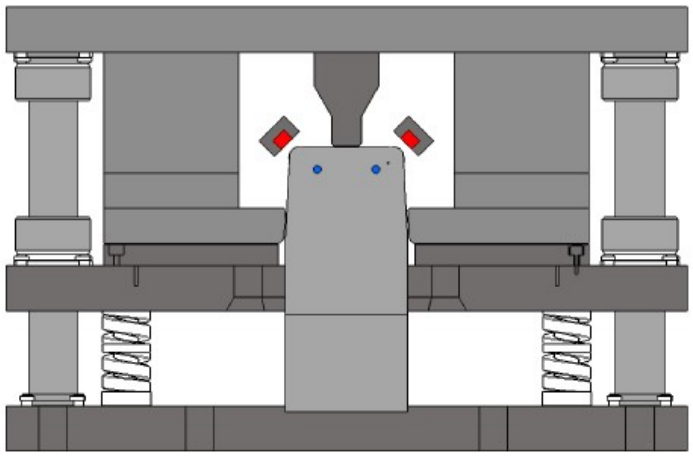

Figure 19 Schematic diagram of the induction heated tool for deep drawing

3 Aims and objectives

In accordance with the state of research and the test environment at the Institute of Material Science, Joining and Forming (IMAT), this thesis focuses on the development of a new method in sheet metal forming for springback compensation of AHSS. This work is based on deductive methods and the hypothesis as solution approach given is that in closed tools the stresses within the radius are at its highest, the heat influence gives a relaxation of stress via targeted heating. The part geometry is defined as a hat profile or U-profile, because here the springback effect is at its greatest.

Hypothesis: "A reduction of residual stresses can be achieved by annealing "

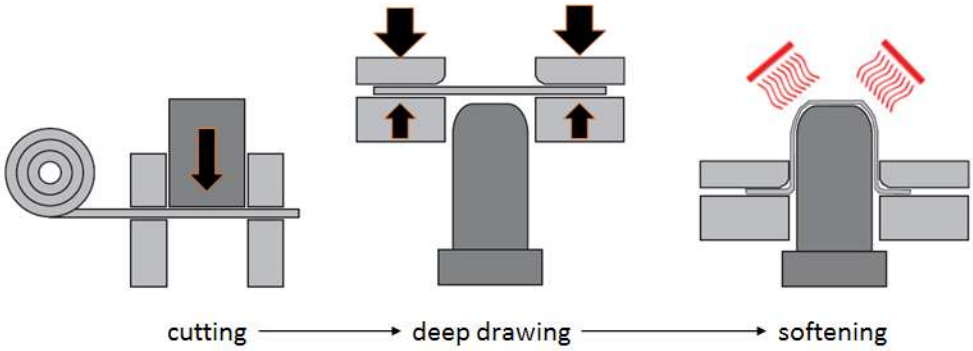

Figure 20 Short principle of local heated area in order to reduce springback

The main objectives of this study are:

- To determine the material properties of different AHS steels by using the experiment data from tensile test as well as metallographic examination.
- Development and the manufacturing of testing tool including induction heating facility
- Analyses the crucial heat treatment parameters using various measurement systems in dies
- To conduct FE simulation for this type of sheet forming

The scientific findings from this thesis should provide knowledge to support the implementation of this type of process in an industrial manufacturing process. This thesis was done in cooperation with Magna Cosma, Weikersdorf.

4 Experimental design

4.1 Material and conducted methods

Within this work, different AHSS materials were tested. In agreement with Magna Cosma as partner, the most used materials in the automotive industry from AHSS group were chosen.

At the very beginning of this study, to observe the influence of various process parameters on springback, the following materials were used:

- TRIP800
- DP1000
- CP-W 1200

The second phase included the effect of material structure from heating up to different peak temperatures. For this phase the following materials were used:

- DP1180HD
- TWIP980

The reason for choosing these materials is the expected change in microstructure at elevated temperatures.

The third phase before the actual tool construction was the influence of material softening within the radius. It was expected that the material would reduce strength when heated. For this purpose, a 3-point bending simulation was conducted. Due to the availability of material cards in the software, the following materials were used:

- DP1000
- DP600

In the experimental part, three materials were used, each of those steels are applied in the automotive industry. The materials were selected in three different strength categories, with the expectation that the influence of annealing on the microstructure of the chosen material and the amount of springback would be observed.

- HCT780X
- CR700Y980T
- CR900Y1180T

Due to the significant drawing depth of the tool of approximately 100mm, a side wall effect appeared. To compare the effect between softer and harder steels, a study was conducted between dual-phase and DC steels:

- DC04
- DP1000

For the first simulation done by PamStamp software, and in order to obtain a complete picture of the impact of heating on the material being processed, a material with a complete material data card was selected:

- 22MnB5

For the second simulation done in Abaqus, a material for cold forming with slight addition in the form of the dependence of the modulus of elasticity on temperature was used

- DP980

4.1.1 Impact of various factors

As explained in Chapter 2, various parameters affect the amount of springback occurrence. In order to determine the materials and the thickness of the material that will be used in this work, a small analysis was made with the already existing tools at the institute. Various tool shapes have been used such as the open U-shaped tool, the upper part of the B-Pillar and the tunnel geometry. The results in this chapter are the product of collaborative work on the master thesis by Mr. Santiago Rinon Arrese, titled "State-of-the-art Springback prediction during Cold Forming of AHSS parts in the Automotive Industry", conducted at the IMAT.

Measurements were made with the aid of the GOM measurement system. This allowed for fast dimensional inspection and produced accurate measurement data. The results from the 3D scanning process were fed into and evaluated by GOM Inspect V8 SR1 (a product of GOM Inspect Software ®). This software allowed for the quick and precise comparison of the measurements in order to formulate the ideal model to be used. The first model (measurement) was imported using the .G3D extension, whilst the second (CAD Modell/punch) used the .IGS format. In order to observe the influence of various parameters throughout the model, the current state forming was compared to punch geometry.

Three materials were evaluated during this study, TRIP800, DP1000 and CP-W 1200. The two variables employed were blankholder force and press force.

Figure 21 displays the influence of press force and blankholder force on the level of springback in the sheet. Naturally, the level of springback observed was greater in the stiffer materials. The RGB colors illustrate the amount of springback in the hat profile tests depending on material, blankholder force and press force.

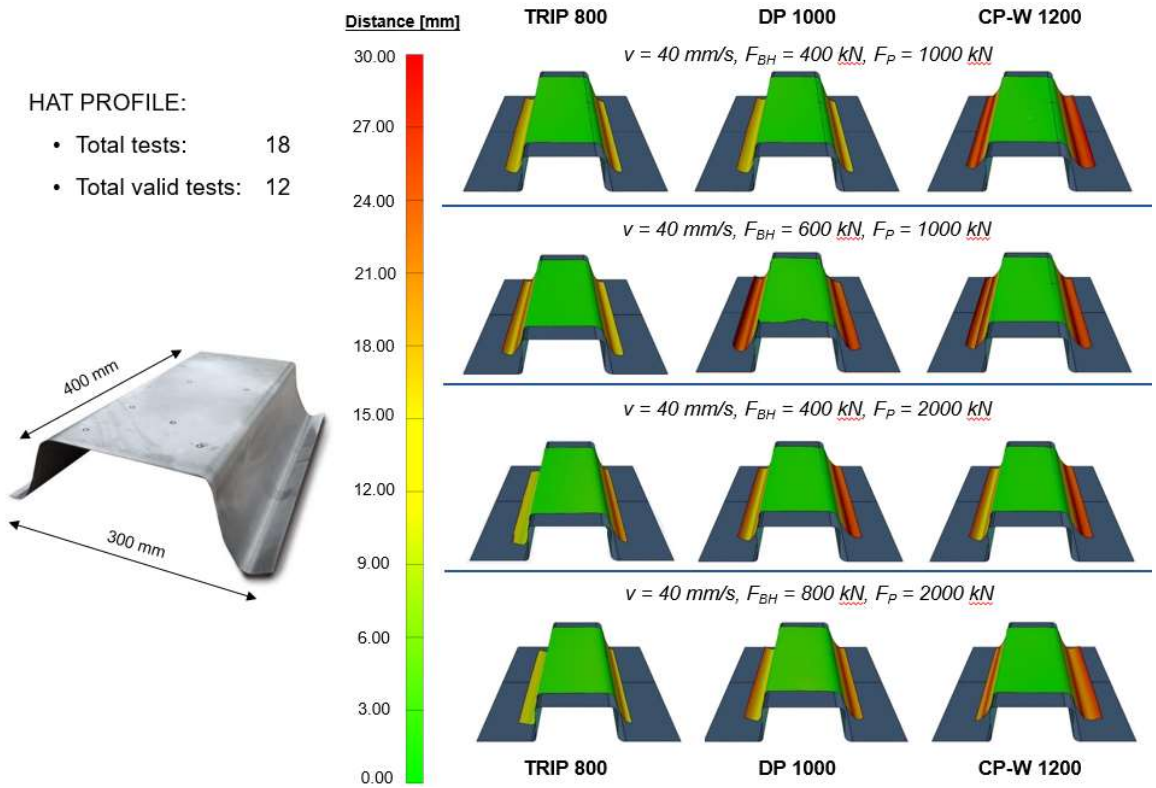

Figure 21 Comparison of different springback states with hat profile geometry

Of the three materials, TRIP 800 has a more defined pattern, when compared to the two other stronger materials. TRIP 800 clearly displays less springback as shown in Fig. 22. This result was true for the hat profile and B-pillar geometries. However, it can be observed, that uniformity of the springback values increases regarding higher press input parameters. The reasoning behind this, could be the strengthening of the material due to the transformation of retained austenite during forming.

Figure 22 is an interval plot, that allows for a more precise view of the influence of each variable on the springback amount in the material.

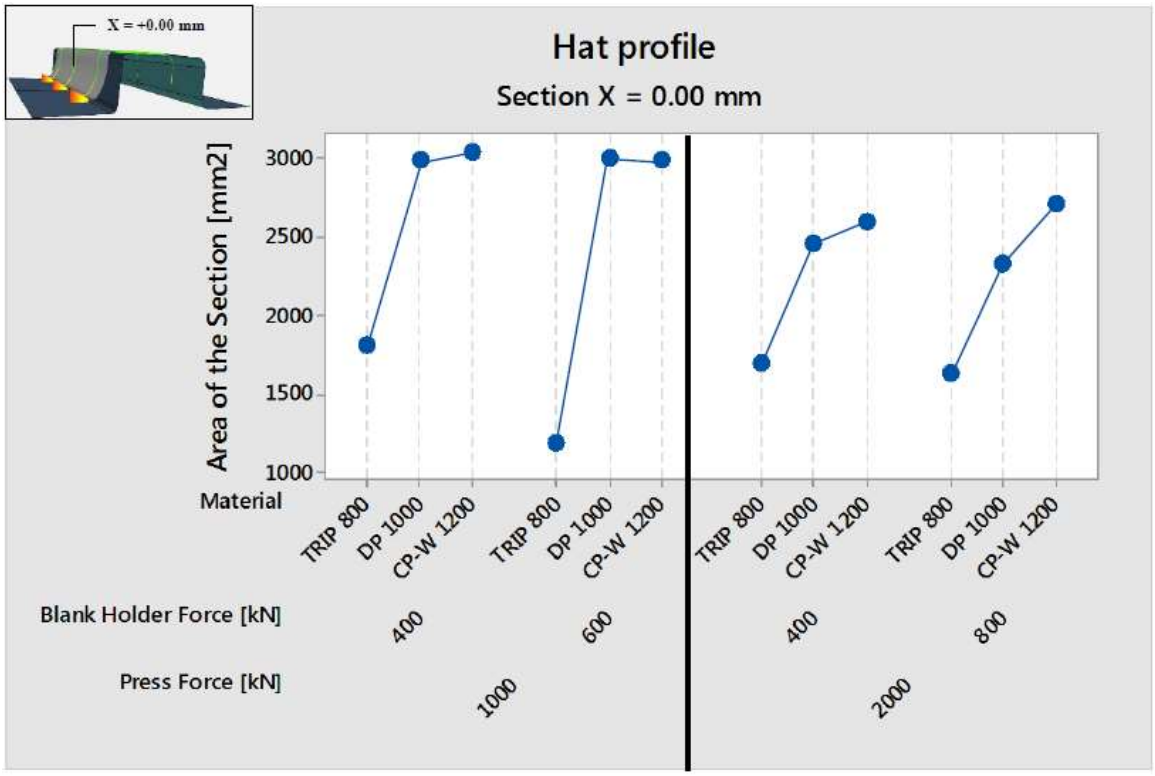

Figure 22 Interval plot of the hat profile, corresponding to the central section X=0 [70]

It should be noted that the interesting behavior concerning the appearance of springback was also seen in DP 1000 and CP-W 1200. These steels did not follow the predicted usual pattern of a decrease in springback after an increased level of press force is applied. This was especially true for the hat profile. For this profile it is suggested that CP-W 1200 has in fact a higher level of springback than the softer, but thinner steel. In addition, the B-pillar shows diverse behaviour of the steel depending on the section. The previous disparity from Fig. 22 was also accentuated when using the maximum press force but less so with regards to different blankholder forces.

Lastly, the factors that had the greatest impact on the level of springback are shown graphically with the aid of Pareto charts of standardized effects. This type of graph is probably the most relevant of all those available, since it shows clearly in decreasing order the relevance of each parameter, as well as the relevance of the combination of effects.

A reference line was designated as a confidence level of 95% in these graphics in order to allow potentially important effects to be observed. The reference line can be seen to have a far higher magnitude for the hat profile, when compared to the other two geometries. This is due to this geometry´s tendency to create springback.

Figure 23 displays the Pareto Charts of the hat profile with the relevance of all important parameter impact on springback.

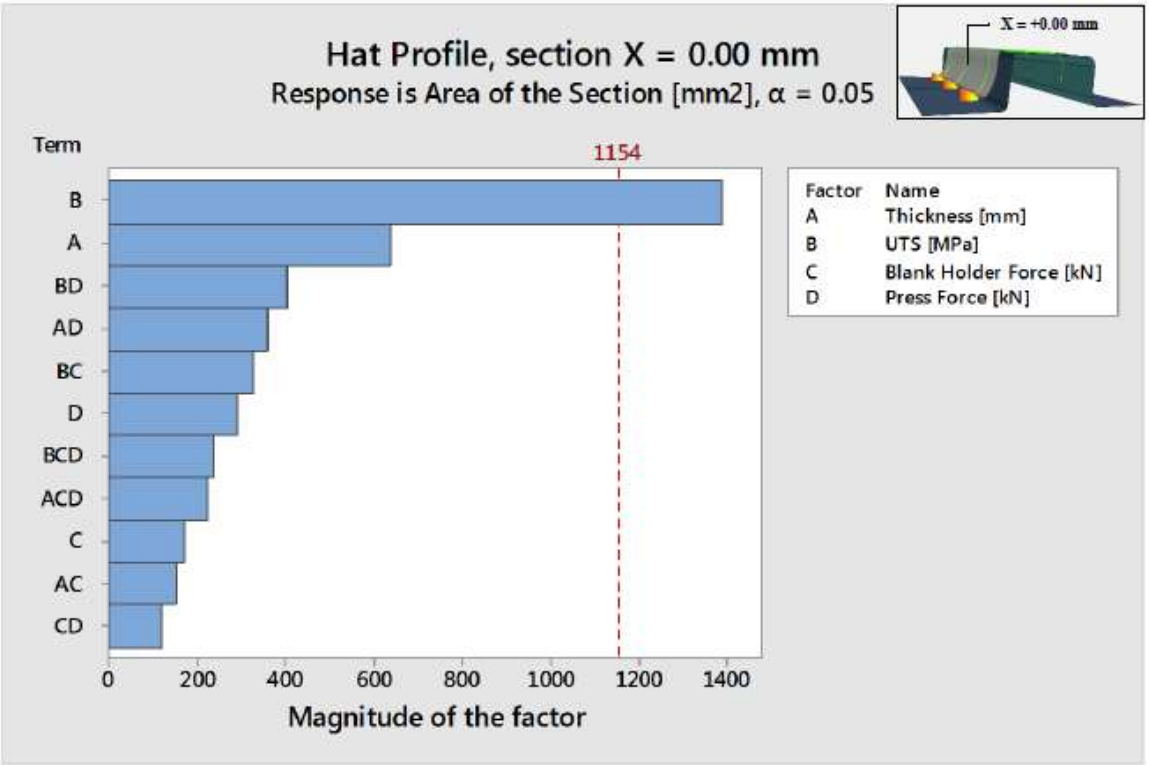

Figure 23 Pareto Chart of standardized effects for the hat profile, corresponding to the central section X=0 [70]

Fig. 24 shows the influence of the parameters on the springback of the B-pillar geometry. The amount of springback in a semi-closed profile is not as great as in an open one, so the focus for further investigation in this work is the open shape geometry such as hat profile.

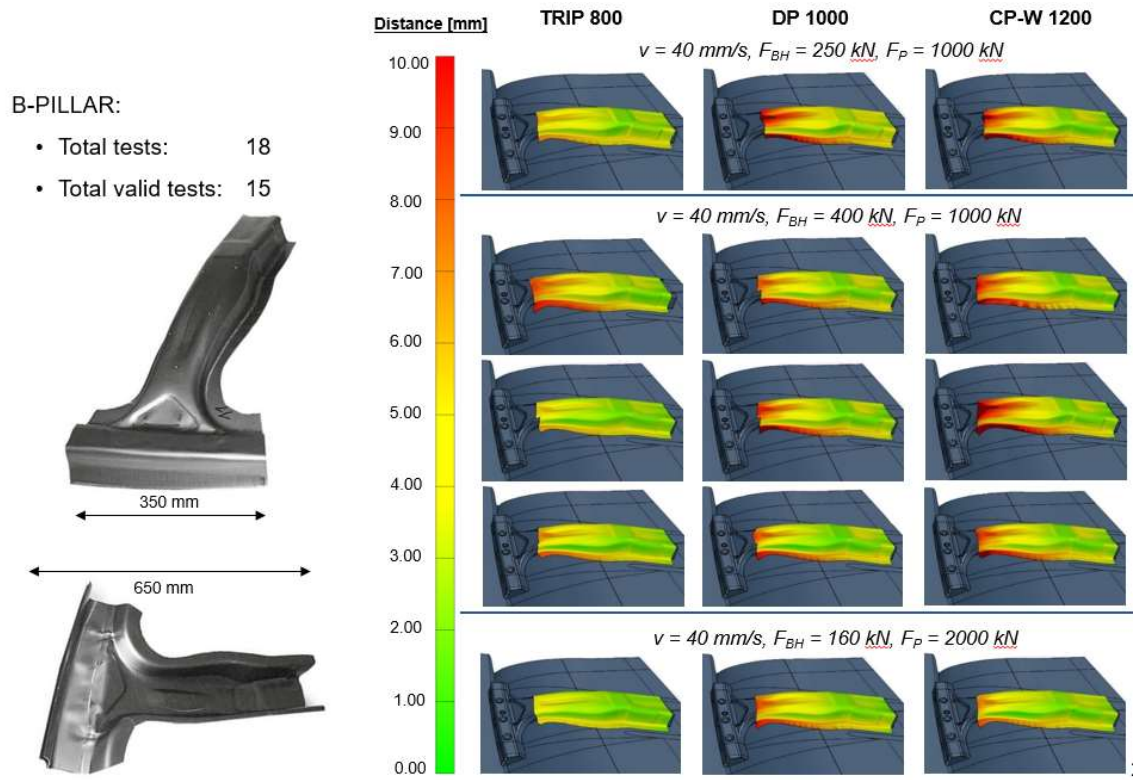

Figure 24 Comparison of different springback states with B-Pillar profile geometry

Figure 25 displays the Pareto Charts of the B-pillar profile with the relevance of all important parameter impacting to springback. It can be observed that the the biggest effect on springback reduction has the press force. Furthermore, it has been observed that the input parameters of the press have a reduced impact on open sections, with the primary influencing factors being the material properties. This is not ideal because in serial production, maintaining control over formability and ensuring the repeatability and validation of all parts is crucial. In situations involving constrained geometries, like the B-pillar, the extent of springback is primarily influenced by the press force. Likewise, increasing the blank holder force has been shown to have a meaningful but relatively less effect on reducing springback compared to the press force.

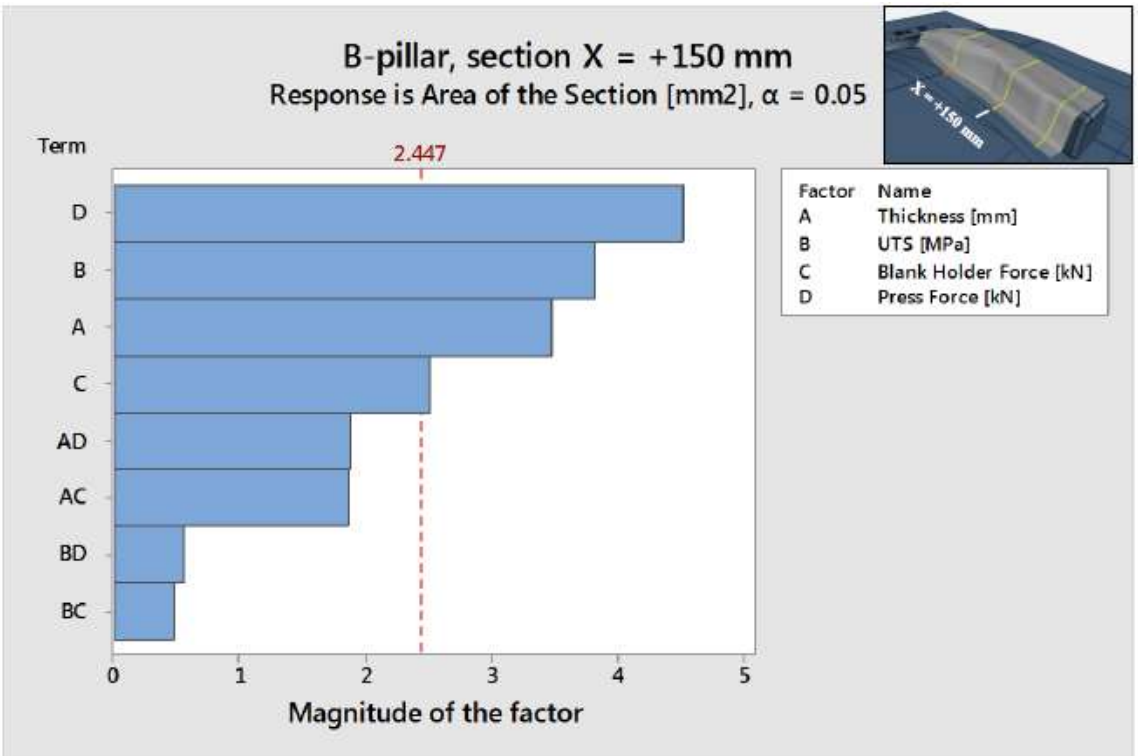

Figure 25 Pareto Chart of standardized effects for the B-Pillar profile, corresponding to the central section X=+150 [70]

To investigate ability to adapt the hat tool accepting different material thicknesses, a similar study was made where the forming parameters were the same, but the thickness was variable with 1mm and 1.6mm.

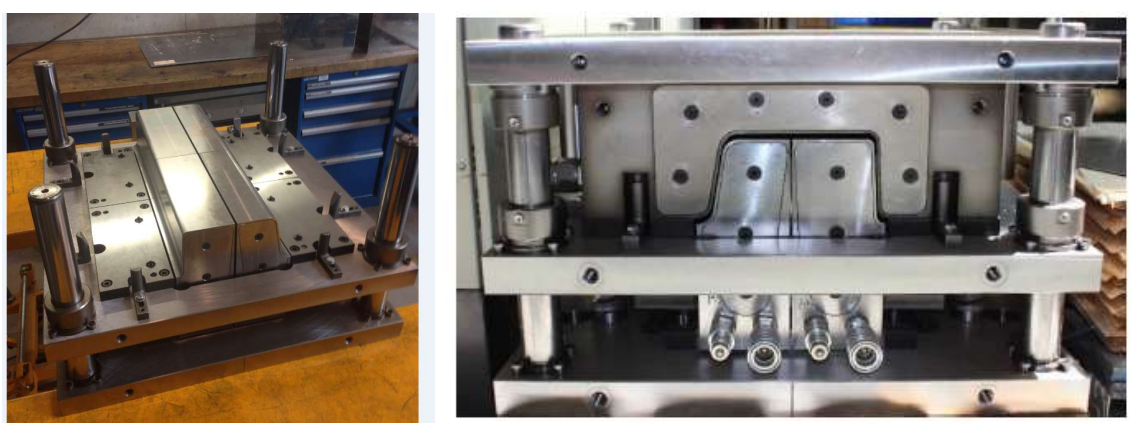

Figure 26 Hat profile tool from segments

Figure 27 shows the difference in the amount of springback with the same steel grade of different thickness. The thinner material exhibits a higher tendency for springback compared to the thicker material.

Figure 27 Springback - influence of material thickness at same steel grade

4.1.2 Investigated materials

In the early stages of the work, two AHSS steels were investigated. Firstly, DP1180HD – a Dual Phase steel and, secondly TWIP980, which is an austenitic high manganese Twinning Induced Plasticity steel. Both of these materials were cold rolled and displayed a uniform sheet thickness of 1.5mm.

In order to evaluate the mechanical properties of the above materials, tensile tests were carried out in accordance to DIN EN ISO 6892 in the rolling direction at room temperature.

The findings of these tests are listed in the following Table 3.

Table 3 Chemical composition (wt %) of the studied UHS steels used in the experiments.

	C	Mn	Si	P	S	Cr	Mo	Al	Ni	Cu	Nb	Fe
DP1180HD	0.21	2.88	0.8	0.006	0.007		<0.5			0.01	<0.02	Bal
TWIP980	0.67	16.56	0.13	0.011	<0.005		<0.2			0.03	<0.005	Bal

Table 4 Mechanical properties of the investigated UHS steels. [71]

Steel	Thickness t in mm	Yield Strength YS in MPa	Ultimate Tensile Strength UTS in MPa	Uniform Elongation U.E. in %	Total Elongation T.E. in %
DP1180HD	1.5	1077	1269	> 6	> 12
TWIP980	1.5	545	1067	> 60	> 60

It can observed at a macroscopic level that both steels exhibit different behaviors. This is due to the differences in characteristics they have in microstructure. DP1180HD has a ferrite matrix containing martensite, bainite, tempered martensite and also small amounts of retained austenite. On the other hand, TWIP980 is characterized by an austenitic microstructure. [71]

The microstructure of both materials when in delivery condition and without the being heat treated is shown in Figure 28 and their chemical compositions can be observed in Table 4.

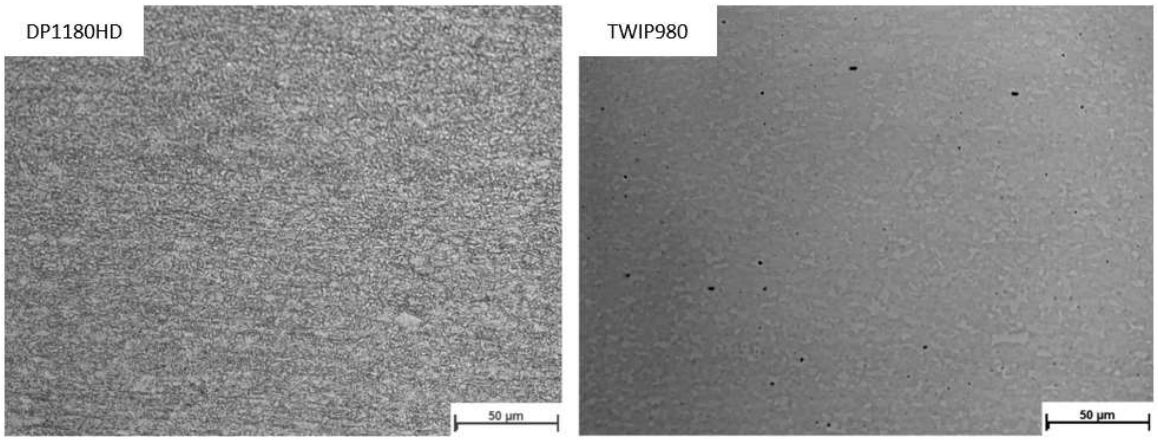

Figure 28 Light optical micrographs after etching in as rolled condition DP1180HD and TWIP980 [71]

4.1.3 Test facilities for material characterization

During the investigations performed within this thesis, TA Instrument´s DIL805T quenching dilatometer was employed. This measuring system was used as it comes with an adapter that allows for tensile tests to be performed on mini-flat samples. This, consequently, allows for the precise measurement of true stress and strain.

When in the quenching mode, the specimen is first heated using induction heating to the required temperature, and subsequently cooled at a rate defined by the user.

In this study, this measuring equipment was not only used to measure elongation of the specimen on elevated temperature, but also to gain better understanding of structure and hardness after heat treatment.

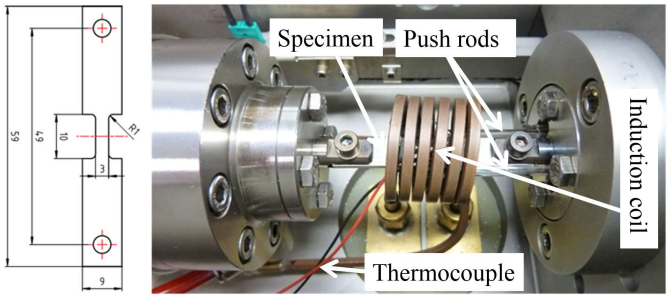

Figure 29 Dilatometer DIL805T, setup

Throughout the dilatometric experiments, a heating rate of 220 °C/s was used. As can be seen in Figure 30-a, the start and finishing temperature of DP1180HD for austenite formation was observed to be A1 = 755°C ± 2°C and A3 = 843°C ± 3°C, respectively for the highest annealing temperature of 900°C. The start temperature at which martensite formation began (Ms) was observed to be approximately 365°C. [71]

Figure 30-b displays the dilatometric curve of TWIP steel without a phase transformation at increased temperatures, normally expected in case of an austenitic steel. The sample expanded to 200 µm. [71]

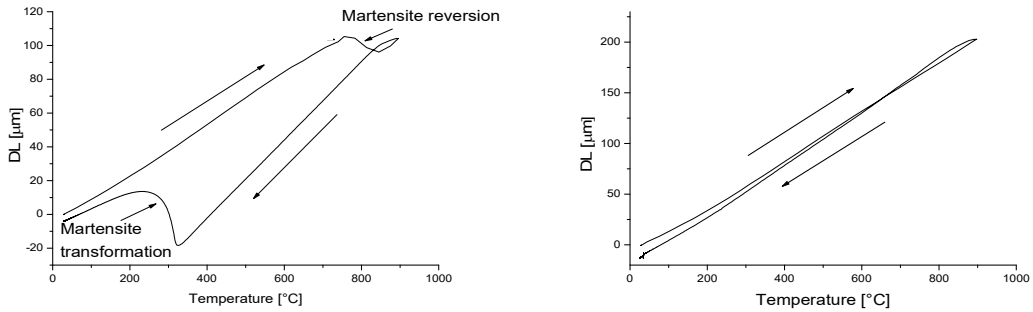

Figure 30 Dilatometric curves of heating and cooling a) DP1180HD and b) TWIP980 with the peak temperature of 900°C [71]

4.1.4 Pre-tests with induction

A testing system with a 10kHz and a 100kHz inverter, with a rated power of 120kW and 160kW respectively, is available for use at The Institute of Material Science, Joining and Forming. During bending experiments with a local induction procedure, the face inductor was employed. To demonstrate a potential for springback reduction during hybrid deep drawing, the preliminary trials were carried out in a simplified process. The samples were bent in a simple tool, both with and without heating in the area of the radii. [71]

Figure 31-a) shows the trial setup employed with the induction heater. In the case of heat treatment, the samples were air cooled to room temperature. Following both procedures, the bending angles were measured, compared and analyzed. To allow an accurate analysis of this procedure, it was essential that the temperature was exactly recorded throughout the whole heat treatment. In order to do this, a hole with a diameter of 0.55mm and a side depth of approximately 30 mm was made into the sheet. A sheathed thermocouple with a diameter of 0.5mm and a maximum sampling rate of 7 Hz, was used to measure the heat inside the blank. The heat trace from this was measured during both the heat and cooling phases. An induction power level of 40% was employed in order to heat the sheet at a rate of 50°C/s to the desired temperature of 900°C. Due to the slower rate of cooling in air, in comparison to quenching, the material did not fully transform to martensite, as observed during dilatometric testing. [71]

As demonstrated in Figure 31-b), the largest potential for springback reduction was observed in DP1180HD. In this case, a 16-degree reduction was achieved. Figure 33 shows the hardness of the DP steel, that reached a level between 310HV10 and 345HV10 after the induction heat treatment, followed by air cooling. The difference in material hardness compared to the reference was 80HV10. Due to the contact between the part and the forming tool during the combination deep drawing and heating in the same process, the cooling rate would be increased and therefore a higher strength would be achieved. In the case of the TWIP steel, no significant reduction in springback was observed during these trials, as presented in Figure 31-c). [71]

Outcomes from the feasibility study: [71]

- New process approaches are regarded essential to optimize the forming process of AHSS in terms of minimizing springback
- The local heat treatment in forming dies with the objective of relieving residual stress, changing the microstructure and reducing therefore springback, can be successfully performed through induction heating
- The heat treatment process i.e., the heating rate, annealing temperature and the cooling rate has a significant impact on the hardness values in case of DP steel, due to it reaching different martensite contents
- DP steel, in comparison with TWIP steel, demonstrated more potential for the hybrid deep drawing process in order to reduce springback. The reason for this effect is the change in the microstructure of the material and its strengthening

During the second phase of pre trials, indirect heating in the bending area by means of an inductive alternating field and a laser process are employed. Through partial heating, a localized reduction in material strength can be achieved. The results are quantified to see whether this process has an impact on the material behavior. The variation of temperature in the forming area, implemented by localized heating of individual tool ranges between room temperature and Ac1. This should shorten the feasibility phase and thus minimize the cost for further development in this work.

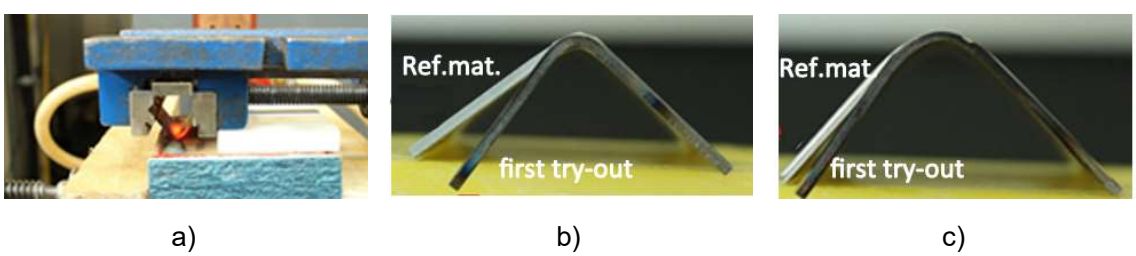

Figure 31 Bending with and without local heat treatment a) Induction heaters, b) DP1180HD and c) TWIP980 [71]

Figure 32 present the positions of hardness measurements. Measurements at points 1 and 2 were taken to determine the reference hardness of the tested material, while positions 3, 4, and 5 indicate the material strength affected by annealing.

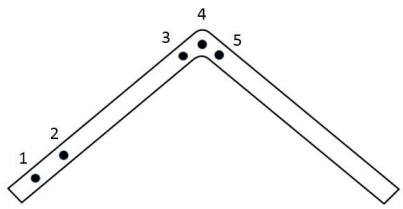

Figure 32 Representation of hardness measurement points

Figure 33 displays the hardness values for both materials used in this study. In the figure, a decrease in the hardness of the DP material in the heating zone can be observed. The reason for this is the slow air cooling. If the process that would be later used in industry, the material cooling would be significantly faster due to the contact between the sheet and the tool.

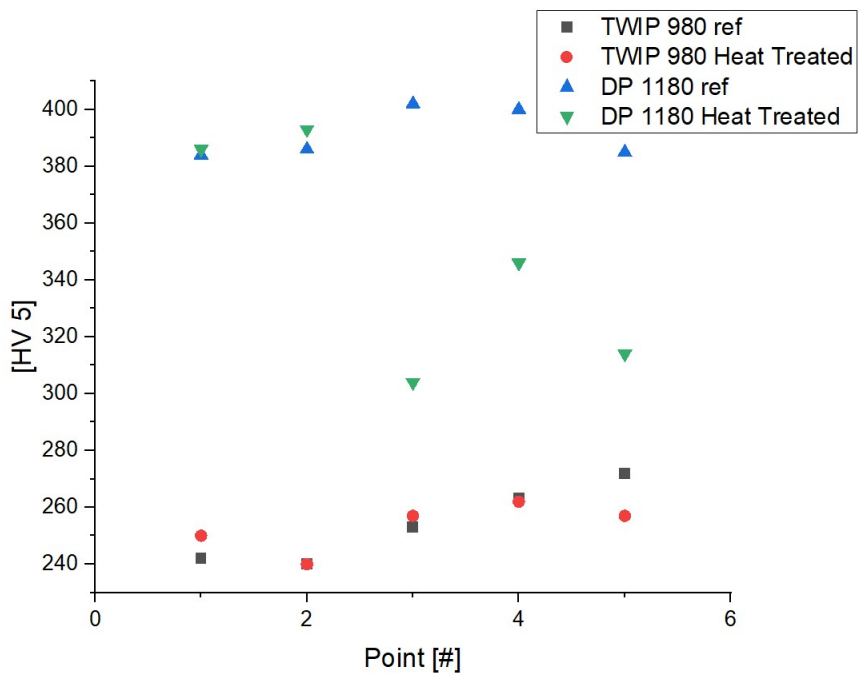

Figure 33 Hardness measurement of two steel grades after induction heating [71]

4.1.5 Softening

Figure 34 shows the microstructures of DP steel at different peak temperatures. It can be observed that the material exhibits a complex phase composition at each peak temperature. Different levels of ferrite, martensite, bainite and residual austenite are present in the microstructure at lower peak temperatures.

Austenitization of the steel occurs at between 700°C and 900°C. This leads to further changes within the microstructure and thus the strength of the steel. At the peak temperature of 900°C, the steel becomes fully austenized and of high cooling rates a martensitic microstructure is formed.

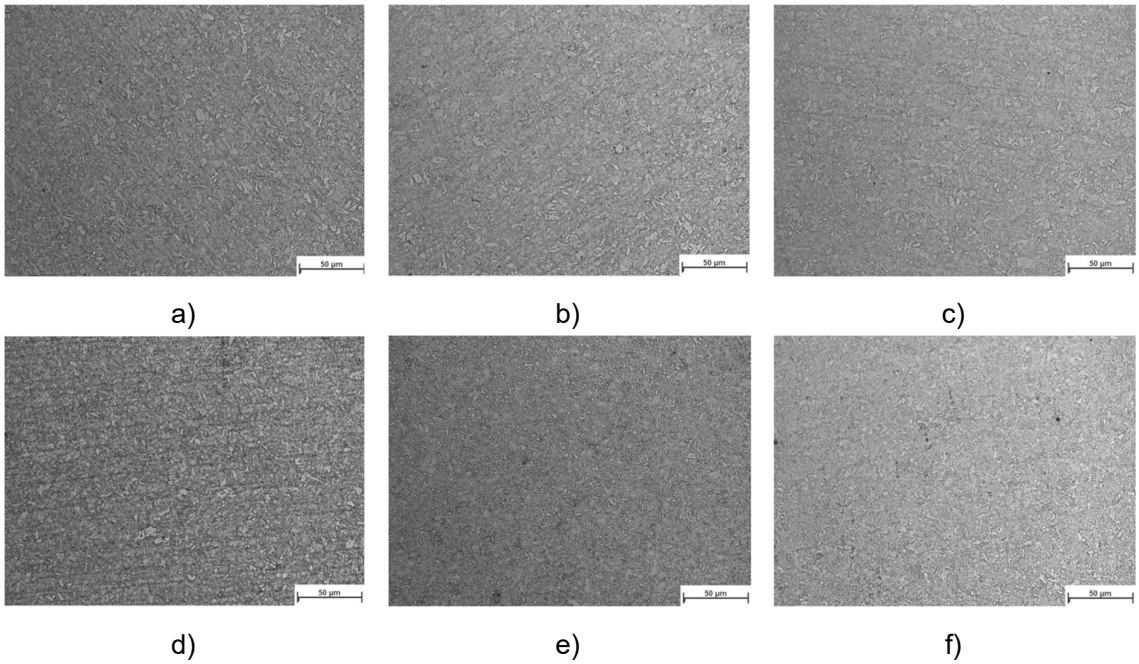

Figure 34 Microstructures of the heat treated DP1180HD samples at various peak temperatures at a) 400°C, b) 500°C, c) 600°C, d) 700°C, e) 800°C and f) 900°C [71]

Following the heat treatment, reaching various peak temperatures, it can be observed that TWIP steel always exhibits an austenitic microstructure, as seen in Figure 35. When not deformed, no changes in the microstructure of TWIP steel were seen when viewed with a light optical microscope. The grain size increased with increasing annealing temperature. [71]

Shown in Figure 36 are the measured hardness of UHS steels after undergoing induction post heating with various peak temperatures (measurement at room temperature is also shown). Comparison of DP1180HD to 385HV10 steels at temperatures below 400°C show a similar hardness, however above a 400°C peak temperature the hardness drops from 385 HV10 to circa 295 HV10 at a heat treatment temperature at 700°C. This decrease is due to annealing of the steel microstructure in this temperature range. A maximum of 518 HV10 was achieved for DP1180HD by heating to a peak temperature of 900°C. The transformation of the metal microstructure into martensite is responsible for this hardness increase. [71]

In a rolled condition the hardness of TWIP980 mas measured as 255 HV10. Upon heating and cooling a small 5% change was observed when compared to the reference material, as shown in Figure 36. [71]

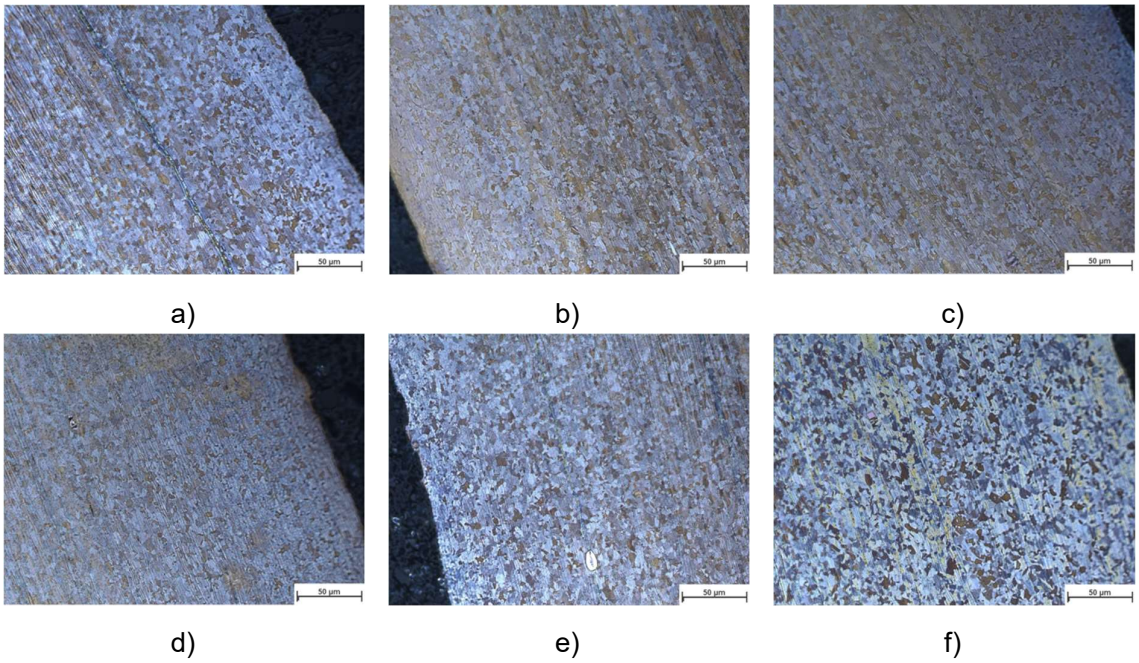

Figure 35 Microstructures of the heat treated TWIP980 samples at various peak temperatures at a) 400°C b) 500°C c) 600°C d) 700°C e) 800°C f) 900°C [71]

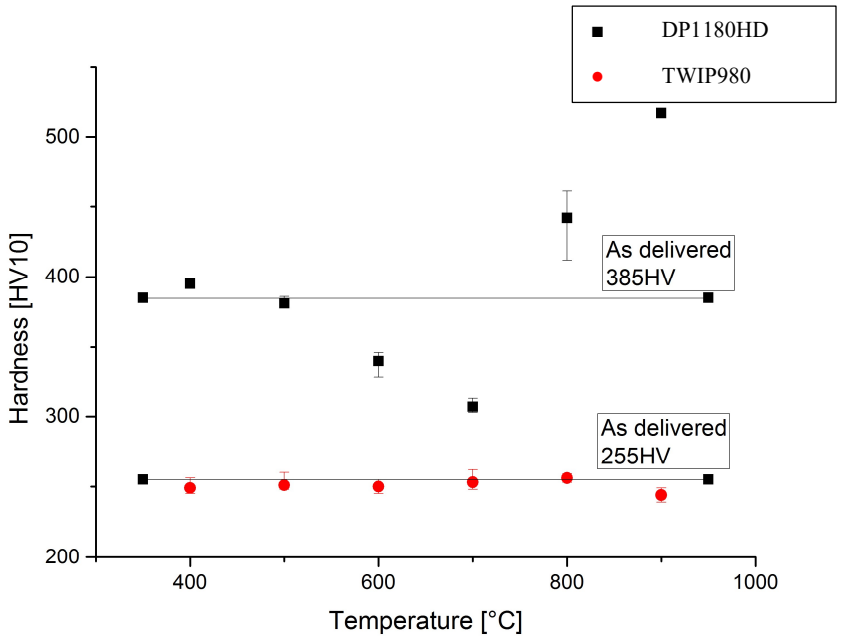

Figure 36 Hardness profile of DP1180HD and TWIP980 across the sheet thickness at various peak temperatures [71]

4.2 Deep drawing tool

In order to obtain a suitable image of the properties of the test material, the construction of a test rig at the IMAT is implemented. As explained in Chapter 4, the biggest influence on the springback, in addition to the strength and the thickness of the material is the radius of the punch and the drawing depth.

Therefore, a rough simulation was conducted to define the shape of the punch. The final part geometry is shown in Fig. 37 with radii of 8 mm and a drawing depth of 100 mm.

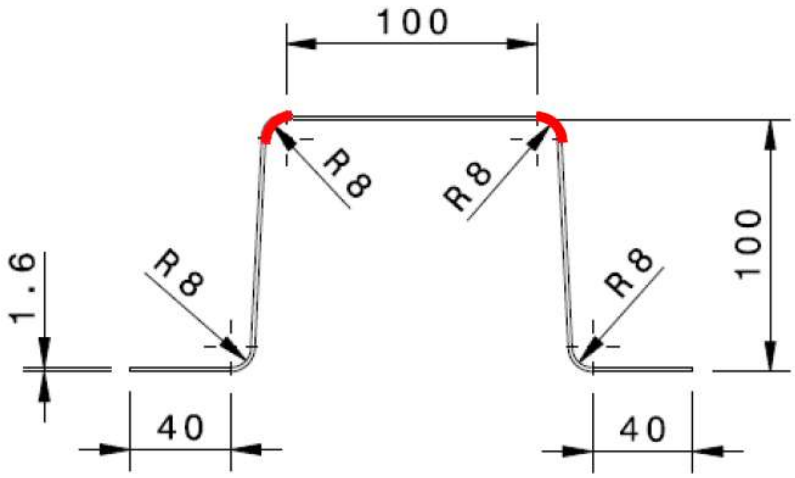

Figure 37 Hat profile dimension for a tool

Fig. 38 shows the main components, such as: central plate, base plates (upper and lower), guiding pillars, inductor (placed near the punch's drawing edges), drawing punch, clamping bar, blankholder and drawing die. A water filled cooling channel, parallel to the drawing edge, is used to prevent excess local heating of the punch. A Schuler 400-tons hydraulic press table is used to fix the lower base plate with the drawing punch and blankholder. The drawing die, fixed to the upper base plate, is attached to the ram of the press. [72]

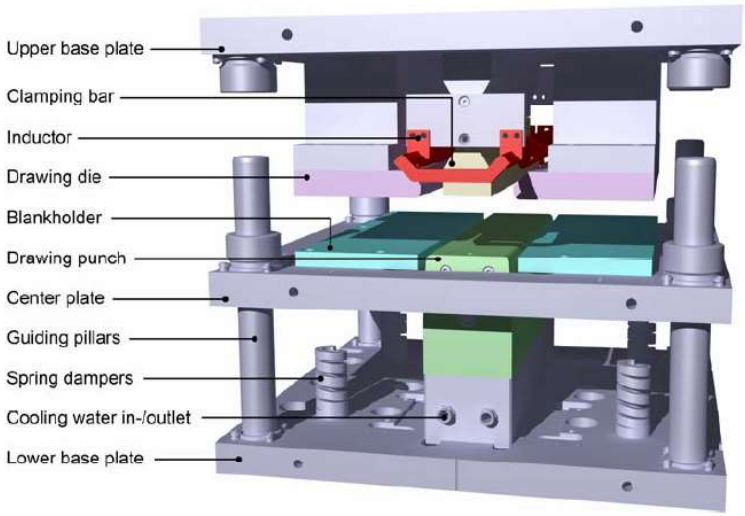

Figure 38 Main components of the hybrid forming-heating tool [72]

Figure 39 is a schematic illustration of the hybrid forming heating process. It functions as follows:

a) The hydraulic press ram downward movement creates a predefined cushion force between the drawing die and the blankholder, where the blank is clamped.

b) The blank is then drawn over the fixed punch via the ram's downward movement to the lower end-position.

c) Now fixed at the lower end position, the now formed blank is locally heated to a predefined peak temperature using the inductor. The formed blank is kept in position until subsequent cooling is completed.

d) The finished formed blank is released once the ram and die move to the upper end position after forming and heating is complete.

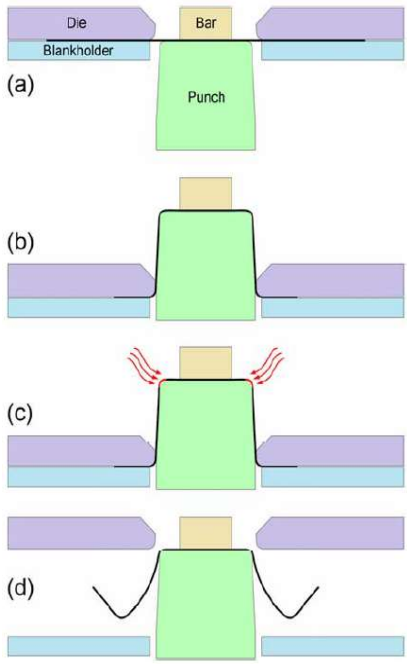

Figure 39 Schematic illustration of the hybrid forming-heating process [72]

For a better observation of the temperature propagation different types of measurement systems were installed. For the measurement of the tool temperature, ten thermocouples were used and for the part temperature pyrometer. Figure 40

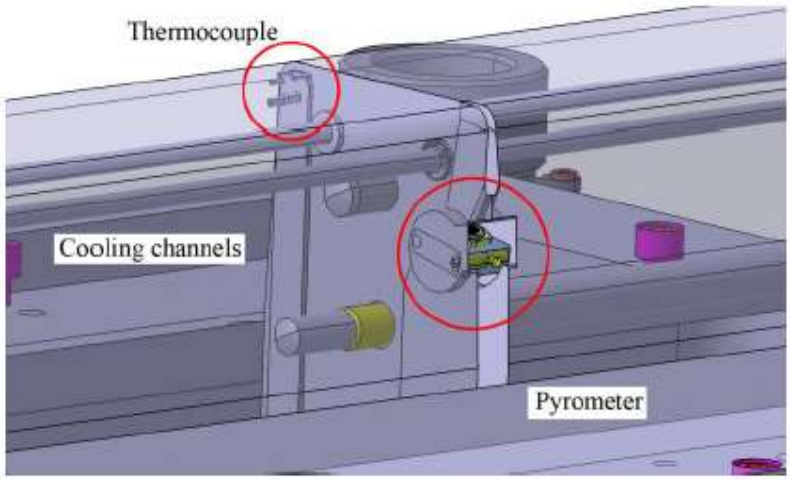

Figure 40 Measurement system integrated in testing tool

Firstly, it was observed how quickly the temperature of the material increased using three different power settings, respectively 30%, 40% and 50% (Fig 41). Since the key temperatures investigated were 500 and 900C, the decision was made that a setting of 50% would produce too steep a rise in temperature, thus making the resulting measurements inaccurate. Likewise, 30% brought on too slow an increase in temperature that would not be efficient if implemented on an industrial level. Therefore, it was decided that 40% would provide the ideal medium between accurate measurements and future compatibility in laboratory investigation.

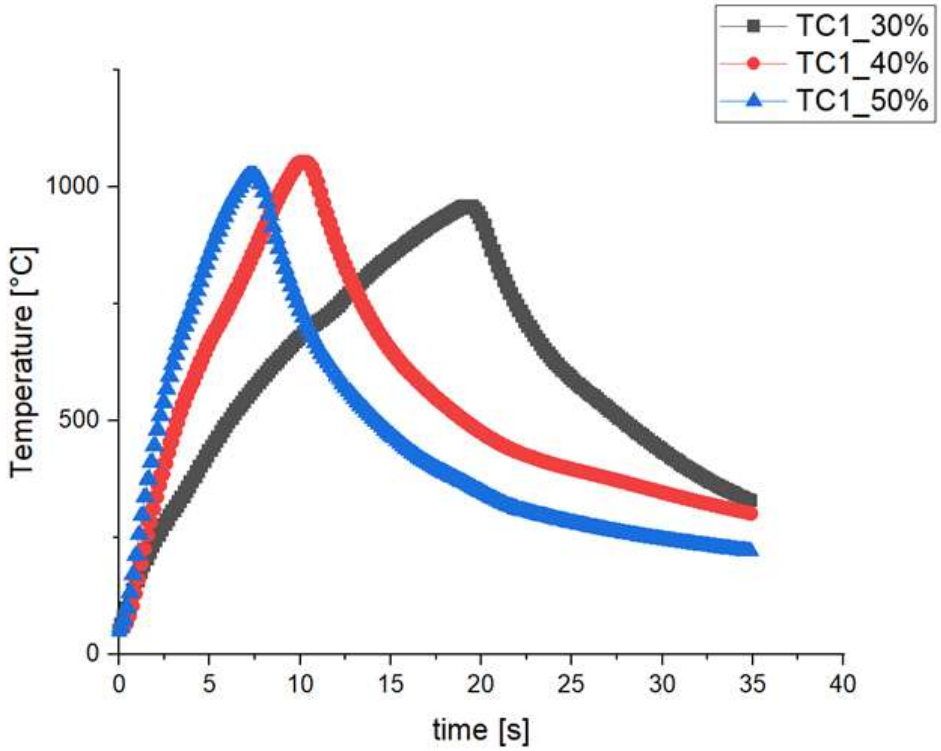

Figure 41 Impact of different electric power settings on heating speed

Figure 42 shows the increase in temperature within the tool as well as on the sheet itself. The induction parameter that was selected for measurement was a power setting of 40%. Within 9 seconds, the warmest measuring thermocouple (TC1) recorded a peak temperature of 220 degrees Celsius. In comparison, the lowest measuring thermocouple (TC10) registered 80 degrees Celsius. The pyrometer has a measuring range of 350-1200, and has measured a peak temperature in this setup of 920°C.

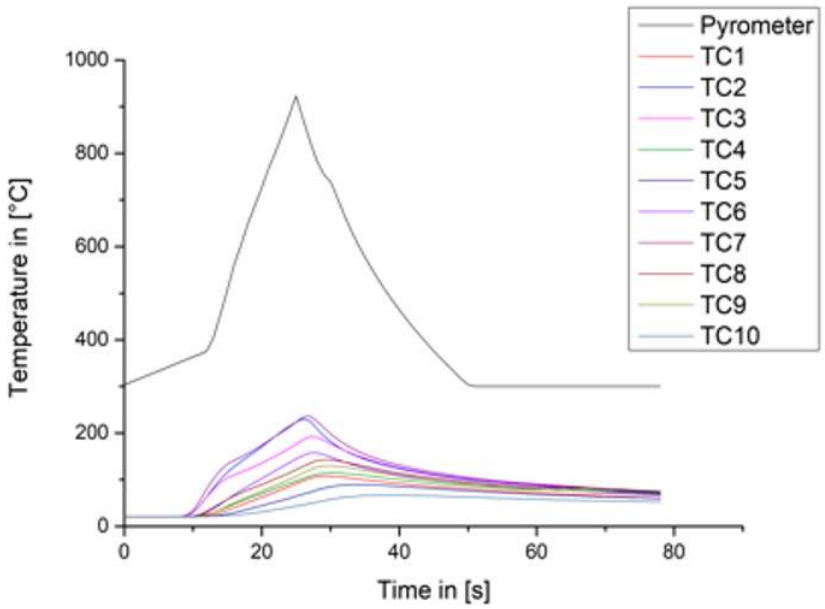

Figure 42 Temperature measurement within the tool as well as on the sheet

Figure 43 shows the temperature distribution throughout the radius of the tool in the process of heating the blank to a temperature of 900°C. At its highest point, the temperature of the upper section of the tool reached approximately 220°C. This demonstrates the necessity of implementing a water-cooling system within the tool to eliminate a gradual overheating through repeated use.

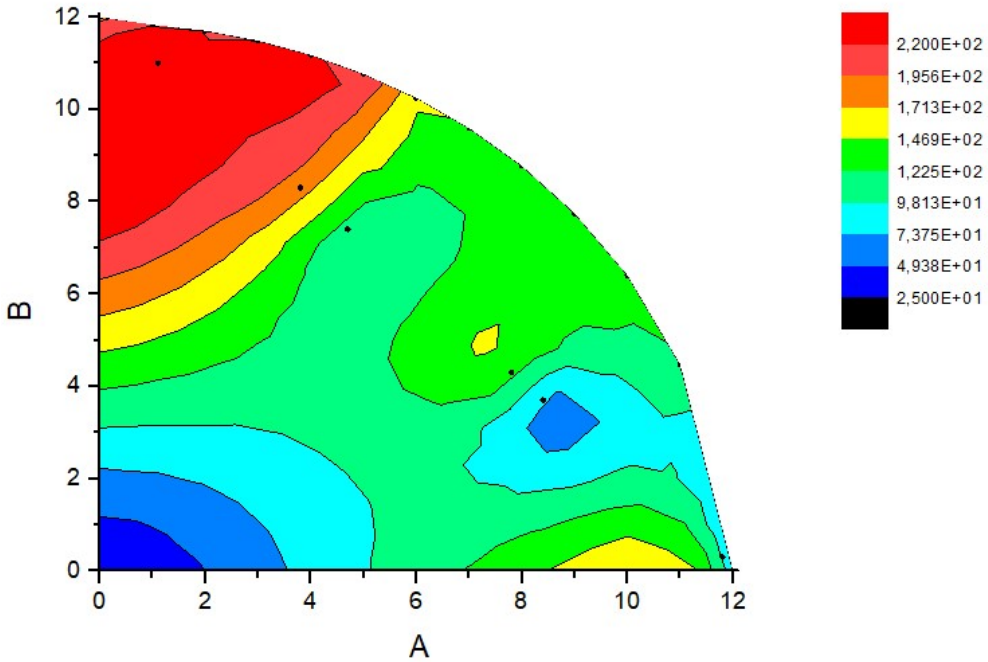

Figure 43 Temperature distribution throughout the radius of the tool

After finishing and assembly of both the tool and induction coils, a check was performed to ensure uniform part heating. For this purpose, 6 thermocouples were welded onto a preformed sheet within the radius (Figure 44), the tool was closed, and heating was initiated.

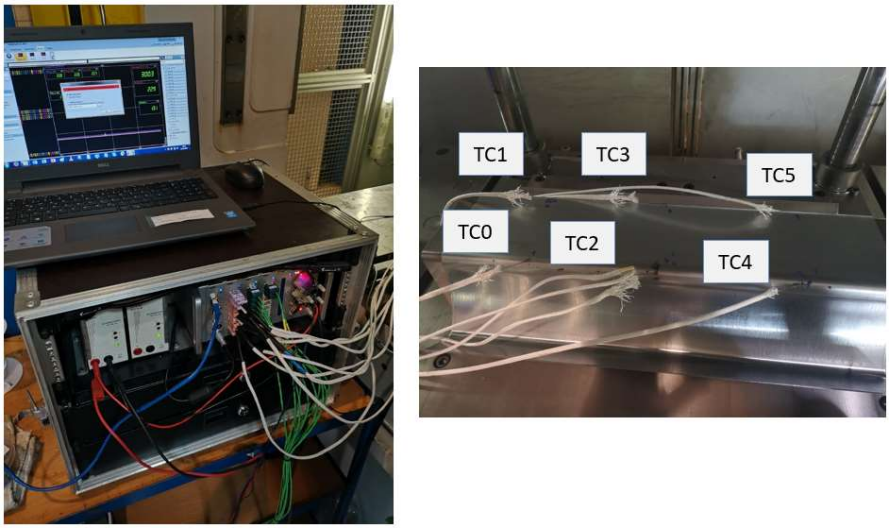

Figure 44 Temperature measurement setup using Dewesoft and thermocouples

In cases where there are significant differences in distance between the induction coil and the heated part, a slower or faster heating may occur. The graph shows a difference of 200°C peak temperature between those 6 thermocouples. To reduce this difference, it was necessary to implement components like ceramic spacers in the tool, which ensure a consistent distance from the coil to the part.

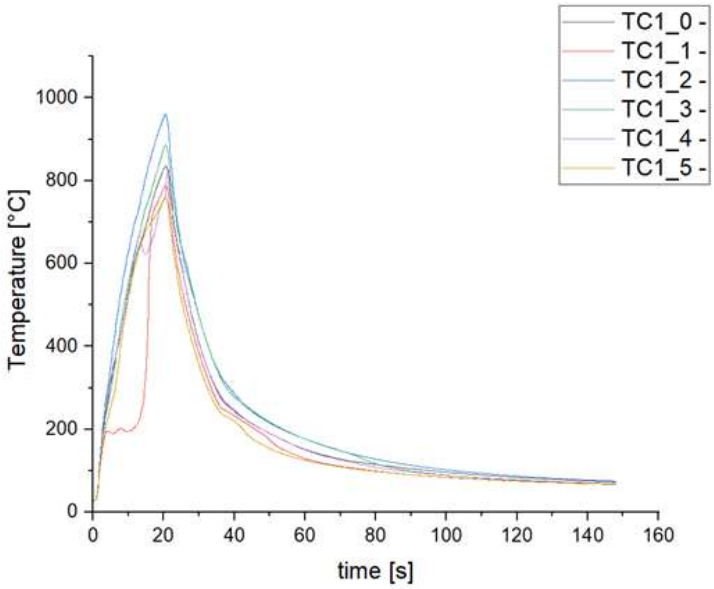

Figure 45 Influence of coil to workpiece air gap on temperature propagation

4.2.1 First simulation of three-point bending part to define test rig geometry

In brief, the design development of the geometry was aided by a feasibility analysis by using FEM software HyperCrash, in order to define the heating area. The material data of DP steels for the conducted simulation was taken from the HyperCrash material library.

The assumption was that material strength in the heating area would decrease by 40%.

A so-called Bumper beam crash simulation was carried out to compare a different deformation, stress, and energy absorbing capacity of various setups. For a crash analysis shell and brick elements were used for the modelling of solid parts (8 node hexa). The mesh preparation and modification were carried out by Altair HyperMesh Software and RADIOSS solver.

Figure 46 presents two different simulations: crash simulation of monolithic DP1000 material on the left-hand side and on the right-hand side the combination of DP1000 and DP600 in the area of the radii.

The difference in energy between the two models is 3% at 10mm of punch affecting.

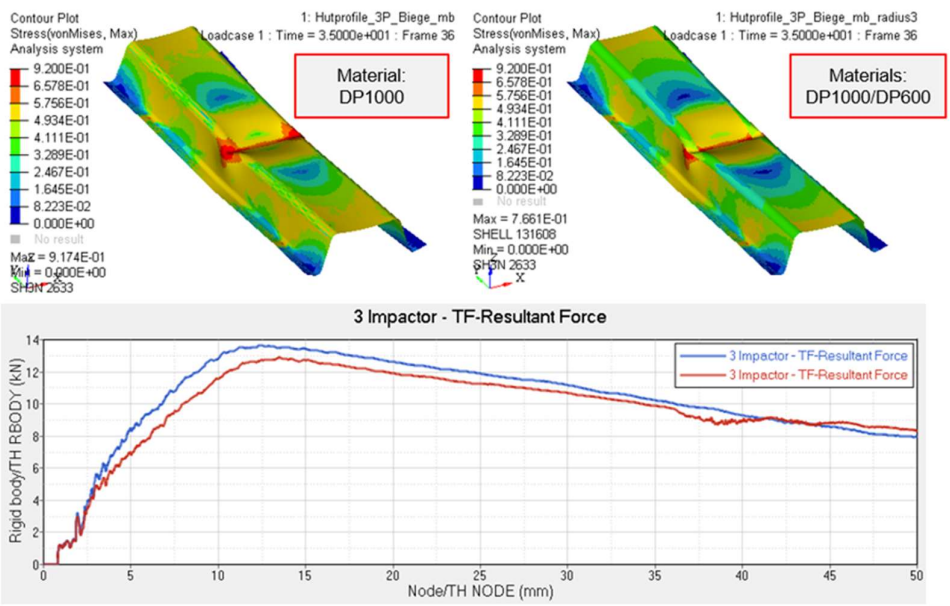

Figure 46 Crash analysis of hat profile for local heated part

Figure 47 schematically represents the difference in heat distribution within a material when using either an inductor or a magnetic flux concentrator. In this investigation, a Magnetic Flux Concentrator was implemented to heat the sheet. Due to the so called “slot” effect, it provides a low reluctance path for the magnetic field and also compacts the inductor current to the surface of the concentrator. This results in a less superficial and more exact heating of sheet upon the tool. Figure 47 displays the positioning of the magnetic flux concentrators in regard to the sheet. This positioning allows for localized heating of the radii of the sheet without affecting the rest of the material.

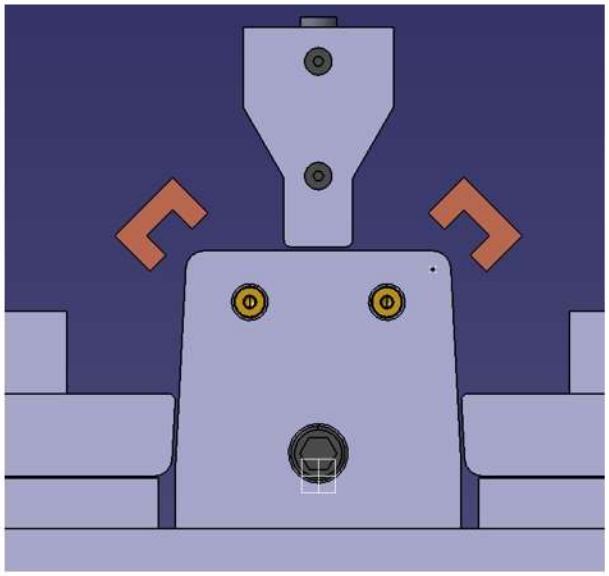

Figure 47 Positioning of the flux concentrators with regard to the sheet

4.3 Test trials

To prove the feasibility of the presented hybrid concept for reducing springback at semi-industrial scale, a test trials was done at IMAT. Figure 48 shows a process flow to valued concept and hypothesis.

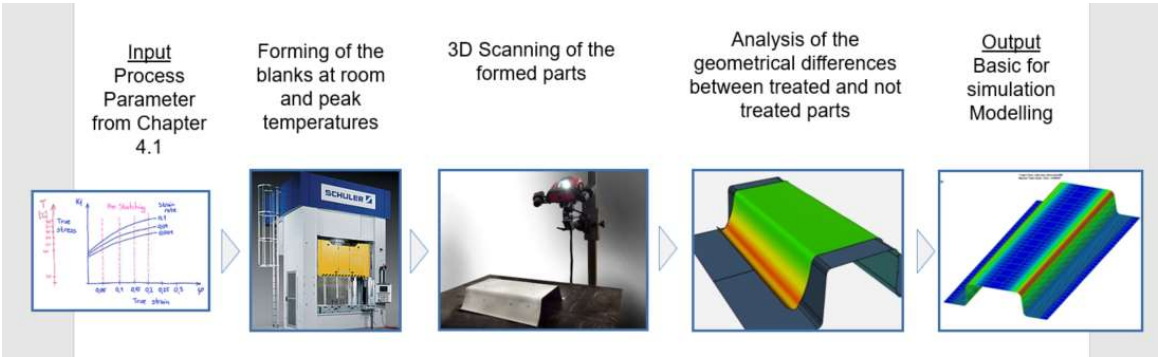

Figure 48 Process flow for test trials

Galvanized dual phase steel (DP) sheets CR700Y980T-DP (YS 700-850 MPa, UTS 980-1130 MPa) with dimensions of L 500 mm, W 400 mm, T 1.6 mm were employed to form U-profiles, following the process conditions displayed in table 5. 0.4ml of Wisura FMO 5010 forming oil was applied to both sides of the blank to aid lubrication. [72]

Table 5 Process conditions for first tryouts

Drawing speed	80 mm/s
Drawing depth (ideal height of U-profile)	100 mm
Blankholder force	300 kN
Peak temperatures for inductive heating	525 °C / 925 °C
Heating time	2.5 s / 5.5 s
Cooling time	12.5 s / 9.5 s
Total heat treatment time (heating and cooling)	15 s

Local inductive heating of the blank's radii zones was conducted immediately following the forming step. Peak temperatures were varied by varying the time duration of inductive heating: 525°C corresponds to 2.5 seconds of heating time, whereas 925°C was achieved after 5.5 seconds of heating time. Natural air convection was used for final cooling of the formed part. In total 15 seconds were used to form and release the part. [72]

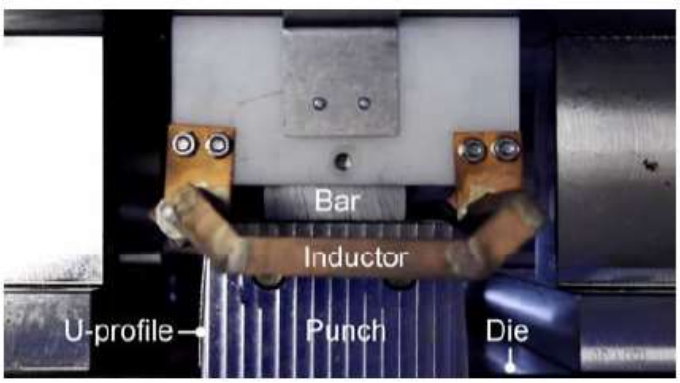

Figure 49 Inductive heating of the radius zones of the U-profile

A GOM ATOS III Triple Scan measurement system was used to capture the geometries of the U-profiles produced during the hybrid forming-heating process, with and without heat treatment of the radius zones. Results of numerical simulations were then validated using the measured geometry data. [72]

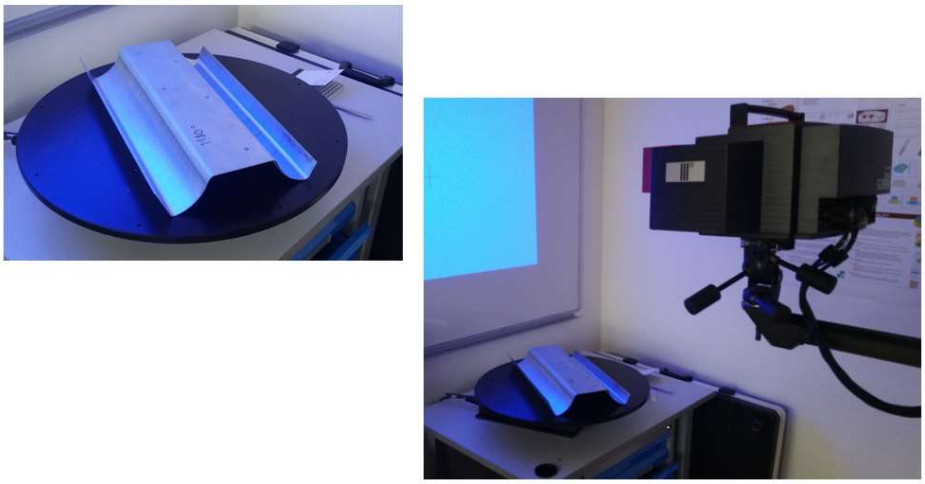

Figure 50 3D Scan of formed parts and analysis

During this investigation, three different materials were used, with HCT780X being the softest and CR900Y1180T being the hardest steel. When testing each material, the shape was initially produced at room temperature (a) to provide reference. The materials were then heated to 500°C (b) and 900°C (c) respectively in order to observe what effect this has on the springback of the material after hot forming.

The results are displayed in Figures 51, 52 and 53 respectively. It can be observed that CR700Y980T, when heated up to 900°C, provided the most desirable result, achieving a greatly reduced springback whilst still having a high level of formability. In comparison CR900Y1180T, whilst having its springback reduced when heated to 900°C, was simply too hard to be formed effectively.

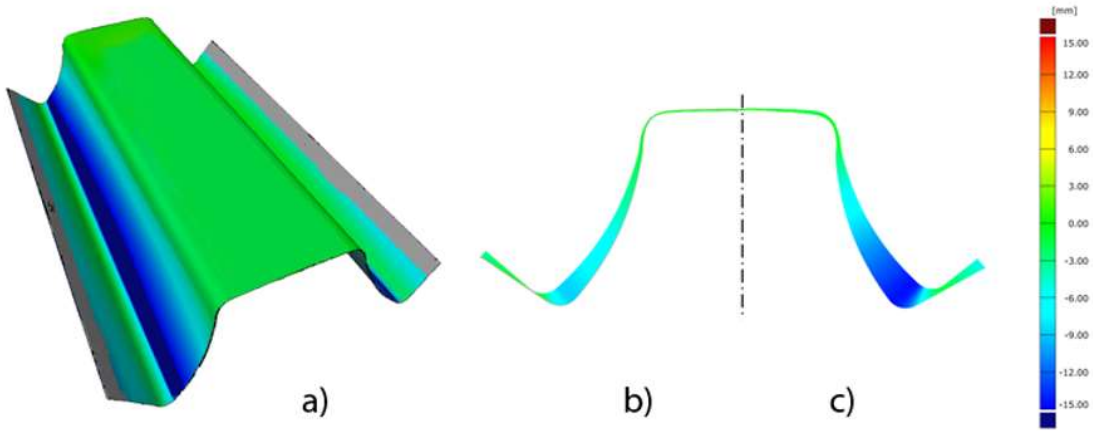

Material HCT780X
a) alignment of the formed part with and without heating the model
b) creation of sections of the formed part with 500°C heating and without heating
c) creation of sections of the formed part with 900°C heating and without heating

Figure 51 3D Scan of HCT780X material after forming

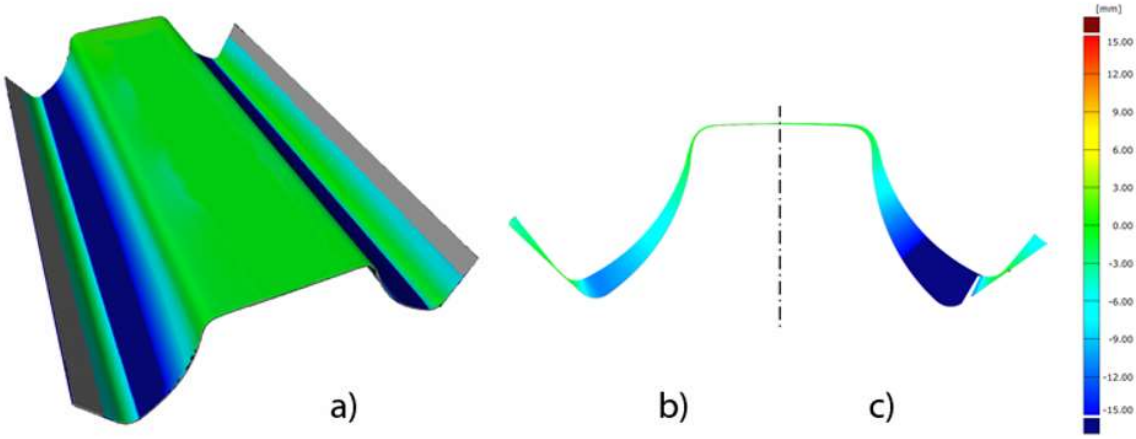

Material CR700Y980T
a) alignment of the formed part with and without heating the model
b) creation of sections of the formed part with 500°C heating and without heating
c) creation of sections of the formed part with 900°C heating and without heating

Figure 52 3D Scan of CR700Y980T material after forming

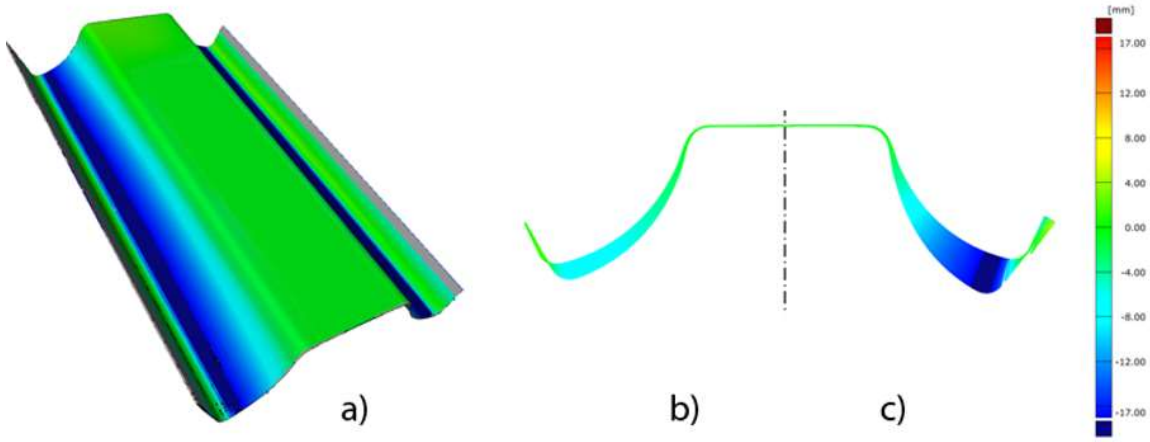

Material CR900Y1180T
a) alignment of the formed part with and without heating the model
b) creation of sections of the formed part with 500°C heating and without heating
c) creation of sections of the formed part with 900°C heating and without heating

Figure 53 3D Scan of CR900Y1180T material after forming

After the 3D scanning of the material to observe more closely how the process of hot forming affected the hardness of each material, cross-sectional cuts were taken and then probed at regular intervals along the radii.

The hardness of the HCT780X steel, measured at room temperature (RT) and after induction post heating with different peak temperatures, shows an initial hardness after forming at room temperature Figure 54a of approximately 230HV10 in the non-forming area, and shows a peak hardness of 290HV10. At a peak temperature of 500°C Figure 54b the hardness is between 260 HV10 and 295 HV10. The hardness of HCT780X achieves values of maximum 275HV10 after the induction heat treatment with a peak temperature of 900°C.

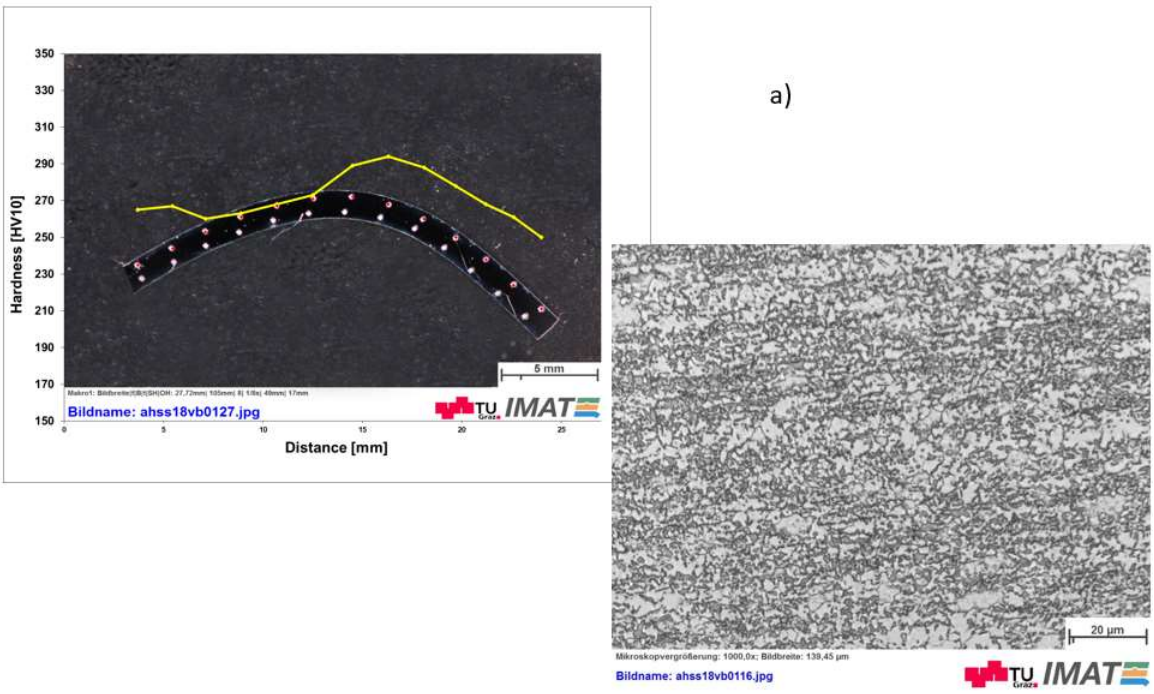

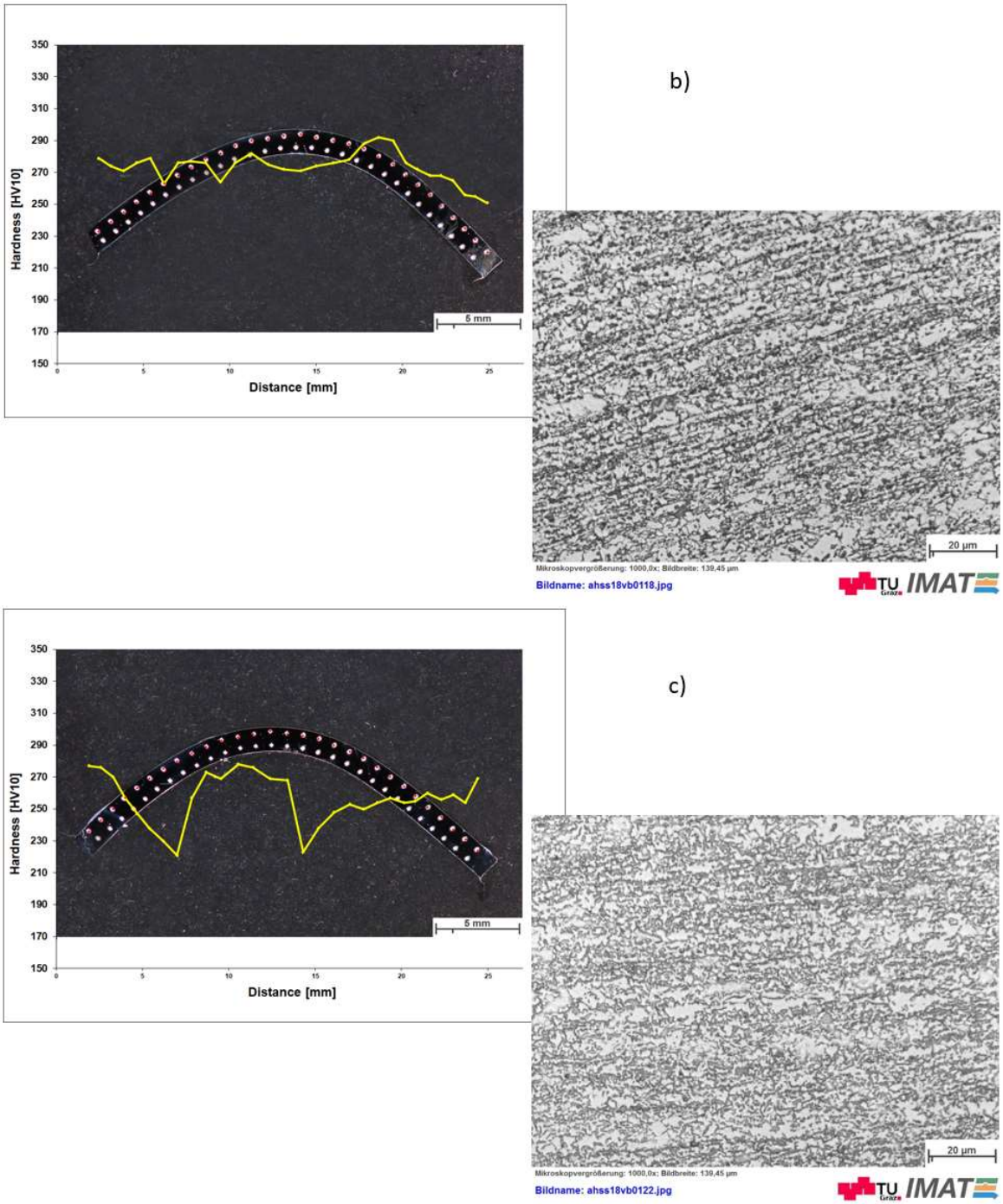

Figure 54 Hardness measurement of HCT780X at temperatures a) RT b) 500°C c) 900°C

Figure 55a demonstrates the initial hardness of CR700Y980T after forming at room temperature of approximately 340HV10. At a peak temperature of 500°C in Figure 55b the hardness is between 330 HV10 and 365 HV10. The hardness of CR700Y980T achieves values of 340HV10 after the induction

heat treatment with the peak temperature of 900°C. It was possible to see a reduction in hardness of 60HV10 due to microstructural phase changes in the heat effected area.

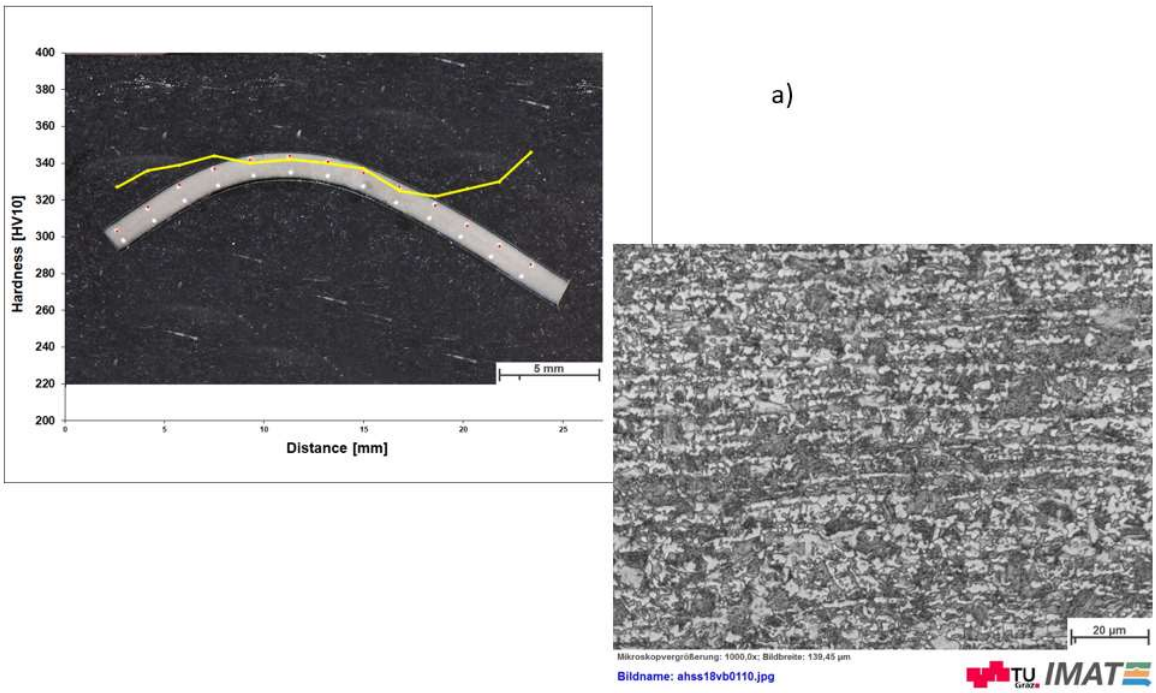

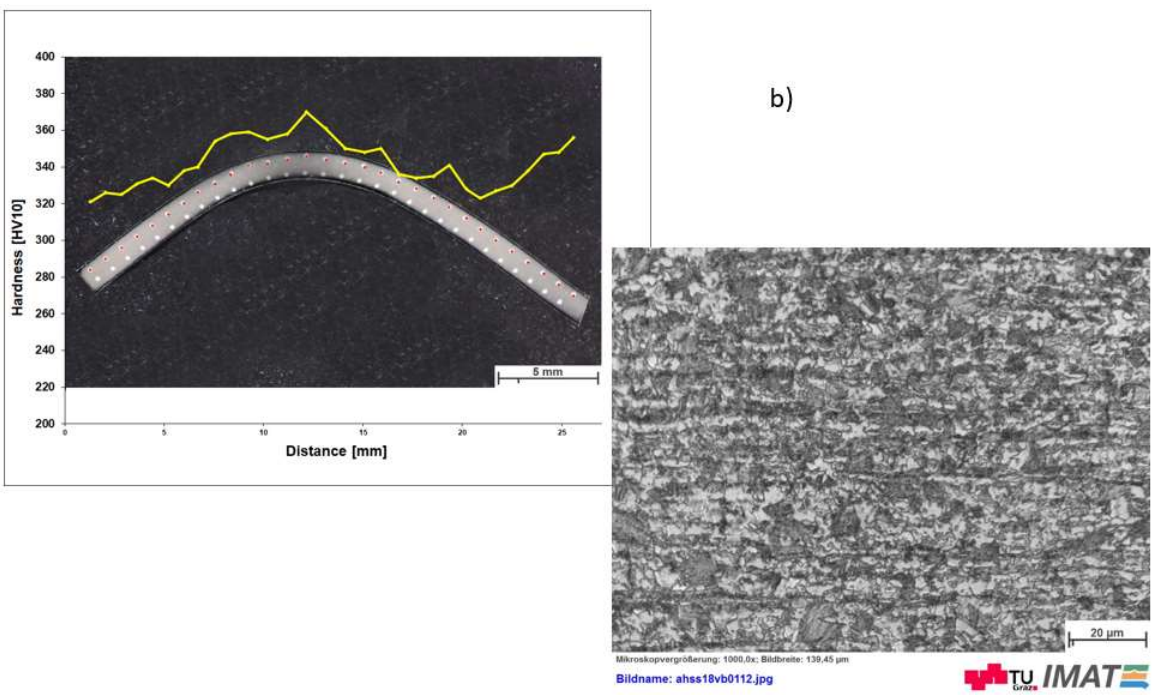

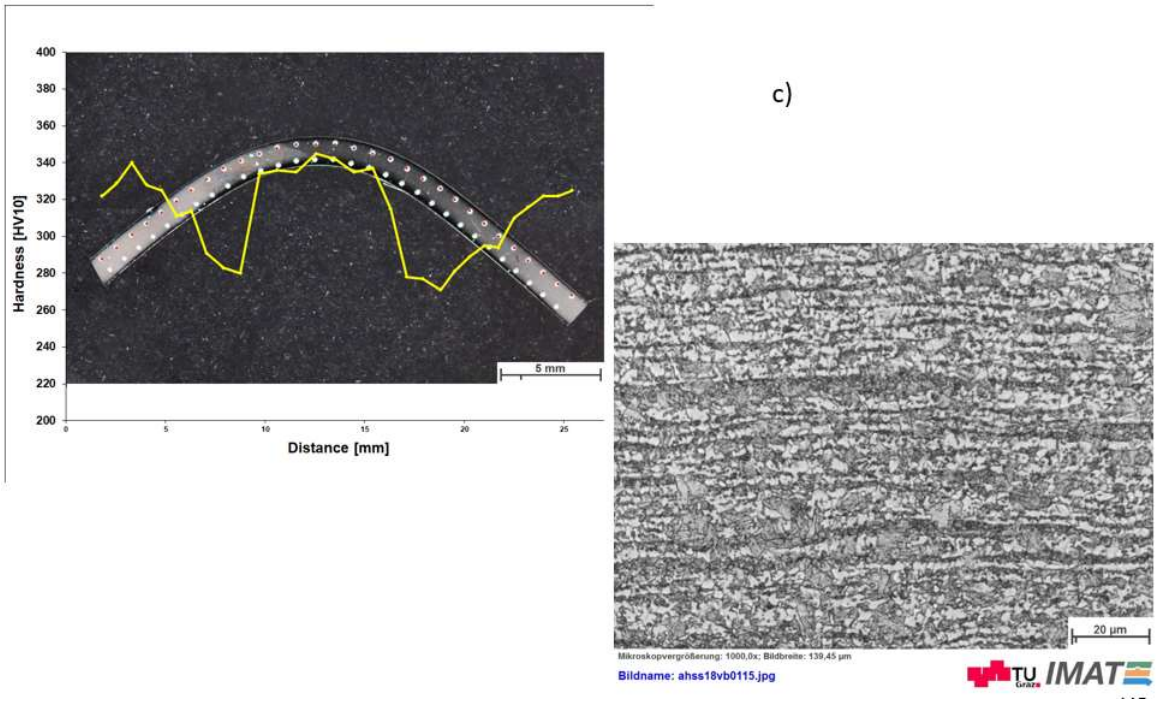

Figure 55 Hardness measurement of CR700Y980T at temperatures a) RT b) 500°C c) 900°C

The steel with the highest UTS of 1180MPa showed a hardness after forming at room temperature (Figure 56a) of approximately 440HV10. At the peak temperature of 500°C (Figure 56b) the hardness is similar to the one at room temperature. The hardness of CR900Y1180T achieves values of 455HV10 after the induction heat treatment with a peak temperature of 900°C. However, a large difference in hardness of 170HV between the maximum and minimum values can be observed. This could lead to a problem later on in case the part is used in a crash part group.

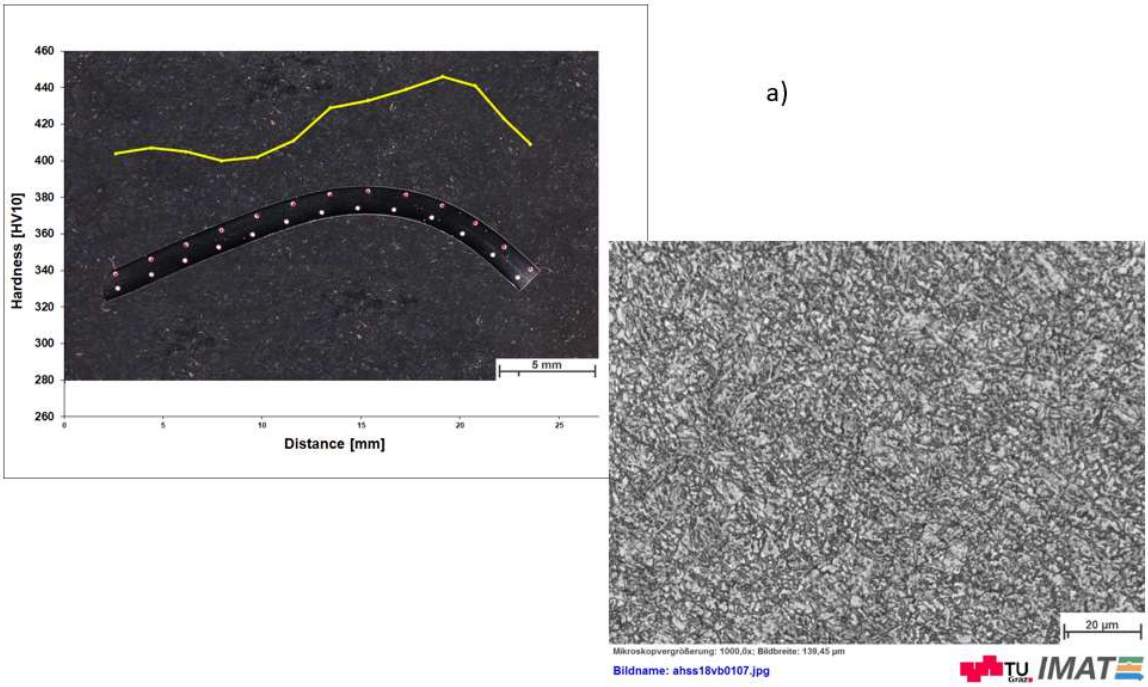
a)
Hardness [HV10]
Distance [mm]
5 mm
20 µm
Mikroskopvergrößerung: 1000,0x; Bildbreite: 139,45 µm
Bildname: ahss18vb0107.jpg
TU Graz IMAT

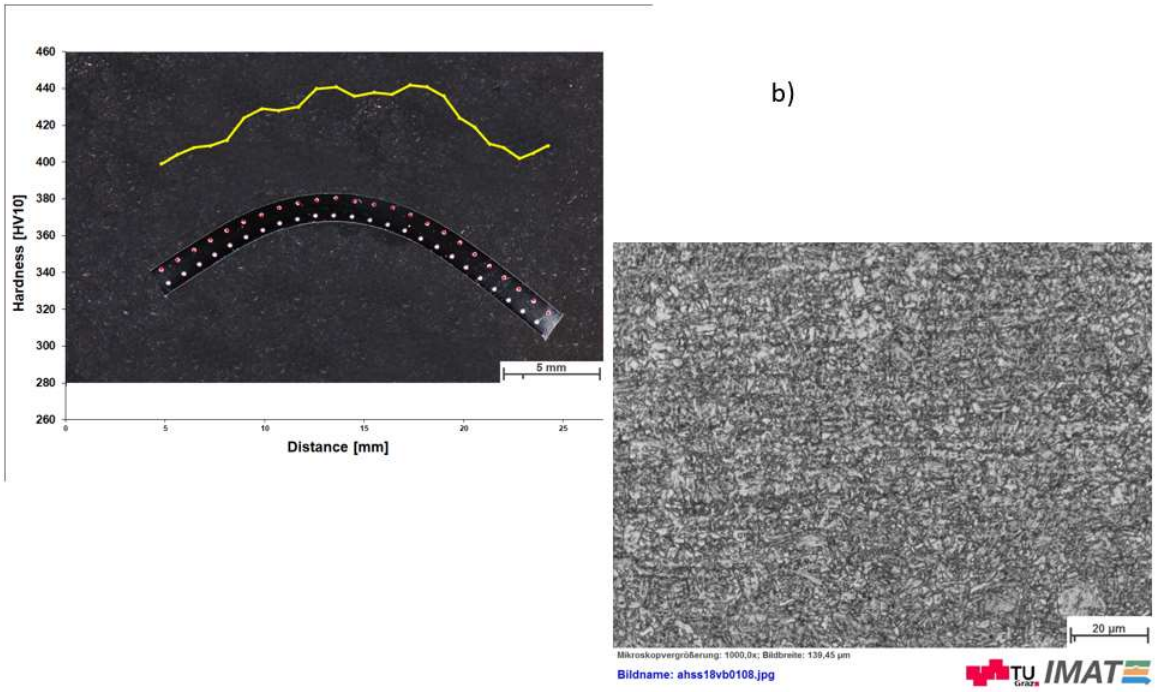
b)
Hardness [HV10]
Distance [mm]
5 mm
20 µm
Mikroskopvergrößerung: 1000,0x; Bildbreite: 139,45 µm
Bildname: ahss18vb0108.jpg
TU Graz IMAT

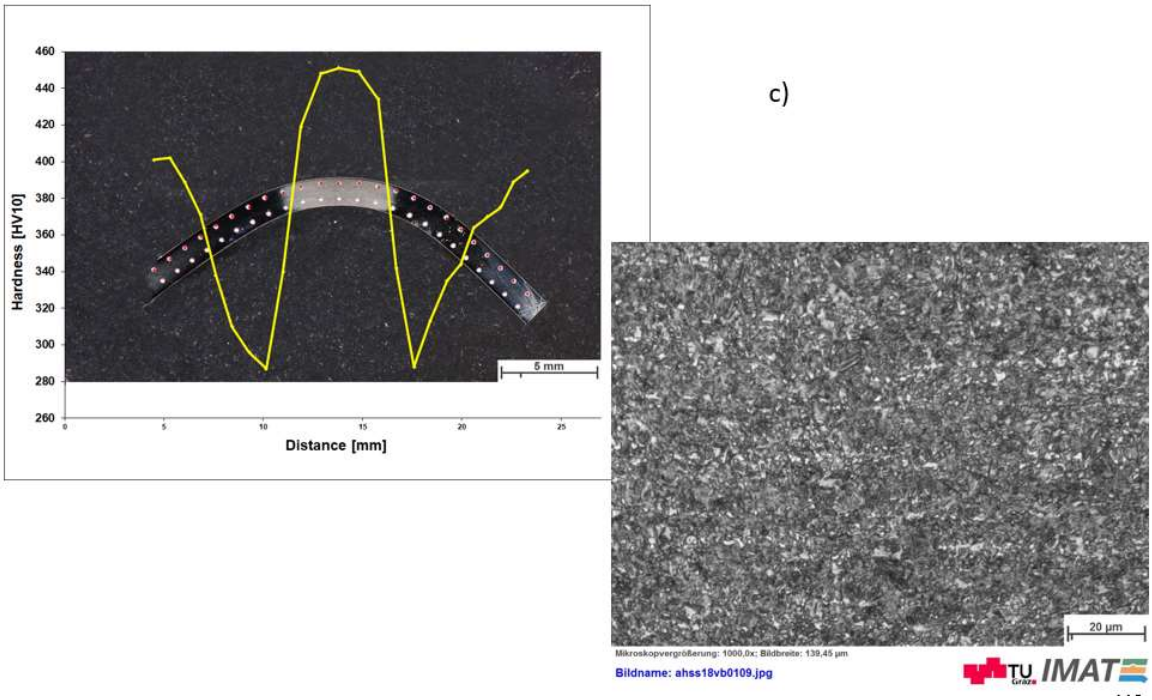

Figure 56 Hardness measurement of CR900Y1180T at temperatures a) RT b) 500°C c) 900°C

Following the above investigation, microscopy was then implemented to measure tangents` angle after forming. The sheets heated to 500°C and 900°C respectively were then once again compared to the reference sheet that was formed without the use of heating. The improvements in the reduction of springback could then be clearly observed. In the following photos, the upper sample is the reference sheet (formed at room temperature), the middle sample is the sheet that was heated to 500 during the forming process and the lower sample is the sheet that was heated to 900 during forming.

For material HCT780X, in comparison to the reference sample with angel of 105.82°, the sample heated to 500°C saw an improvement of 9° and the sample heated to 900 saw an improvement of 8°.

Figure 57 Bending angle after forming of HCT780X at temperatures a) RT b) 500°C c) 900°C

For the material CR700Y980T, in comparison to the reference sample with an angle of 111,75°, the sample heated to 500°C improved by 10° and the sample heated to 900°C by 13°.

Figure 58 Bending angle after forming of CR700Y980T at temperatures a) RT b) 500°C c) 900°C

Finally, the material CR900Y1180T in comparison to the reference sample with an angle of 114.09°, the sample heated to 500°C improved by 8° and the sample heated to 900°C by 15°.

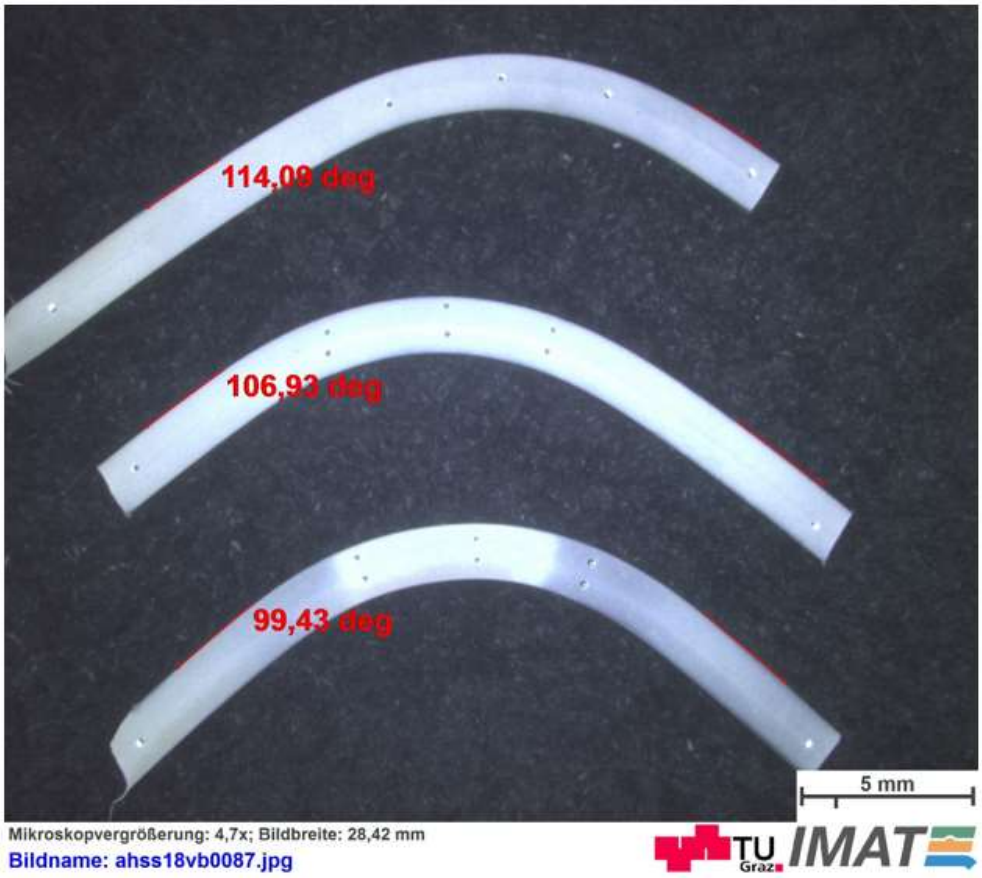

Figure 59 Bending angle after forming of CR900Y1180T at temperatures a) RT b) 500°C c) 900°C

As a result of the forming process, the blank undergoes stretching, bending and unbending deformations as it passes the tool radius. These deformations apply a complex stress to the sheet that results in the formation of so-called sidewall curl. The side curl becomes more pronounced for higher strength materials as showed on Figure 60 and Figure 61. The geometry of the formed part will deviate from the shape imposed by the tooling, which may well give rise to problems for subsequent assembly operations. [73]

Figure 60 Sidewall curl after forming of DC04

Employing stake beads during the forming of Advanced High-Strength Steel is a prevalent technique for controlling the residual stresses in stamping. These stake beads are incorporated into the part's addendum and become active at the bottom of the stroke, leading to heightened sidewall strain. This action serves to secure the plastic deformation, thereby minimizing curl and angular changes in the sidewall. [74] The goal of this work was to achieve a maximum springback in cold forming tool, which was why tool adaptation was not considered.

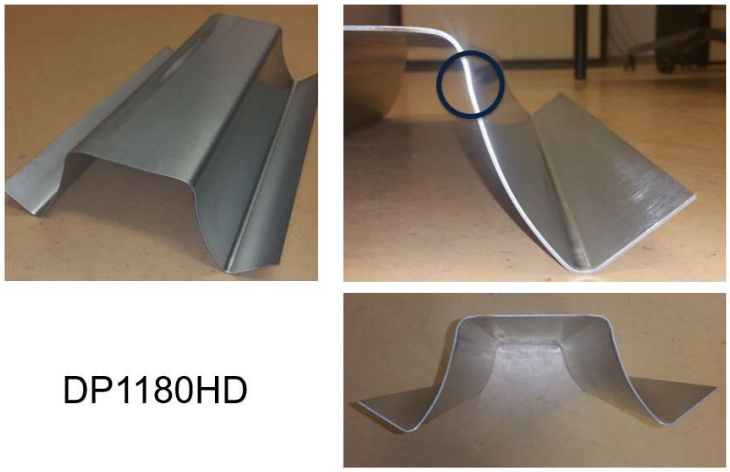

Figure 61 Sidewall curl after forming of CR900Y1180T

During hot forming, when the sheet became heated to a temperature of over 1000°C, waving of the upper surface was observed (a). This can clearly be seen when compared to the sheet formed at room temperature (b).

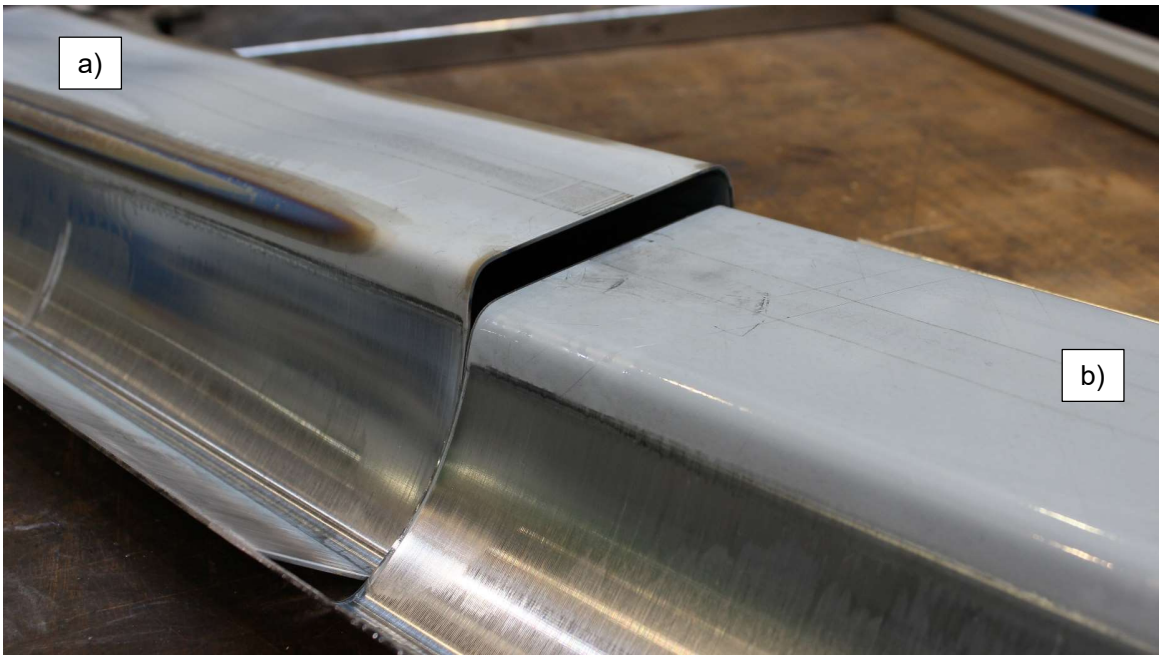

Figure 62 Overheated part above 1000°C and failure

As mentioned previosly, in order to accurately measure temperature, a pyrometer was placed inside the tool and a slit was cut. However, this produced a highly undesirable result as the slit redistributed the eddy currents unevenly, causing localized overheating. Therefore, the investigation focused on the areas of the sheet where this overheating was not observed, Figure 63.

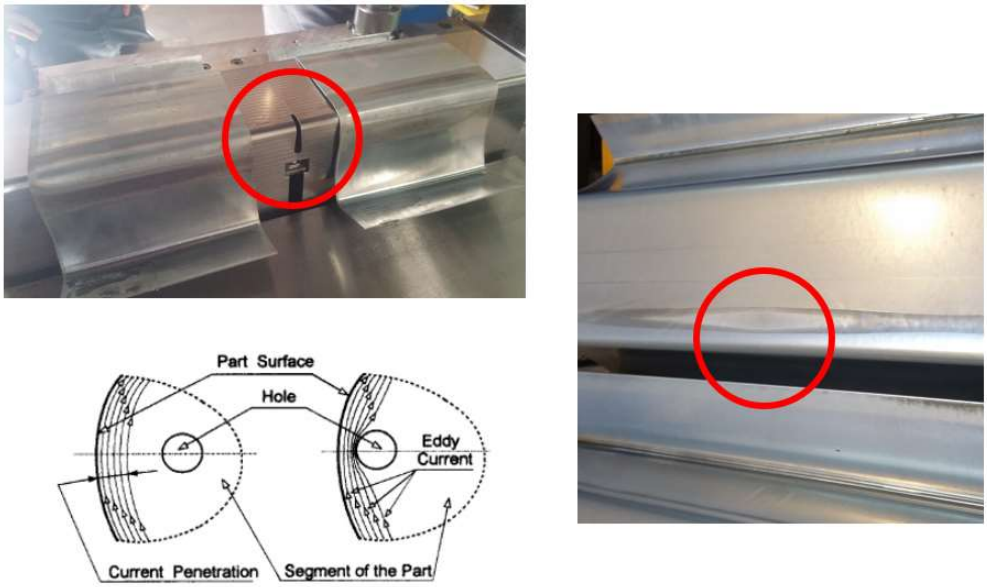

Figure 63 Measurement position cause hot spot in a part [69]

In summary, experimental investigations have showcased the viability of employing the concept for deep drawing U-profiles from AHSS steels using a prototype tool on a semi-industrial scale, aimed at mitigating springback. Local inductive heating before the tool is opened serves to alleviate internal stresses and consequently has the potential to significantly reduce springback. Furthermore, elevating the peak temperature during the heating process correlates with a decrease in the springback angle. Heat treatment conducted at peak temperatures of 925°C, coupled with conductive tool cooling, leads to the partial development of martensite and yields advantageous hardness properties. [72]

4.4 Modeling and simulation

4.4.1 Hat Profile Simulation using PamStamp for material 22MnB5

It was essential that commercially available FEM software was used in order to model the FEM simulation. This is because the simulation model achieved from the experimental data collected through the heat treatment and process must be validated. The development and the manufacturing of a heat treatment tool should be made with the ability to work under near-production conditions.

Due to cost restrictions for this project, material cards intended for hot forming, instead of those for cold forming were used. This is due to the fact that material cards a very highly priced and it would not be cost effective to purchase them, purely for this thesis. In order to provide a more accurate simulation, a material card for 22MnB5 was employed, as it is itself a material that is suitable for warm forming.

Fig 64 displays the simulation of the warm forming of 22MnB5. The light blue stripe that can be observed represents the exact area of heating. This area was varied in both width and peak temperature. The following parameters were selected for the simulation: Shell hourglass control - Stiffness using elastic

modulus, shell element type: for OP forming process Belytschko-Tsay with strain order 2 and for OP springback Batoz Q4 gamma with strain order 1. Thermal behavior to imposed temperature of 900°C and thermal exchanges by contact with blank at constant surface heat transfer coefficient 1E-005.

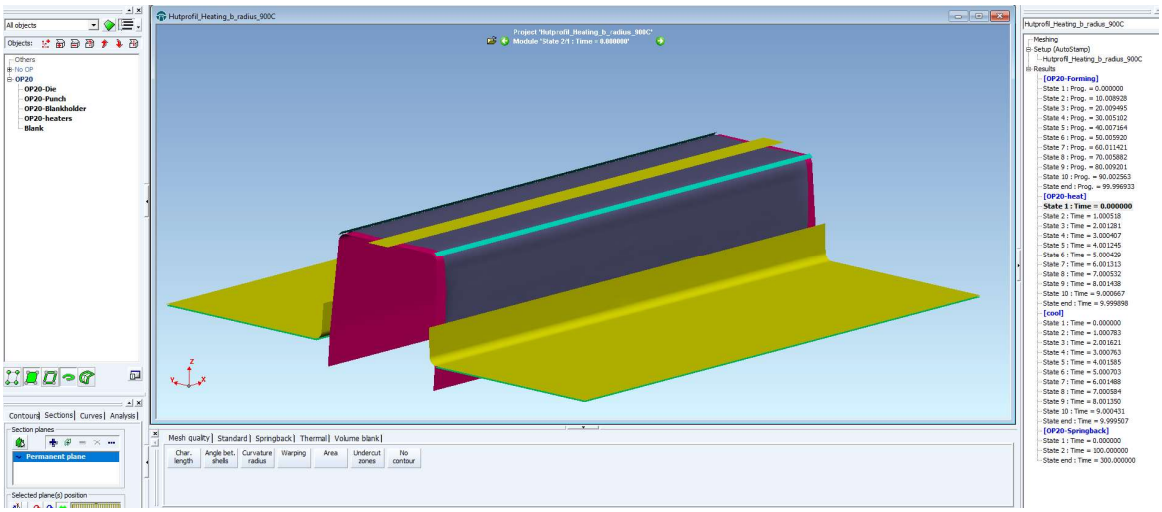

Figure 64 Simulation of a partially hot treated deep drawing process of 22MnB5

Figure 65 shows the extrapolated flow curves at different temperatures for Material 22MnB5. This data was subsequently fed into PAM-Stamp software.

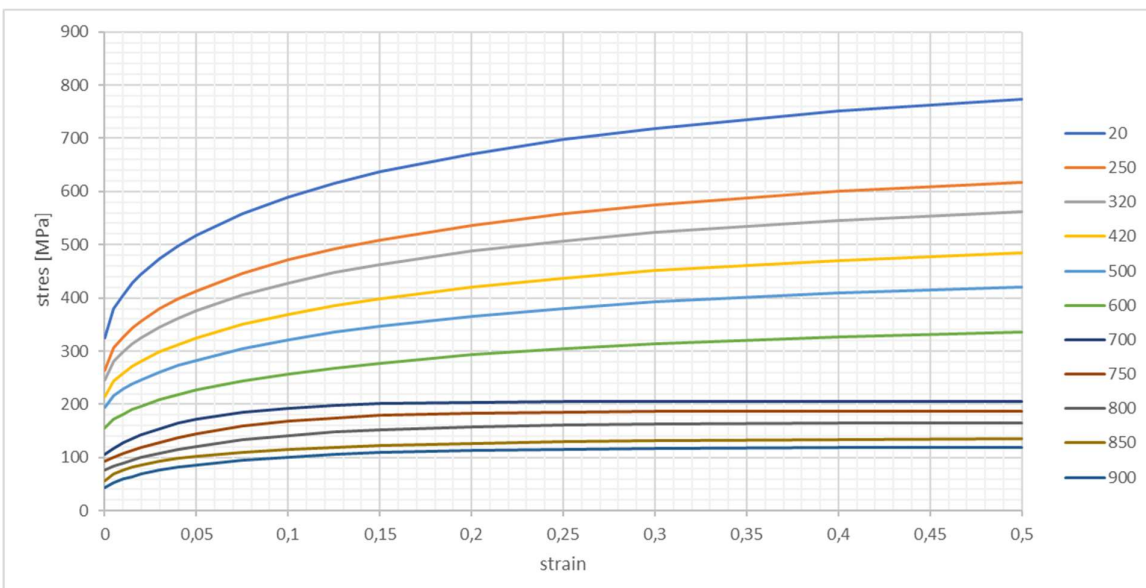

Figure 65 Extrapolated flow curves at different temperatures for material 22MnB5

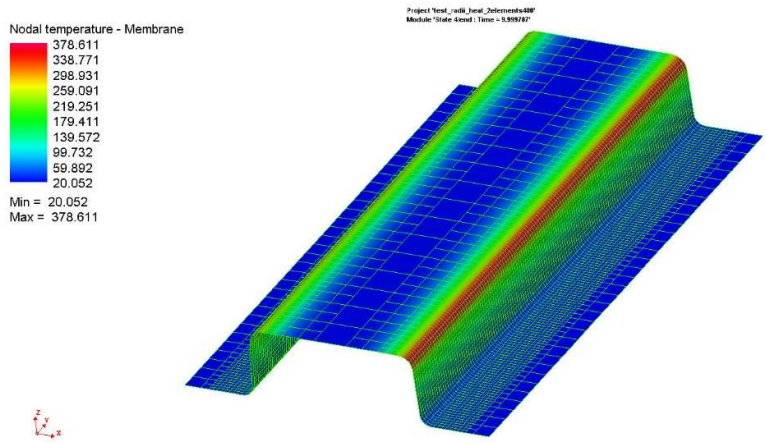

Figure 66 Meshed part model and partial heated to 500°C

It can be observed in Fig. 66 that a variation in both width of the area heated and peak temperature produced various levels of springback in the material. The simulation matrix is listed in Table 6.

Table 6 Heated area determinate to nodes affected and peak temperature of a FEM

	a)	b)	c)	d)
Peak Temp. [°C]	900	900	500	500
Nodes affected [#]	5	10	5	10

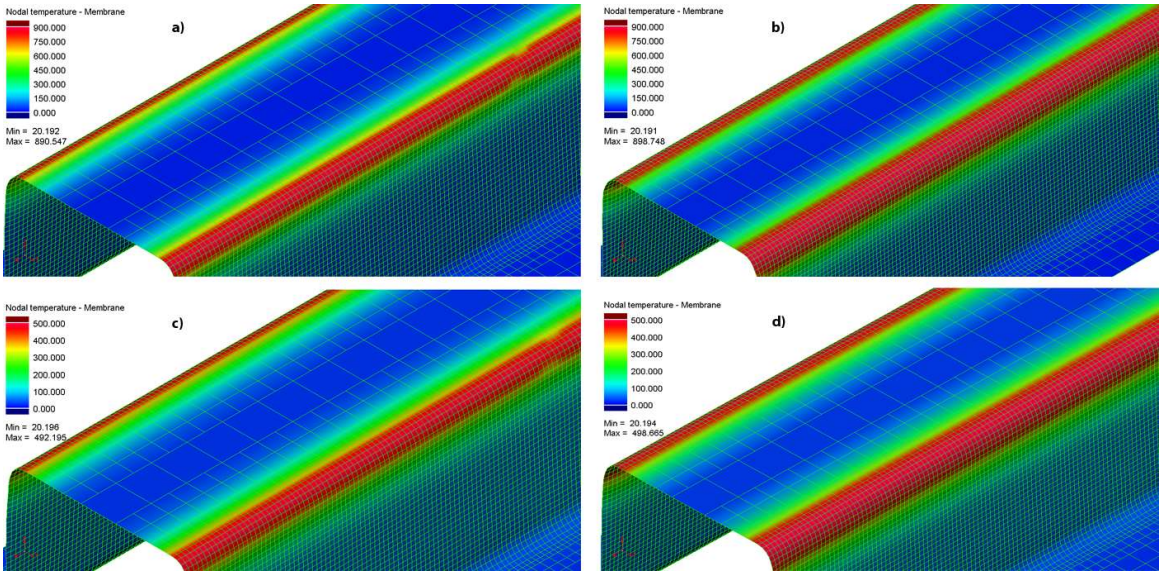

Figure 67 Simulation of different heating areas and peak temperatures

All the simulations exhibit, Figure 67, a reduction in the amount of springback in comparison to forming without heating. With these simulations, it is clear that a peak temperature of 900°C, concentrated on a smaller area produced the best result in terms of springback. It is interesting to note that the amount of springback of the simulation with 900°C with a wide area and with 500°C and small area of heating have similar values of springback, Figure 68.

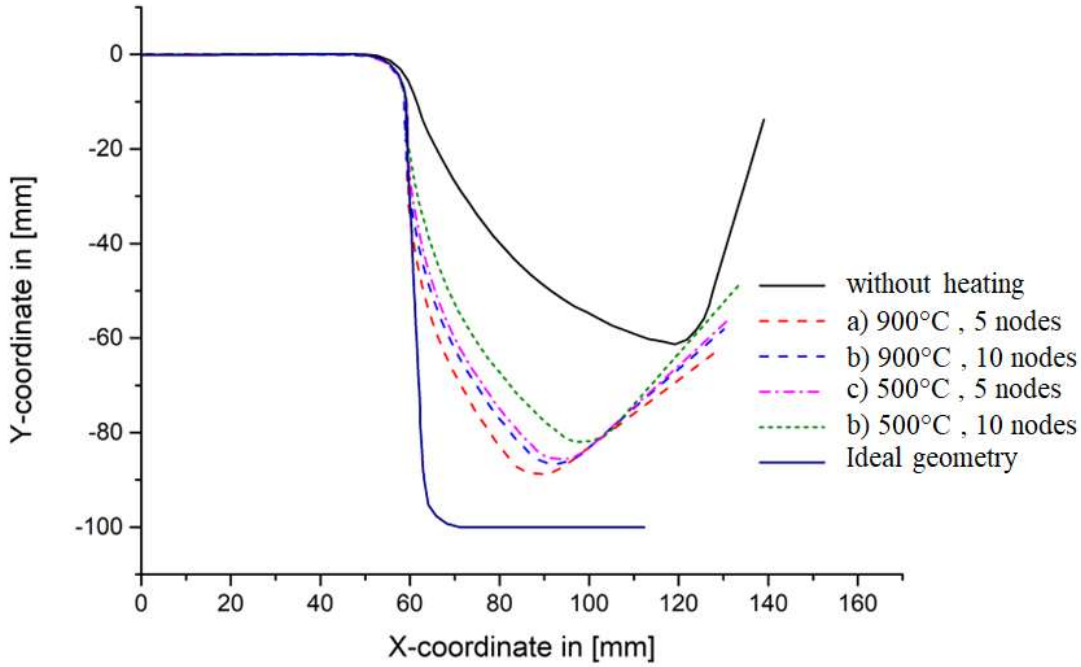

Figure 68 Springback simulation of 22MnB5 with influence of temperature in radii

4.4.2 Hat Profile using Abaqus for material DP980

Due to the formed U-profile's length dimension being much greater than overall height and width, the strain in the length direction is comparatively negligible. Furthermore, the cross-sectional dimensions also remain practically constant. This makes it possible to simplify the three-dimensional (3D) setup by using a two-dimensional (2D) plane strain model as shown in Fig. 69. A Abaqus Standard software package was used to construct a 2D model with one deformable component (the blank) and four analytical rigid components (die, blankholder, clamping bar and punch). Only the blank component was meshed using the so called "4-node bilinear plane strain quadrilateral, hybrid, constant pressure, reduced integration, hourglass control" (CPE4RH) elements of 0.005 mm × 0.05 mm. Shown in Fig. 69 is the rectangular cross-section of the 1.6 mm thick and 200 mm wide blank half. It was meshed using 128,000 elements and organized into 32 rows and 4000 columns. [72]

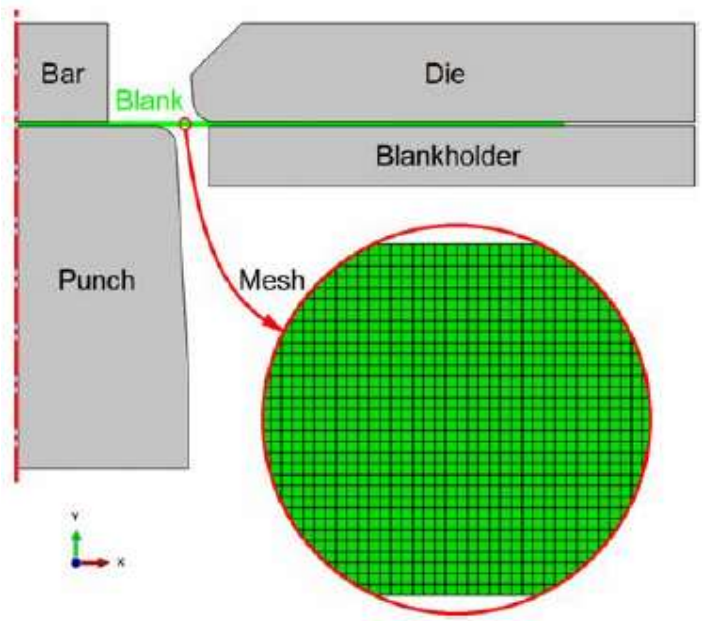

Figure 69 Symmetric 2D plane strain model with rigid (grey) and deformable (green) components for the FEM [72]

A Bähr DIL 805 D/T dilatometer equipped with an inductive heater was used to determine the flow curves and temperature-dependent elastoplastic properties (including Young's modulus) of DP steel. As shown in Fig. 70, a clamp was used to hold the tensile samples in the induction heater of the dilatometer. Prior to testing, samples were inductively heated to various temperatures (ranging from room temperature to 1000°C). [72]

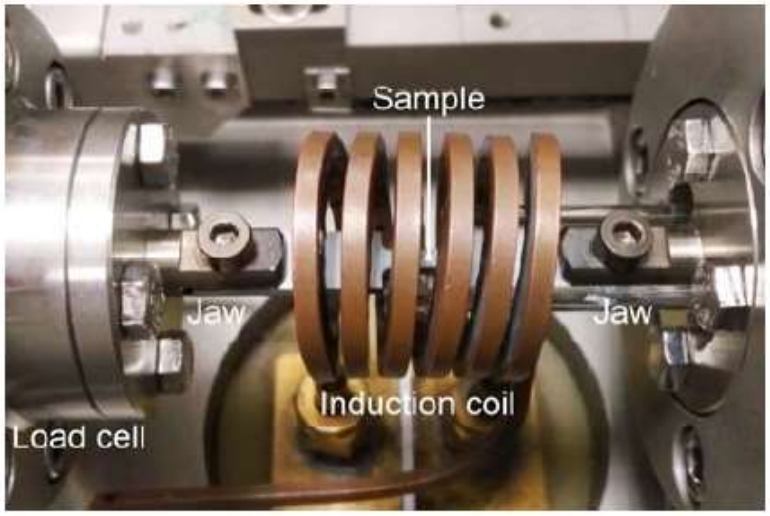

Figure 70 Tensile testing of samples using the dilatometer [72]

The tensile force and sample elongation were continuously monitored during testing and the corresponding true stress-strain curves were calculated. The Hollomon equation was then used to determine the temperature-dependent flow curves from the true stress-strain curves as illustrated in Fig. 71(a).

In addition, the Young's modulus temperature-dependence was calculated and is shown in Fig 71(b). The ratio of Young's modulus at high temperature versus room temperature (25°C) was calculated to be 204 GPa. Throughout the analysis a constant Poisson's ratio of 0.3 was assumed. [72]

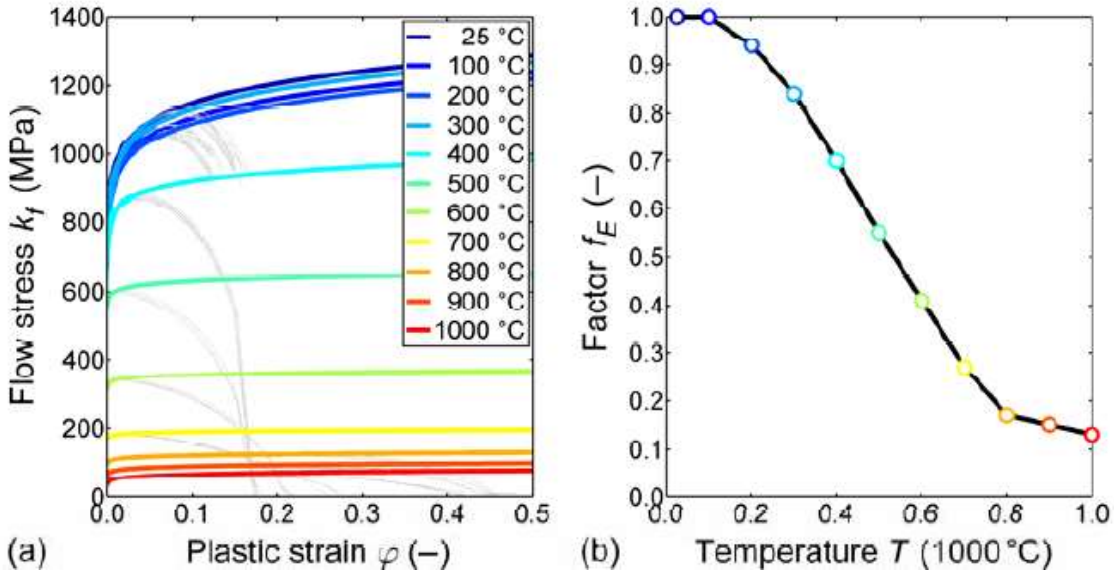

Figure 71 a) Temperature-dependent flow curves and b) temperature dependence of the Young`s modulus of the DP steel [72]

Shown in Fig. 39 are the four steps used to simulate the hybrid process. Note that the drawing die movement was restricted to the vertical direction, whereas the punch and clamping bar were fixed in position. The blankholder was forced against the direction of movement of the die and other process conditions, shown in Table 5 were included into the numerical model. Direct modeling of local inductive heating was not performed. Instead, measured peak temperature versus time curves from deep drawing experiments at the radii zones were included (shown in Fig. 72(a) are the two time-curves for 525°C and 925°C peak temperatures). In order to only consider local heating, both peak temperature time-curves were multiplied by the corresponding trapezoidal functions illustrated in Fig. 72(b). It must be noted that the temperature factor fT is equal to zero outside the radii zones. Constraints for the current model include: temperature allocation is based on the width coordinate of the initial unformed blank, a constant temperature along the thickness direction is assumed and a constant Coulomb's friction coefficient of 0.1 was set for each contact interface. [72]

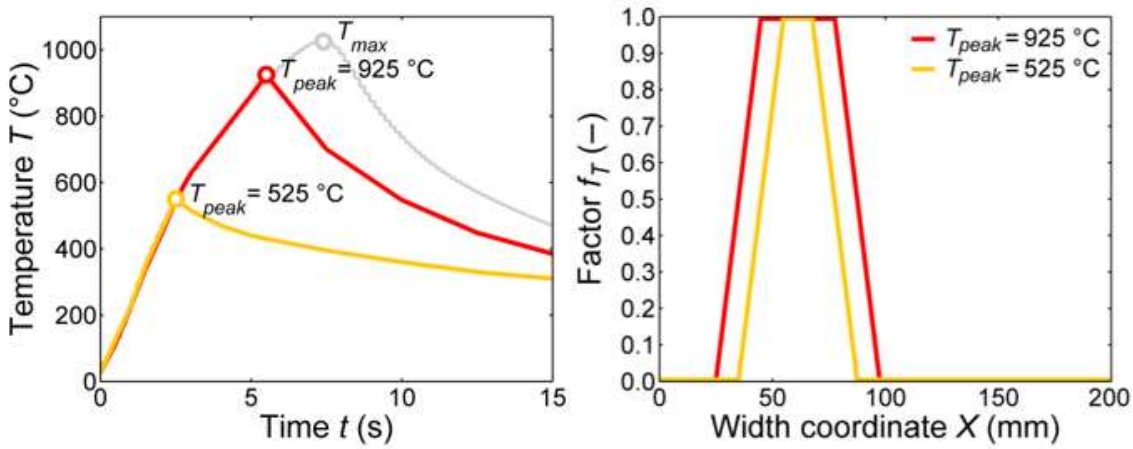

Figure 72 (a) Peak temperature-time curve and (b) trapezoidal temperature distribution [72]

Various processing conditions for the dual-phased steel were examined for etched microstructures and local hardness curve measurements: (a) as-bent with no heat treatment, (b) bent with heat treatment of 525°C peak temperature and (c) beat and heat treated up to a peak temperature of 925°C. The fraction of ferrite (light grey) and martensite (dark grey) are nearly equal, as shown in Fig. 8(a) and (b). Thus, it is clear that a peak temperature of 525°C did not alter the microstructure significantly. Conversely, as shown in Fig. 73 (c) heat treatment to 925°C does exhibit changes to the microstructure arising from decomposition of martensite into ferrite. The result of this change in microstructure is a reduction in the hardness, as shown in Fig.74. [72]

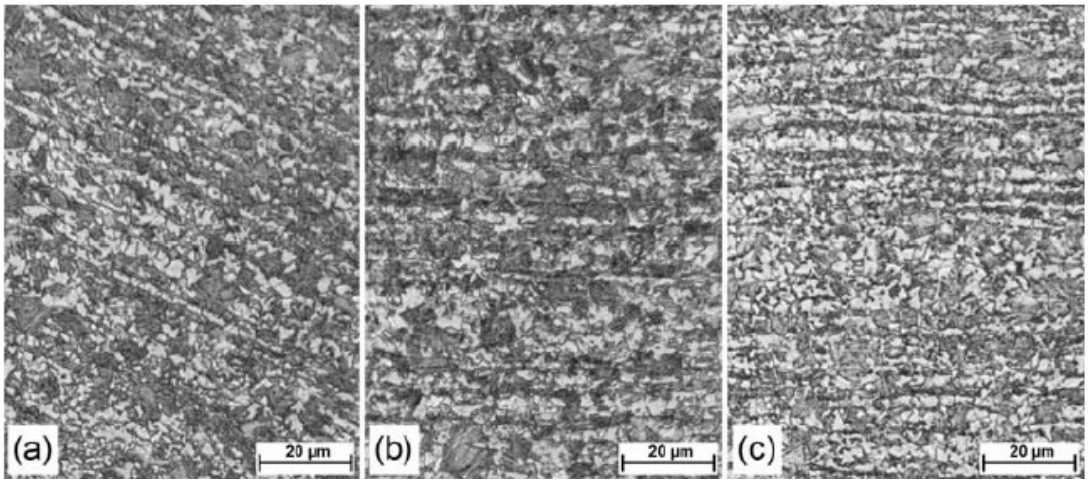

Figure 73 Microstructure of the dual phase steel a) without heat treatment and heat-treated with peak temperatures of b)525°C and c) 925° [72]

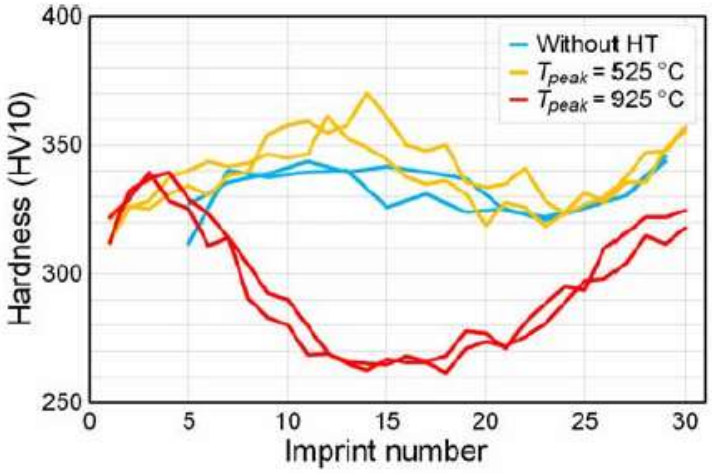

Figure 74 Local hardness of DP steel along the radius of the U-profile produces with and without heat treatment [72]

A comparison of the U-profile cross-sections produced with and without local heat treatment is shown in Fig. 75. These cross-sections are representative of the deep drawing experiments measured in the middle of the U-profile. As can be seen, springback angles decreased significantly with increasing peak temperatures. Some variability in drawing depth resulted in various profile leg lengths. However, this variation in length does not influence the measured springback angles. Finally, Fig. 75 shows the accuracy of the simulation model in predicting the influence of heat treatment on the measured springback angles. [72]

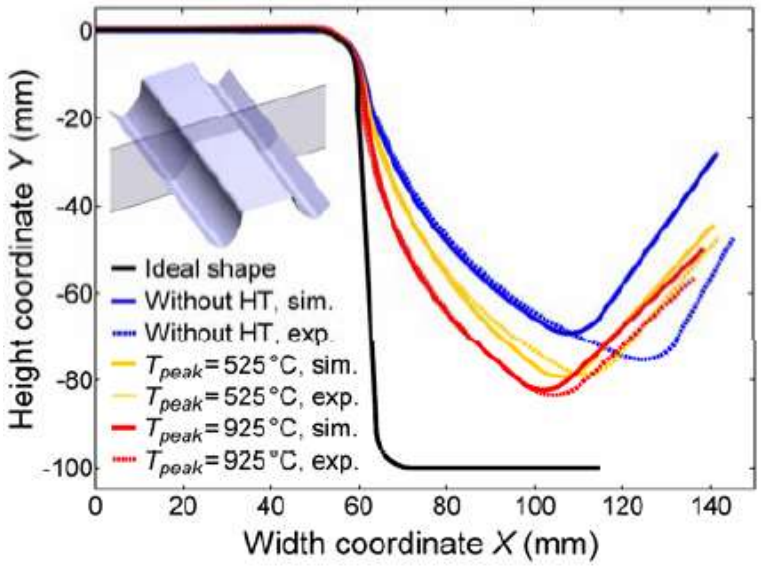

Figure 75 Comparison of springback with and without heat treatment (HT) of the radius zones of the U-profile [72]

In summary, both simulations show potential for such a hybrid process. The only drawback is the lack of complete material cards for cold/hot forming, which are very expensive nowadays. Therefore, an approach through simulation optimization in Abaqus reduces costs. Ideally, a study involving around ten different steels with various forming temperatures would be optimal. This data could later be incorporated into an AI model to create a database for further simulations.

5 Summary and outlook

In recent years, a trend in the steady increase in the use of high-strength steel (HSS) and advanced high-strength steel in the facilitation of the deep drawing of automotive components has become apparent. This is due to the fact that these steel types show great potential for not only producing lightweight structures, but also for improved crash resistance. However, a considerable obstacle manufacturers face in the production of these components when attempting to control their dimensional specifications is elastic springback. Springback is can essentially be described as an elastic deformation, occurring when the formed component is released from the forming tool. Springback can give rise to inaccurate geometries when forming components, therefore, refining the forming process to reduce the appearance of springback is seen as an extremely worthwhile progression within the automobile industry. Various different technological concepts were proposed for reducing springback in the sheet forming of HSS or AHSS, respectively: variation of the blankholder force, press force, drawbeads, heating of the flange region in deep drawing or using a counterpunch in sheet bending.

This thesis presents the concept of a hybrid forming-heating process to reduce the appearance of springback as a result of the deep drawing of AHSS. Both the experimental and numerical investigations performed within this thesis demonstrated the feasibility of the concept for deep drawing of U-profiles from DP steel using a prototype tool at semi-industrial scale.

The work within this thesis can be divided into two parts, experimental and numerical. In order to carry out the experimental side of the work, a tool was designed and produced at IMAT. The designed tool allowed for the localized heat treatment of deep drawn components, specifically immediately after completing the forming stroke i.e. just prior to the formed component becoming released from the tool.

For the purpose of this experimental analysis, two materials were proposed by the project partner, namely DP and TWIP. Tensile tests, employing the use of a quenching and deformation dilatometer, were performed in order to characterize the phase structure of the material after undergoing the influence of heating. As a result of these tests, it can determined how temperature will influence the mechanical properties of the material due to changes in its microstructure.

As a result of the first performed tests with the dilatometer, a decision was made to further investigate, utilizing dual phase materials. This was because dual phased materials are, at present, the most commonly used within the automotive industry. The steel grades that were selected to be tested on the tool were have a ultimate tensile strength of 780MPa, 980MPa and 1180MPa.

After shaping in the tool, the parts were scanned with the aid of the 3D measurement system GOM. The data from these scans was then analyzed in order to observe the influence of heating on both the occurrence and amount of springback deformation. It was observed, that materials that were heated to a temperature of 900°C, displayed a lesser occurrence of springback in comparison to materials that were heated to 500°C. However, one negative drawback was observed when heating the material to a temperature above 900°C. This was that a strengthening of the material was seen in the middle of the heating zone, but likewise a weakening of the material that occurs in the area between the part at peak temperature and the part that is cooler than 500°C. This conclusion was reached through the analysis of hardness measurements recorded after tests.

Measurements of the tangential angle between the upper part and the sidewall were also performed, as well as monitoring of the process and its optimization with the use of thermocouples and pyrometer embedded within the tool.

The second, numerical part of the thesis was carried out with the aid of various pieces of software. Firstly, the user-friendly, commercial software PAM- Stamp was used. A 22MnB5 material card was utilized in order to observe the effects of heating, inductor sizes and different peak temperatures. Similarly to the experimental tests mentioned above, a difference was seen between the parts that were heat treated in comparison to the parts which became formed at room temperature. Subsequently, in order to quantify how localized heat treatment effects the internal stresses inside a U-profile, a 2D model of the hybrid heat forming process was constructed using the Abaqus finite element (FE) software package. The flow curves required for this model were determined through the tensile testing of dual-phase (DP) steel sheets at temperatures between 25°C and 1000 °C.

Based on the results of these investigations the following conclusions can be drawn:

- Local inductive heating before opening the tool, decreases internal stresses and, therefore, may reduce significantly the occurrence of springback.
- Increasing the peak temperature of the heating process decreases the springback angle but will have a resulting impact on the phase structure.
- Heat treatment with peak temperatures of 925°C, combined with convective air cooling causes partial decomposition of martensite and loss of hardness. Comparatively, heat treatment with peak temperatures of 525 °C does not significantly influence the original microstructure.
- The FE model of the hybrid forming-heating process can predict the springback tendency based on the peak temperature-time curve recorded during heat treatment.

Outlook

Due to time restrictions when working on the project, some questions remained unanswered. Firstly, how the power of the conductor could be increased in order to reach speeds suitable for the industrial application of the system. Secondly, whether embrittlement would occur on the coating of the material when utilizing such high temperatures. And finally, whether the employing of such a system would be cost effective, particularly in the current economic environment where energy prices are constantly rising.

6 List of references

[1] M.Pudar, L.Malik, F. Mittermayer and R.Vallant, “Dissimilar Joining of Magnesium in body construction,” Wien, Austria, 2012.

[2] S. A. Nikolaevich, A. A. Valerievich, G. A. Igorevich, A. Alexandrovich and S. M. Alexandrovich, “Advanced materials of automobile bodies,” 2014.

[3] B. Zuidema, “The Role of Body-in-White Weight Reduction,” 2013.

[4] The Steel Recycling Institute, “Steel LCA study: lightweighting with advanced high-strength steel produces lower GHG emissions than with aluminum,” 2018.

[5] M. Kutz, “Handbook of Materials Selection,” 2002.

[6] S. Xu, K. Zhao, T. Lanker, J. Zhang and C. T. Wang, “Springback Prediction, Compensation and Correlation for Automotive Stamping,” 2005.

[7] WorldAutoSteel, “https://ahssinsights.org/forming/springback/,” 2018. [Online].

[8] K. Lange, Umformtechnik, Handbuch für Industrie und Wissenschaft, 1990.

[9] S. GmbH, Handbuch der Umformtechnik, Berlin: Springer, 1996.

[10] E. Doege and B.-A. Behrens, Handbuch Umformtechnik: Grundlagen, Technologien, Maschinen, 2010: Springer.

[11] G. Oehler and F. Kaiser, Schnitt-, Stanz- und Ziehwerkzeuge, Springer, 2001.

[12] Y. Zhang, Q. Zhang, X. Qin and Y. Sun, “A consistent relationship between the stress and plastic strain components and its application in deep drawing process,” Mathematical Problems in Engineering, 2017.

[13] A. Birkert, S. Haage and M. Straub, Umformtechnische Herstellung komplexer Karosserieteile: Auslegung von Ziehanlagen, Springer, 2013.

[14] M. Klamser, “Ziehen von Blechformteilen auf einfachwirkenden Pressen mit hydraulischer Zieheinrichtung im Pressentisch,” Stuttgart, Univ., Diss., 1994.

[15] B. Smallman, Metals and Materials, Butterworth - Heinemann, 1995.

[16] L. Larsson, Warm Sheet Metal Forming with Localized In-Tool Induction Heating, Lund: Faculty of Engineering, Lund University, 2005.

[17] E. Billur and T. Altan, “Three generations of advanced high-strength Steels for automotive applications, part I,” 2013.

[18] E. Billur and T. Altan, “Three generations of advanced high-strength Steels for automotive applications, part II,” 2013.

[19] E. Billur and T. Altan, “Three generations of advanced high-strength Steels for automotive applications, part III,” 2013.

[20] E. Shalash, “Optimal Automotive Door-Body Fitting for Body-In-White Assembly,” University of Widnsor, Ontario (Canada), 1996.

[21] E. C. B. Conference, “www.automotive-circle.com/,” [Online].

[22] W. Schatt and H. Worch, Werkstoff-Wissenschaft, Deutscher Verlag für Grundstoffindustrie, 1996.

[23] W. Beitz and K.-H. Grote, Dubbel Taschenbuch für den Maschinenbau, Springer, 1997.

[24] K. Schmitt-Thomas, Metallkunde für das Maschinenwesen - Band 1, Springer, 1990.

[25] K. Pöhlandt, “Testing strain-rate sensitive materials in the torsion test,” 1980.

[26] D. Banabic, H.-J. Bunge, K. Pöhlandt and A. Tekkaya2017, “Formability of metallic materials”.

[27] S. Benson, “Bending Basics: The hows and whys of springback and springforward,” 2014. [Online].

[28] “Sheet Metal Forming - bending,” 2009. [Online]. Available: https://www.custompartnet.com/wu/sheet-metal-forming.

[29] S. Sumikawa, A. Ishjwatari, J. Hiramoto and T. Urabe, “Improvement of springback prediction accuracy using material model considering elastoplastic anisotropy and Bauschinger effect,” vol. Journal of Materials Processing Technology, 2016.

[30] M. F.Horstemeyer, “Damage influence on bauschinger effect of a cast A356 Aluminum alloy,” 1998.

[31] M. Vable, “Mechanics of Materials,” 2014.

[32] R. K. Gupta, C. Mathew and P. Ramkumar, “Strain Hardening in Aerospace Alloys,” 2015.

[33] Z. Marciniak, J. Hu and J. Duncan, Mechanics of sheet metal forming, Butterworth-Heinemann, 2002.

[34] A. Sluzalec, Theory of Metal Forming Plasticity, Classical Advanced Topics, Springer, 2004.

[35] R. Schmidt-Jürgensen, “Untersuchungen zur Simulation rückfederungsbedingter Formabweichungen beim Tiefziehen,” 2002.

[36] A. Albut, “The influence of the sheet thickness on springback effect in case of TWB's forming,” Circuits, Systems and Sign, 2008.

[37] N. Woellner, S. Lajarin and P. Marcondes, “Blank Holder Force Influence on the Springback of Advanced High Strength Steels,” 22nd International Congress of Mechanical Engineering, 2013.

[38] R. Srinivasan, D. Vasudevan and P. Padmanabhan, “Influence of friction parameters on springback and bend force in air bending of electrogalvanized steel sheet: an experimental study,” 2013.

[39] A. Albut and G. Brabie, “The influence of the rolling direction of the joined steel sheets on the springback intensity in the case of O-shape parts made from tailor welded strips,” 2006.

[40] S. Chikalthankar, G. Belurkar and V. Nandedkar, “Factors Affecting on Springback in Sheet Metal Bending: A review,” 2014.

[41] G. Sachs, Principles and Methods of Sheet Metal Fabrication, Literary Licensing, LLC, 2013.

[42] R. Radonjic and M. Liewald, “Approaches for springback reduction when forming ultra high-strength sheet metals,” 2016.

[43] Y. Kuriyama, “The Latest Trends in Both Development of High Tensile Strength Steels and Press Forming Technologies for Automotive Parts,” 2001.

[44] Auto/Steel partnership, High Strength Steel Stamping Design Manual 20-48.

[45] S. Sadagopan, D. Urban, M. C. Wong, Huang and B. Yan, “AISI/DOE Technology Roadmap Program: Formability Characterization of a New Generation of High Strength Steels,” 2003.

[46] M. Linnepe, P. Sieczkarek, M. Kibben and F. Botz, “Dimensionally Accurate Parts Made Of High Strength Steels – Compressive Stress Superposition Instead Of Tool Compensation,” 2021.

[47] J. Born, “Smarter Forming,” *Compact Steel - The ThyssenKrupp Steel Magazine,* 2018.

[48] C. Löbbe and A. E. Tekkaya, “Mechanisms for controlling springback and strength in heat-assisted sheet forming,” 2018.

[49] T. Yoshida, E. Isogai, K. Sato and K. Hashimoto, “Springback Problems in Forming of High-Strength Steel Sheets and Countermeasures,” NIPPON STEEL TECHNICAL REPORT, 2013.

[50] C. Löbbe, Temperaturunterstütztes Biegen und Wärmebehandeln im mehrstufigen Werkzeugen, Dortmunder Umformtechnik, 2018.

[51] C. Löbbe, O. Hering, L. Hiegemann and A. E. Tekkaya, “Setting Mechanical Properties of High Strength Steels for Rapid Hot Forming Processes,” *Materials,* 2016.

[52] W. A. Siswanto, A. D. Anggono, B. Omar and K. Jusoff, “An Alternate Method to Springback Compensation for Sheet Metal Forming,” *.e Scientific World Journal,* 2014.

[53] U.Ulibarri, I.Gil, J.Mendiguren, L.Galdos and E. S. d. Argandoña, “Influence of heat treatments on springback and formability of Inconel 718 alloy in multi-stage deep drawing processes at room temperature,” Linz, 2016.

[54] X. Cui, Z. Zhang, H. Yu, X. Xiao and Y. Cheng, “Springback Calibration of a U-Shaped Electromagnetic Impulse Forming Process,” *Metals - MDPI,* 2019.

[55] T. Pepelnjak, B. Baranoglu, E. Kayhan and B.Kaftanoglu, “Numerical Simulation of the Deep Drawing Process with Local Heating at the Flange Region,” 8th International Conference and Exhibition on Design and Production of MACHINES and DIES/MOLDS, 2015.

[56] T. Pepelnjak, E. Kayhan and B. Kaftanoglu, “Analysis of non-isothermal warm deep drawing of dual-phase DP600 steel,” 2018.

[57] Y. Lim, MIMO Adaptive Process Control in Stamping Using Punch Force, University of Michigan, 2010.

[58] K. Lawanwong, H. Hamasaki, R. Hino and F. Yoshida, “Double-action bending for eliminating springback in hat-shaped bending of advanced high-strength steel sheet,” 2020.

[59] N. Woellner, S. F. Lajarin and P. V. P. Marcondes, “BLANK HOLDER FORCE INFLUENCE ON THE SPRINGBACK OF ADVANCED HIGH STRENGTH STEELS,” 2013.

[60] T. Maeno, K.-i. Mori and T. Nagai, “Improvement in formability by control of temperature in hot stamping of ultra-high strength steel parts,” 2014.

[61] Y. Jia, C. Pu, F. Zhu, D. Zhou, C. Du, Y.-W. Wang, Z. Qin and a. C.-K. Hsiung, “Numerical Study of Twist Spring-back Control with an Unbalanced Post-stretching Approach for Advanced High Strength Steel,” 2018.

[62] D. Zhou and K. Kannan, “The Effect of Combination Beads on Springback: Experimental Study & Virtual Study,” 2021.

[63] Y. Jia, C. Pu, F. Zhu, K. Schmid and Y. W. Wang, ““A New Hybrid Bead with Post-stretching Method to Effectively Control Spring-back for Advanced High Strength Steel”.

[64] A. Konieczny, “Dual Phase Steel Applications in Tailor-Welded Blank Technology,” 2004.

[65] J. Fekete, “Product and Process Effects On Stamping Performance Of Advanced High Strength Steels,” 2006.

[66] A. Mihail, M. Rodzik and G. Nadkarni, “Design & Manufacturing a DP980 B-Pillar Inner for the GM Chevy Equinox / Pontiac Torrent,” 2007.

[67] A. Mousavi and A. Brosius, “Improving the springback behavior of deep drawn parts by macrostructured tools,” 2018.

[68] S.-M. Park, S.-R. Lee and S. Hong, “Springback Minimization using Bottoming in Al Can Deep Drawing Process,” 2016.

[69] V. Rudnev, D. Loveless, R. Cook and M. Black, Handbook of induction heating, Marcel Dekker, 2003.

[70] S. R. Arrese, State-of-the-art Springback prediction during Cold Forming of AHSS parts in the Automotive Industry, Graz: Master thesis, TUGraz, 2016.

[71] V. Boskovic, C. Sommitsch and M. Kicin, “Development of a Hybrid Deep Drawing Process to Reduce Springback of AHSS,” Journal of Physics: Conference Series, Volume 896, 2017.

[72] J. Domitner, V. Boskovic, I. Baumgartner, F. Grünbart, C. Sommitsch and M. Kicin, “Local Heat Treatment for Springback Reduction in Deep Drawing of Advanced High-Strength Steel,” The Minerals, Metals & Materials Series , 2022.

[73] K.-H. Chang, “Chapter 13 - Sheet Metal Forming Simulation,” *e-Design, Computer-Aided Engineering Design,* no. Academic press, pp. 685-741, 2015.

[74] WorlAutoSteel, “AHSS Aplication Guidelines,” https://ahssinsights.org/.

[75] S. C. Spathopoulos and G. E. Stavroulakis, “Springback Prediction in Sheet Metal Forming,,” *Applied Mechanics,* pp. 97-110, 2020.

[76] E. Billur, J. Dykeman and T. Altan, “Three generations of advanced high strenght steel for automotive applications,” 2014.

[77] H. JH, “Tensile Deformation. Metals Technology 12(4):268–289”.

7 List of figures

8 List of tables